الجمهورية الجزائرية الديمقراطية الشعبية

Republique Algerienne Democratique Et Populaire

وزارة التعليم العالي والبحث العلمي

Ministère de l'Enseignement Supérieur et de la Recherche Scientifique

جامعة العربي التبسي – تبسة

Université Larbi tébessi – Tébessa –

Faculté des Sciences et de la Technologie

Département de Génie Civil

THESE DE DOCTORAT

Présentée pour l'obtention du **diplôme** de **Doctorat LMD**

En : Génie Civil

Spécialité : Structures et matériaux avancés

Par : **Abuteir Baker Wael**

Sujet

Non-linear dynamic analysis of FGM plates and shells with a degenerated shell finite element

Présenté et soutenue publiquement, le 10/03/2022, devant le jury composé de :

Président	Ninouh Tarek	Pr.	Université de Tébessa
Encadreur	Harkati El-haddi	Pr.	Université de Tébessa
Examinateur	Djeghaba Kamel	Pr.	Université de Annaba
Examinateur	Mamen Belgacem	MCA.	Université de Khenchla
Examinateur	Yahiaoui Djarir	MCA.	Université de Batna
Co-Encadreur	Boutagouga Djamel	Pr.	Université de Tébessa

Promotion : 2021/2022

ACKNOWLEDGEMENTS

First, I would like to thank my family for allowing me to realize my own Potential, all the support they have provided me over the years was the greatest gift anyone has ever given me. Also, I must express my very profound gratitude to my advisors, Prof. Harkati El-Haddi and Prof. Boutagouga Djamel for providing me with unfailing support and continuous encouragement throughout my years of study and through the process of researching and writing this thesis, I would like also to thank Dr. Harkati Amine and his family, they were always supporting me and encouraging me with their best wishes. This accomplishment would not have been possible without them. Thank you all.

Finally, I would like to thank all my friends for supporting me in this research.

ملخص

في هذا العمل، تمت دراسة الاستجابة الديناميكية الغير خطية والالتواء الديناميكي للهياكل الصدفية المصنعة من المواد ذات الخصائص المتدرجة (FGM) في البيئات الحرارية مع اعتبار الخصائص المادية متغيرة بالحرارة. أخذنا بالاعتبار أن الخصائص الفعالة للمادة المتدرجة وظيفيًا تعتمد على درجة الحرارة ويمكن أن تتغير وظيفيًا في اتجاه السماكة فقط. للتغلب على قفل القص والقفل الغشائي، تم اعتماد تكامل مخفض معدل وفعال. تم استخدام مخطط تكامل زمني محافظ / مبدد من اجل تكامل الزمن مع عنصر صدفي منحني مكون من 8 عقد. تمت صياغة العنصر المحدد الصدفي في إطار الصيغة اللاخطية الهندسية الكلية لـ Lagrange مع اعتبار الإجهادات حرارية باستخدام Green-Lagrange. تظهر النتائج العددية التي تم الحصول عليها أن العنصر الصدفي المنحني المطور مع مخطط تكامل الوقت المحافظ / المبدد قادر على حل مشاكل الالتواء الديناميكي غير الخطي والمشاكل الديناميكية ذاتا الإزاحة الكبيرة للهياكل الصدفية المصنعة من المواد ذات الخصائص المتدرجة في البيئات الحرارية الشديدة. تم بعد ذلك دراسة تأثير المادة المكونة، وتدرج المادة، والخصائص الإنشائية والحمولات الحرارية-ميكانيكية على السلوك الديناميكي. على وجه الخصوص، تم عرض ومناقشة تأثيرات قانون التدرج ودرجة الحرارة خلال السماكة على السلوكات غير الخطية الستاتيكية والديناميكية.

الكلمات المفتاحية: *عنصر صدفي; FGM ; متدرج وظيفيا; ميكانيكي-حراري ; ديناميكية غير خطية ; التواء ديناميكي ; التأثير الحراري.*

Abstract

In this work, the nonlinear time history response and dynamic-buckling of functionally graded material (FGM) shell structures in thermal environments with temperature-dependent material properties are studied. The effective properties of the functionally graded material are assumed to be temperature-dependent and can vary through the thickness only. To overcome shear and membrane locking, an efficient modified reduced integration is adopted. An implicit conservative/decaying time integration scheme and a curved 8-node degenerated shell element are used for the time and spatial discretization respectively. The shell element is formulated in the framework of the Total Lagrangian Formulation with thermal strains/stresses taken into account using the Green-Lagrange geometric nonlinearity. Numerical results obtained here, show that the developed curved shell element with the implicit conservative time integration scheme is capable of solving nonlinear dynamic-buckling and large displacement dynamic problems of FGM shell structures in severe thermal environments. The effects of the constituent material, material gradient, parameters of structural geometry and thermo-mechanical loadings on the dynamic behavior are then investigated. In particular, the effects of the power-law indexes and temperature gradient through-thickness on the nonlinear static, dynamic and dynamic-buckling phenomena are presented and discussed.

***Keywords**:* Degenerated shell; FGM; Functionally graded; Thermo-mechanical; Nonlinear dynamic; Dynamic-buckling; Thermal effect.

Résumé

Dans ce travail, la réponse dynamique non linéaire et le flambement dynamique des coques en matériaux fonctionnellement graduées (FGM) dans des environnement thermiques avec des propriétés de matériau dépendantes de la température sont étudiés. Les propriétés effectives du matériau à gradation fonctionnelle sont supposées dépendantes de la température et ne peuvent varier que suivant l'épaisseur. Pour surmonter les blocages de cisaillement et de membrane, une intégration réduite modifiée efficace est adoptée. Un schéma d'intégration dynamique implicite conservatif/dissipatif et un élément de coque dégénéré courbe à 8-nœuds sont utilisés pour la discrétisation dans le temps et dans l'espaces respectivement. L'élément de coque est formulé dans le cadre de la Formulation Lagrangienne Totale avec prise en compte des déformations/contraintes thermiques en utilisant la déformation non-linéaire géométrique de Green-Lagrange. Les résultats numériques obtenus montrent que la formulation d'élément coque courbe développée avec le schéma d'intégration implicite composite est capable de résoudre les problèmes de la dynamique non-linéaire et les problèmes de flambement-dynamique des structures de coque FGM dans des environnements thermiques sévères L'influence de différents constituants, l'indice de gradient de matériau, des paramètres de géométrie structurelle et des chargements thermomécaniques sur le comportement dynamique sont étudiés. En particulier, les effets des indices de loi de puissance et du gradient de température à travers l'épaisseur sur les phénomènes non linéaires statiques, dynamiques et de flambement dynamique sont présentés et discutés.

Mots-clés: Coque dégénéré ; FGM ; Fonctionnellement gradué; Thermo-mécanique ; Dynamique non linéaire; Flambement dynamique ; Effet thermique.

CONTENTS

CHAPTER 01

General Background on Functionally Graded Materials

CHAPTER 02

Plates and shells theories

CHAPTER 03

Formulation of a nonlinear curved 8-node degenerated shell element in thermal environments

CHAPTER 04

Direct time integration dynamic analysis

CHAPTER 05

Results and discussion

List of figures

CHAPTER 01

CHAPTER 02

CHAPTER 03

CHAPTER 05

List of tables

CHAPTER 05

SYMBOLS

---------- CHAPTER 01 ----------

V_c	Volume fraction of ceramic.
z	Thickness direction coordinate.
h	Shell thickness.
n	Power-law index.
V_m	Volume fraction of metal.
E	Elastic modulus.
ν	Poisson's ratio.
ρ	Mass density.
α	Thermal expansion coefficient.
K	Thermal conductivity.
$P(z)$	Through-thickness material properties of an FGM.
T	Temperature.
$P_0, P_{-1}, P_1, P_2, P_3$	Coefficients of temperature.
T_0	Reference temperature.
ΔT	Temperature change.
$ZrO_2 / Ti-6Al-4V$	Zirconium oxide / titanium alloy.
$Si_3N_4 / SUS304$	Silicon nitride / stainless steel.
Al / ZrO_2	Aluminum / Zirconia.

---------- CHAPTER 02 ----------

u_0, v_0, w_0	Displacements of a point on the mid-surface.
ζ	Distance from the middle surface to the point considered.
σ_{33}	Transverse normal stress.
$\psi(\zeta)$	Transverse shear function characterizing the theories corresponding.
K_T	Tangent stiffness matrix.
M	Mass matrix.
r	Nodal load vector.
f	Function to be integrated.
w_i	Weighting factor.
α	Indicates the location of integration points.
U_1	The transverse shear energy obtained for a 3D stress distribution.
U_2	The energy associated with the 2D shell model.
τ_{xz} τ_{yz}	Transverse shear stresses.
T_x T_y	Transverse shear forces.

$H_\tau \quad H_c$	The 2x2 reduced transverse local and global shear stiffness matrix.
$G(z)$	The transverse shear modulus at location (Z).
ε	In plane strain.
$M_x \quad M_y \quad M_{xy}$	The bending moments.
$H(z)$	The 3x3 reduced in plane elasticity tensor which is given for an FGM.

---------- CHAPTER 03 ----------

X, Y, Z	Cartesian global 3D coordinate system.
ξ, η, ζ	Curvilinear coordinate system.
$\vec{v}_{1i}, \vec{v}_{2i}, \vec{v}_{3i}$	Nodal coordinate system.
g_1, g_2, g_3	Covariant coordinate system.
x', y', z'	Local coordinate system.
e_1, e_2, e_3	Unit vectors.
$\boldsymbol{r}_{0j}$	The position vector of a point on the reference surface.
$N_j(\xi_i, \eta_i)$	The 2D shape function of node *j*.
B_0	The linear strain-displacement matrix.
$r_i^{top} \quad r_i^{bot}$	The position vectors for the top and bottom surfaces at each node *i*.
n	The number of element nodes.
$\boldsymbol{u}$	Displacement vector.
${}^0(.), {}^t(.)$	The initial configuration and the configuration at time " t ".
$\alpha_i \quad \beta_i$	The incremental rotation angles of the director vector ${}^t\boldsymbol{v}_{3i}$.
$u \quad v \quad w \quad \theta_x \quad \theta_y$	Global nodal displacements.
$\boldsymbol{\varepsilon}_{ij}$	Green–Lagrangian strain components in the global Cartesian system.
$\tilde{\boldsymbol{\varepsilon}}_{ij}$	Covariant Green–Lagrangian strain components.
$\boldsymbol{Q}$	Transformation matrix.
$\boldsymbol{e}_{ij}$	linear Green–Lagrangian strain in the global Cartesian system.
$\boldsymbol{\eta}_{ij}$	Non-linear Green–Lagrangian strain in the global Cartesian system.
$\boldsymbol{J}$	The Jacobian matrix.
I	Unit matrix.
j_{ij}^{-1}	The element *ij* of the inverse of the Jacobian ***J***.
$\boldsymbol{A}$	Auxiliary matrix.
$\boldsymbol{B_{NL}}$	Nonlinear strain-displacement matrix.
ε^{th}	Thermal strain.
k_s	Shear correction factor.
$\boldsymbol{C}$	Constitutive matrix.
${}^{t+\Delta t}_{0}S_{ij} \quad {}^{t+\Delta t}_{0}\varepsilon_{ij}$	The second Piola-Kirchhoff stress tensor and the incremental Green-Lagrange strain tensor at ($t+\Delta t$) referred to the configuration at a time (t = *0*).
${}^{t+\Delta t}W$	Represents the external virtual work.

${}^{t+\Delta t}_{0}t_k$	Surface traction.
${}^{t+\Delta t}_{0}f_k$	Stands for body forces.
B	Represents the overall strain-displacement matrix.
H^m H^{th}	Mechanical and thermal stress.

---------- CHAPTER 04 ----------

$F_I(t)$	The inertia forces.
$F_D(t)$	The damping forces.
$F_{int}(t)$	The internal (nodal) forces including forces due to initial stresses in the system.
$F_{ext}(t)$	The external forces.
C	The damping matrix.
$f(u)$	The nonlinear internal nodal force vector.
u_0 $\dot{u}_0$	The given initial displacement and velocity.
β γ	Parameters that control the stability and accuracy of the algorithm.
${}^{t+\Delta t}R$	The effective load vector.
α β	The damping coefficients.
$\boldsymbol{S}$	Stands for the displacement matrix.

INTRODUCTION

As Functionally Graded Material (FGM) plates/shells are devoted to work in thermal environments with high temperature, there is a growing concern on considering the effect of temperature on the effective properties of the FGM constituent materials. Consequently, several works handling the linear and nonlinear analysis of FGM structures with temperature-dependent material properties have been presented in recent years.

The main purpose of this work is to develop a powerful and reliable numerical tool to efficiently study nonlinear dynamic behavior, dynamic-buckling and post-buckling of FGM shell structures in thermal environments. The salient features of this numerical too consists of using: curved geometry, membrane/bending/thermo-mechanical coupling, efficient numerical quadrature, and an implicit conservative dynamic scheme. These considerations are expected to be efficient to perform nonlinear transient dynamic and dynamic-buckling analysis with minimum mesh and larger time steps in order to minimize the computational time which is a prime advantage in the field of nonlinear transient dynamic analysis.

Then, the aim of this thesis is considering the effect of temperature on the effective properties of the FGM constituent materials on the nonlinear transient dynamic, dynamic-buckling, and post-buckling behaviours of FGM cylindrical and spherical shells in thermal environments using an implicit conservative/decaying time integration scheme, which, can be considered as an important addition to the state of the art of large-displacement dynamic behaviour of FGM shells. For this purpose, an 8-noded curved degenerated shell element is used for finite element discretization. The shell element is formulated in the framework of the Total Lagrangian Formulation with thermal strains/stresses taken into account using the Green-Lagrange geometric nonlinearity.

The material properties are assumed to be temperature dependent and are graded in the thickness direction according to the power-law distribution in terms of volume fractions of the constituents of the material. The bending and membrane strain-coupling considered in the element formulation allows to efficiently capture the high membrane-bending interaction in FGM plates/shells. In addition, the mass matrix formulation includes translational and rotary inertia effects. Consequently, a minimal number of elements can be used to mesh plane and curved geometries, which is a crucial concern to minimize the computational time, especially in

nonlinear dynamic analysis. Moreover, to overcome membrane and transverse shear locking, an efficient modified reduced numerical integration scheme is adopted allowing for more gain in computational time.

It is much common to use explicit schemes for solving highly nonlinear dynamic buckling and post-buckling problems, despite the fact that implicit dynamics time integration schemes are generally more stable and accurate than explicit ones, and can use larger time steps. Therefore, the present thesis examined dynamic buckling behaviour of functionally graded material shells in thermal environments based on an implicit time integration scheme. Indeed, an implicit conservative/decaying direct time integration scheme is used herein to obtain the time-history responses and to study the dynamic-buckling phenomena of FGM shell structures subjected to dynamic loading. The conservative/decaying scheme is expected to be efficient in energy conservation and parasitic high-frequency dissipation providing stable and accurate dynamic responses. It is important to remark that implicit schemes for shell buckling and post-buckling are still generally lacking in the FE analysis literature.

The present thesis has been subdivided in five chapters as follows:
An introduction is being given to describe the scope and objective of the present research work and explaining the way to achieve the planned objectives.

Chapter 1: Presents a general background, summary and the topics that are related to functionally graded materials (FGMs). In addition, a literature review of recent studies of functionally graded plate/shell structures is provided.

Chapter 2: In this chapter, gives a different shell theory, including different kinematics is presented. Additionally, different finite element approaches to generate shell elements is represented. Finally, an in-depth review of the literature focused on the development of degenerated shell elements, with a focus on recent published work.

Chapter 3: Dealing with the derivation of the degenerated curved shell element in the geometrically nonlinear formulation based on the total Lagrangian approach with regarding thermal environment is described.

Chapter 4: In this chapter, the nonlinear dynamic and buckling response of FGM shells in a thermal environment with temperature-dependent properties are obtained using direct time integration method.

Chapter 5: Results and discussion on FGM plate/shell structures based on the resulting formulation described in the previous chapters.

Finally, we present a general conclusion which incorporates all the results obtained in the previous sections of the numerical analysis.

Chapter 1

General Background on Functionally Graded Materials

1. Introduction

Composite materials have been playing a significant role during the history, and widely used in various industrial applications due to their improved properties, such as automobiles, energy and aerospace engineering fields. Composite materials reached great attention from researchers because they have enhanced properties, in which they are lighter, can also offer design flexibility and provide resistance to corrosion as well as wear. In spite of traditional composites that may suffer high amounts of stress concentration at dissimilar material interfaces, leading to delamination failure. However, the traditional composite material is incapable to employ under the high-temperature environments [1]. In general, the metals have been used in the engineering field for many years on account of their excellent strength and toughness. In the high-temperature condition, the strength of the metal is reduced similar to the traditional composite material. The ceramic materials have excellent characteristics in heat resistance. However, the applications of ceramic are usually limited due to their low toughness.

This chapter is an attempt to give a general introduction, identify and highlight the topics that are most relevant for functionally graded material (FGM) structures. Thus, a brief representation that define the effective properties of the materials.

2. Functionally graded materials concept

As stated above, the traditional composite materials were unable to withstand such extreme working conditions, the failure mode was due to delamination [2], that is, this was as a result of the mismatch in the properties of the two materials. The discontinuity at the interface is responsible for the high-stress concentration that exists at this interface. Hence, when the thermal load is applied to this composite material, the thermal mismatch caused the two materials to be separated, because of the different expansion properties of the two materials, which eventually resulted in the failure of the composite material. The researchers knew that if the sharp interface between the two materials that form the composite material could be eliminated. Then the problem would be solved. The researchers changed this sharp interface into a gradient interface

by gradually introducing the second material into the first material as against joining 100% of one material and 100% of the second material together, that is, using this process of gradually introducing the second material into the first material helped to exchange the sharp interface with the gradually changing interface and the composite material thus developed was able to withstand the intended high-temperature application.

This composite material that was developed with the gradient interface is referred to as "Functionally Graded Materials (FGMs)". The schematic diagram of the functionally graded composite material is shown in Figure 1.1.

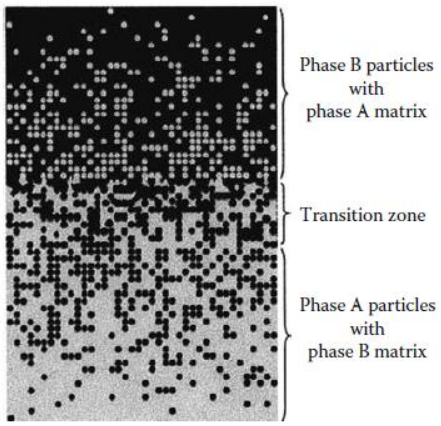

Fig. 1.1 An FGM with the volume fractions of the constituent phases graded and vary in the thickness direction [3].

Functionally graded materials (FGMs) are novel composite materials in which the volume fraction of constituent materials varying gradually through the thickness direction as shown in Figure 1.2, their mechanical and thermo-physical properties exhibit a smooth and continuous variation from one surface to another presented in Figure 1.3, thus eliminating interface problems and mitigating thermal stress concentrations [4]. This is because the ceramic constituents of FGMs can withstand high-temperature environments due to their better thermal resistance characteristics, while the metal constituents provide stronger mechanical performance. FGMs can survive in a harsh working environment with high-temperature gradation without losing their properties, and without failing during the service, see for instance [5-7]. The idea of functionally graded material for engineering application was first introduced in 1984, by a group of Japanese researchers for the core purpose of their aerospace project [8-10] that required thermal barrier with the outside temperature of 2000 K and inside 1000 K within 10 *mm*

thickness. FGMs were initially designed as thermal barrier materials for aerospace structures and fusion reactors [11-13].

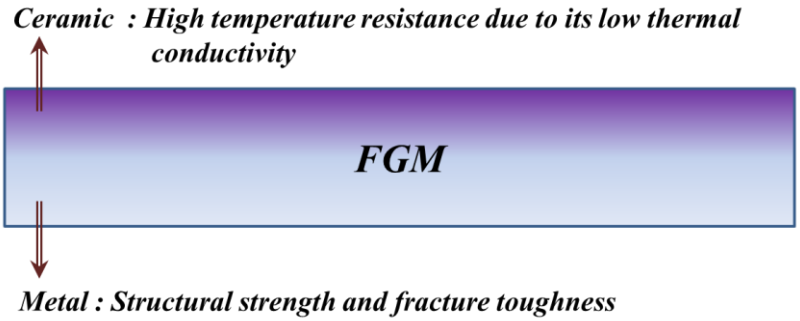

Fig. 1.2 Schematic representation of functionally graded material.

The applications of functionally graded materials have now been extended to other practices, such as in an environment of extreme wear-resistant application [14, 15], and they are being used in several industries and sectors like aerospace, nuclear, defence, automotive, communication, energy etc. as well as they are produced artificially, the primitive forms of FGMs exist in nature. Bones, human skin, the bamboo tree can be considered as organic forms of FGM.

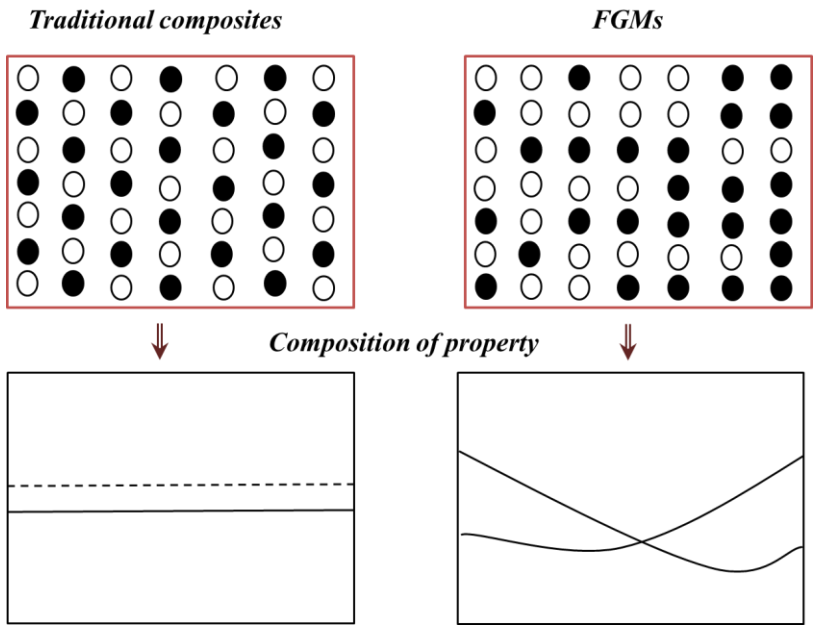

Fig. 1.3 Variation of properties in traditional composites and FGM [16].

The application areas of FGMs can be summarized as follows:

- ***Aerospace***: Spacecraft heat shields, heat exchanger tubes.
- ***Biomedical***: Artificial bones, skins, teeth.
- ***Communication***: Optical fibres, lenses, semiconductors.
- ***Nuclear field***: Fuel palettes, plasma-wall of fusion reactors.
- ***Energy sector***: Thermoelectric generators, solar cells, sensors.
- ***Automotive***: Power transmission systems, braking systems.

Moreover, Potential applications of FGM are both diverse and numerous have recently been reported in the open literature, FGM sensors [17] and actuators [18], FGM metal/ceramic armour [19]. Figure 1.4, represents the hierarchy of modern material.

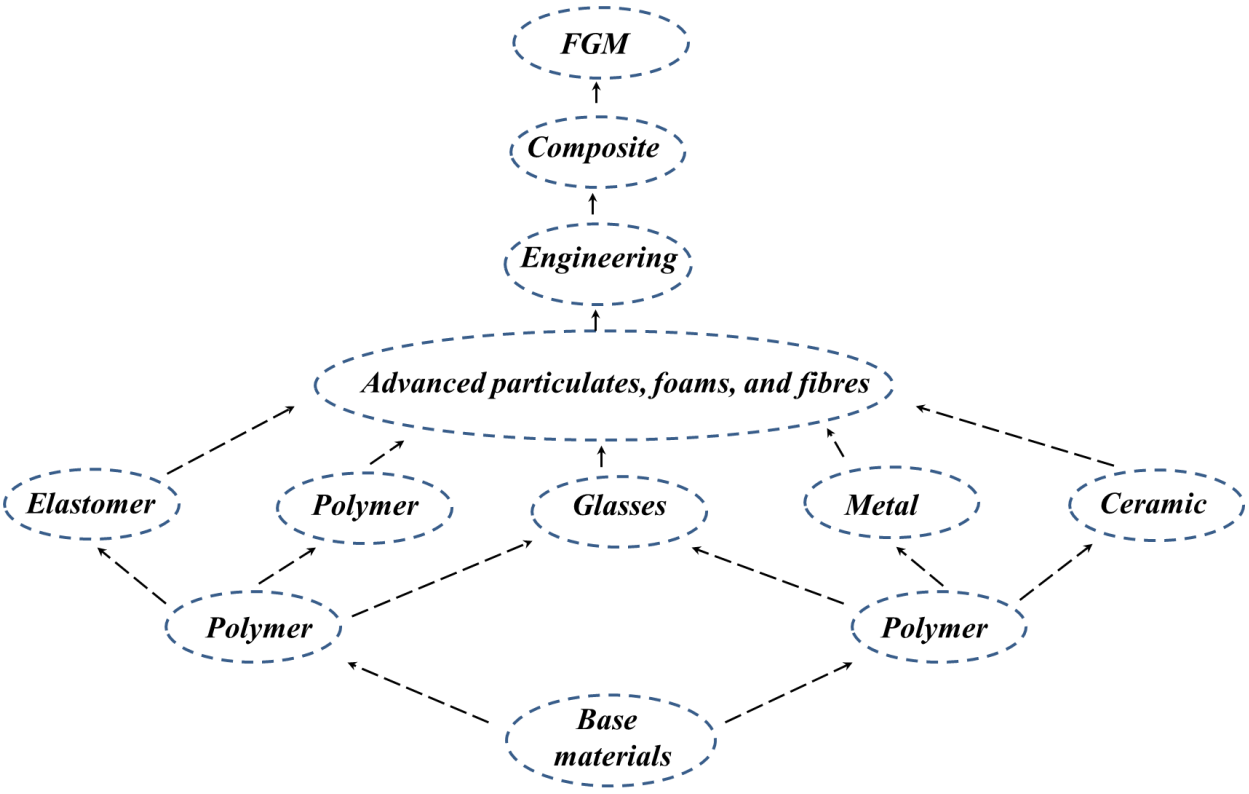

Fig. 1.4 Representation of modern material hierarchy [20].

3. Literature review of recent studies of FGM plates/shells

With the growing concern on FGMs in recent years, numerous studies have been performed to predict the dynamic behaviour " free vibration/transient response " of FGM plate/shell structures. Tornabene et al. [21] analysed the dynamic behaviour of moderately thick FGM conical and cylindrical shells, and annular plates, using the FSDT and the Generalized Differential Quadrature (GDQ) method. They concluded that the power-law distribution choice does not affect the free vibrations frequencies for shells with zero curvature such as annular panels and plates. On the other hand, for curved shells, it has been observed that the influence of the distribution choice is marked and can be considered. However, it can be concluded that the frequency vibration of functionally graded shells depends on the type of vibration mode, thickness, power-law distribution, power-law exponent and curvature of the structure. Yas et al. [22] developed a layer-wise finite element formulation for the analysis of FGM cylindrical shells with finite length under dynamic loads. In this study, the FGM cylinder was divided into many sub-layers and then the full layer-wise shell theory was used. In the research by Jung et al. [23] interesting research on the transient analysis of FGMs and laminated composite structures using a refined 8-node ANS shell element by taking into account the effects of shear deformations and rotatory inertia was presented. A study on the dynamic behaviour of double-curved shells made of functionally graded materials was presented by Tornabene et al. [24] using various higher-order equivalent single layer theories. The three dimensional double directors shell element with third-order shear deformation theory for FGM shell structure analysis was presented by Wali et al. [25]. In his work, static, free vibration and buckling analyses of FGM shells were carried out. Asemi et al. [26] investigated the static and dynamic behaviour of functionally graded skew plate structures based on a 3D theory of elasticity, the equation of motion was solved via Newmark's time integration method. Mahmoudkhani [27] analysed the nonlinear vibration and normal shapes of functionally graded cylindrical shell structures using an efficient analytical method, the equations of motion are based on Donnell's nonlinear shallow shell. In Khan et al [28] the authors investigated the static behaviour and free vibration of the functionally graded material beam using one-dimensional finite element model based on the effective Zig-Zag concept, eigenvalue problem was solved using the subspace iteration method to obtain natural frequencies and the corresponding mode shapes. Jin et al. [29] worked on thick functionally graded plates

and cylindrical shells using the three-dimensional vibration analysis employing the Rayleigh-Ritz procedure to yield an accurate solution. Dynamic behaviour of FGM shell structures subjected to time-varying excitation using a 3D-shell model based on a discrete double directors shell element was examined by Frikhaa et al. [30] using the Newmark method. Hajlaoui et al. [31] worked on the nonlinear dynamics analysis of FGM shell structures using a solid shell element with higher-order transverse shear stress based on the Enhanced Assumed Strain (EAS) formulation. The free vibration analysis of functionally graded carbon nanotubes-reinforced shell structures was predicted by Mellouli et al. [32] using the mesh-free radial point interpolation method (RPIM) and modified first-order shear deformation theory. Moita et al. [33] studied the axisymmetric free-vibration analysis of FGM plate-shell structures. The finite element model was formulated on the Kirchhoff-Love theory that includes the transverse shear deformations by introducing a penalty function to study both thin and thick axisymmetric plate/shells structures. Considerable literature [34-37] exists on the topic of general dynamic analysis of FGMs beam, plate and shell structures.

As a consequence of their outstanding features, FGMs have been extensively used as thermal barriers and protective coating in various applications, especially in the energy and aerospace engineering. In these applications, FGM plates/shells frequently subject to extreme static and dynamic loadings, which leads to vibratory responses of large amplitude. Therefore, in order to efficiently assess the transient response of FGM structures, a reliable nonlinear dynamic analysis of functionally graded plates and shells in thermal environments is highly required. Huang et al. [38] investigated the nonlinear transient response and vibration of FGM plates in thermal environments. Heat conduction and temperature-dependent material properties were considered. The formulations were based on the higher-order shear deformation plate theory and general von Kármán-type equation. Pradyumna et al. [39] analysed the nonlinear dynamic response of functionally graded shell panels in thermal environments having initial geometric imperfection. The material properties were assumed to be temperature-dependent. Aliaga et al. [40] examined the nonlinear static and dynamic thermo-elastic response of functionally graded plates using third-order shear deformation theory based on the von Kármán geometric nonlinearity. Newmark time integration scheme was used for direct time integration of the nonlinear algebraic equations.

Recent studies in the field of nonlinear dynamic analysis are focused on the dynamic-buckling and post-buckling behaviour of structures made of composite and advanced materials. In practice, the FGM structures, which have been developed to withstand thermal stresses in extremely high-temperature environments, are usually subjected to thermo-mechanical dynamic loading. The dynamic response of thin structural FGM shells may lead to the phenomenon of dynamic-buckling. Hence, the nonlinear dynamic behaviour and dynamic-buckling phenomena in thermal environment of such structures, in particular, cylindrical and spherical shells, must be considered during the design of FGM structures for their optimum design. As above mentioned, in addition to static analysis and thermal stress, the dynamic studies of FGM shell structures are mainly limited to linear transient and free-vibration response of beam, plate and shell structures. Works on nonlinear transient response of FGM plates in thermal environments have also reported in the literature. Static buckling analysis of stability for functionally graded plates under mechanical, thermal, thermo-mechanical and Thermo-Electro-Mechanical loads are being reported by several authors, see for instance [41-53]. However, As far as the authors know, works on the dynamic-buckling and post-buckling behaviour of functionally graded material cylindrical and spherical shells in thermal environments are meagre in the literature, moreover, nonlinear transient dynamic behaviour of shell structures with temperature dependent material properties have not yet presented in the literature. Therefore, as such studies are important to the structural designers.

A comprehensive survey for bending, buckling, and vibration analysis of plate and shell structures made of FGMs was presented by [54, 55]. Recently, [56] presented a review of the principal developments in FGMs that includes heat transfer issues, stress, stability and dynamic analyses, testing, manufacturing and design, applications, and fracture.

4. Effective properties of an FGM

The material properties of an FGMs plate/shell structures are assumed to change continuously through the thickness, according to the volume fraction of the metal and ceramic constituent materials. Hence, several models were proposed to define the variation of the volume fraction of each constituent material [57]. Three main functions are usually employed, which are: The power-law function (P-FGM), the exponential function (E-FGM) and Sigmoid function (S-FGM).

4.1. Power law function (P-FGM)

The power law function is quite a simple model that pertains to grading attributes of functionally graded shells through the thickness path from a bottom to the top surface. The variation in material properties of FGM along thickness direction is represented as [58]:

$$V_c(z) = \left(\frac{z}{h} + \frac{1}{2}\right)^n \tag{1.1}$$

Which, should add up to unity for all the constituents materials:

$$V_c + V_m = 1 \tag{1.2}$$

In which, the power-law index (n) is a non-negative real number, h is the shell thickness and z is the thickness direction coordinate ($-0.5h \le z \le 0.5h$). According to Eq. (1.1), when $n = 0$ a fully ceramic material is represented, though, when n approaches infinity a fully metallic structure is retrieved. Figure 1.5, illustrates the through-thickness volume fraction variation with the power-law index (n).

4.2. Sigmoidal law function (S-FGM)

Sigmoidal law function was first introduced by Chinese mathematician [59], by combining two power law functions. This law is used to mitigate stress intensity factor of fractured FGM. The sigmoidal function is also helpful to ensure the continuous distribution of stress at the junction of FGM having ceramic core surrounded by metal or vice versa. The variation of volume fraction of the constituents from upper to lower surfaces of FGM are given by:

For $0 \le z \le \frac{h}{2}$: $P(T,z) = (P_c - P_m)V_{c_1}(z) + P_m$ with $V_{c_1}(z) = 1 - \frac{1}{2}\left(1 - \frac{2z}{h}\right)^n$ (1.3)

For $-\frac{h}{2} \le z \le 0$: $P(T,z) = (P_c - P_m)V_{c_2}(z) + P_m$ with $V_{c_2}(z) = \frac{1}{2}\left(1 + \frac{2z}{h}\right)^n$ (1.4)

4.3. Exponential law function (E-FGM)

The exponential law (E-FGM) is basically used to deal with problems related to fracture mechanism of FGM. The effective material properties of FGM from given surface to any other point is shown as follows:

$$P(T,z) = Ae^{B(z+h/2)} \qquad \text{with} \qquad A = P_m \ , \quad B = \frac{1}{h}\ln\left(\frac{P_c}{P_m}\right) \tag{1.5}$$

In the present work, a simple power-law distribution function is adopted here to describe the volume fraction variation $V_c(z)$.

The through-thickness material properties of an FGM, such as elastic modulus E, Poisson's ratio ν, mass density ρ, thermal expansion coefficient α, and thermal conductivity K, can be stated as:

$$P(z) = (P_c - P_m)V_c(z) + P_m \tag{1.6}$$

Where, P_c and P_m denote the effective material properties of the ceramic and metal phases, respectively. Since the material properties of an FGM constituent experience significant changes with the temperature rise, the temperature-dependency of the constituent material properties is considered.

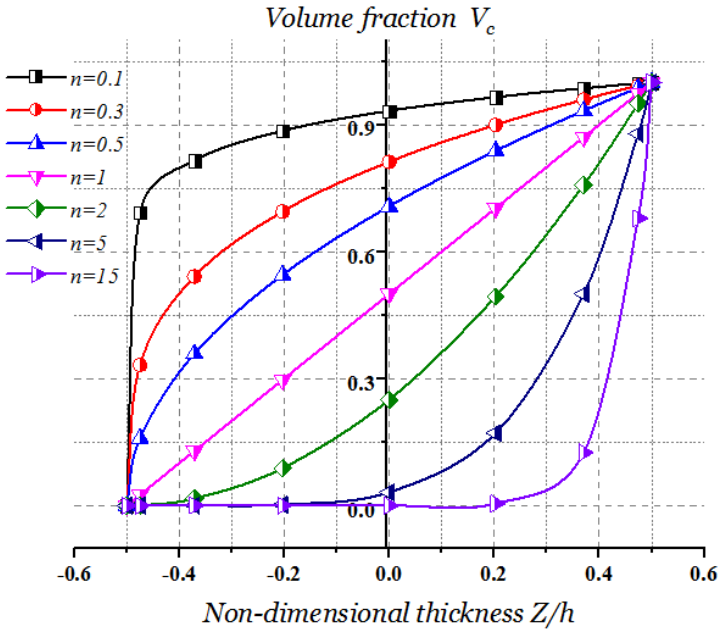

Fig. 1.5 Variation of the volume fraction versus the non-dimensional thickness.

In this study, the temperature variation is assumed to occur in the thickness direction only [60]. The temperature dependence of the mechanical and thermophysical properties of the metal or ceramic phases is given by:

$$P(T) = P_0\left(P_{-1}T^{-1} + 1 + P_1T + P_2T^2 + P_3T^3\right) \tag{1.7}$$

Where, T is the temperature (in Kelvin), P_0, P_{-1}, P_1, P_2 and P_3 are the coefficients of temperature, which are unique for each constituent. The temperature rise is expressed by $T = T_0 + \Delta T$, with T_0 denotes reference temperature at which there are no thermal strains (usually taken as 300 K), and ΔT denotes the temperature change.

Figures 1.6 and 1.7 show the variation of the Young's modulus E, thermal conductivity K, coefficient of thermal expansion α and Poisson's ration v for the constituent materials $ZrO_2 / Ti-6Al-4V$ and $Si_3N_4 / SUS304$ with temperature. These properties vary significantly with temperature.

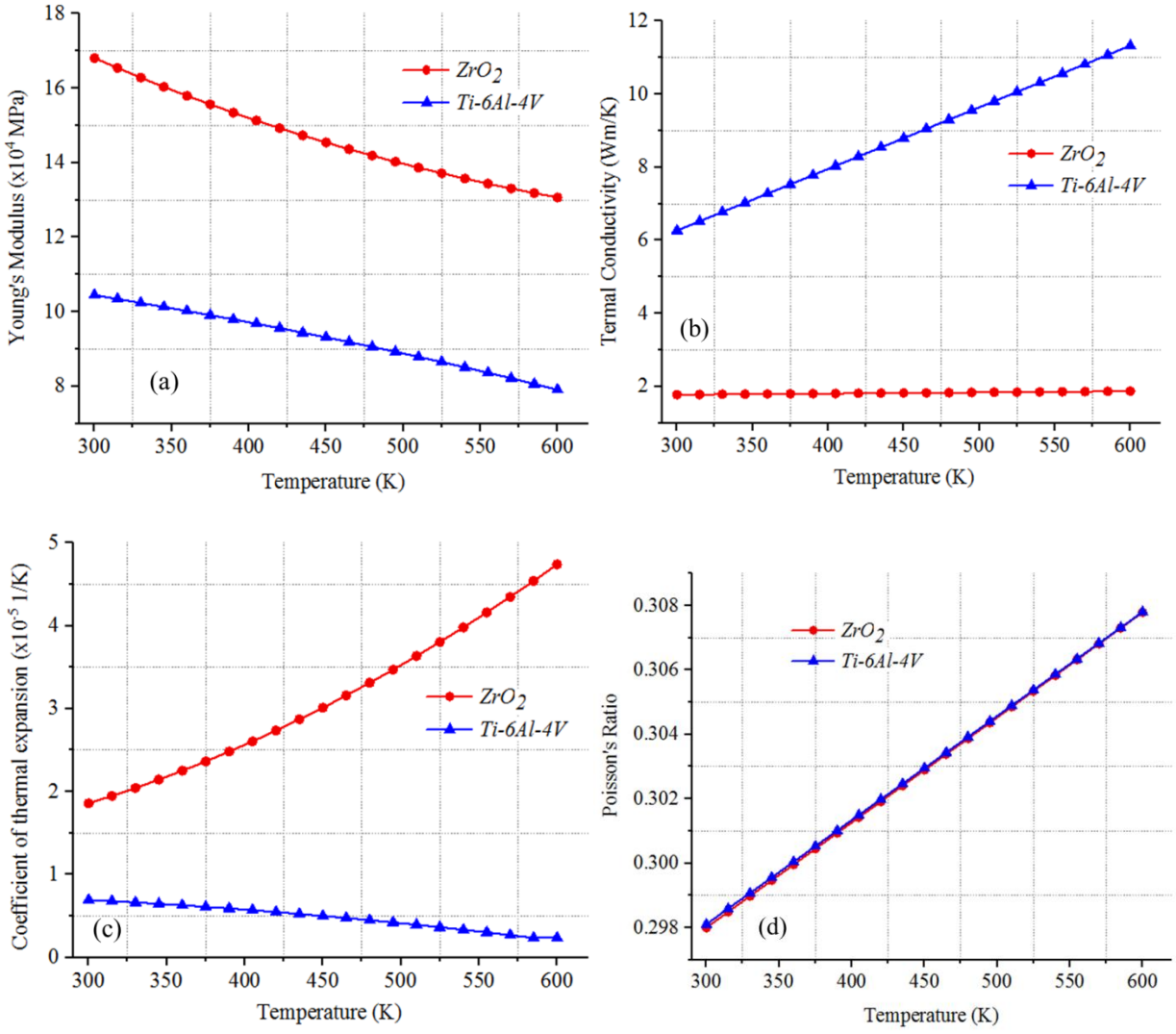

Fig. 1.6 Variation of material properties of $ZrO_2 / Ti-6Al-4V$ with temperature: (a) Young's modulus, (b) thermal conductivity, (c) coefficient of thermal expansion and (d) Poisson's ration.

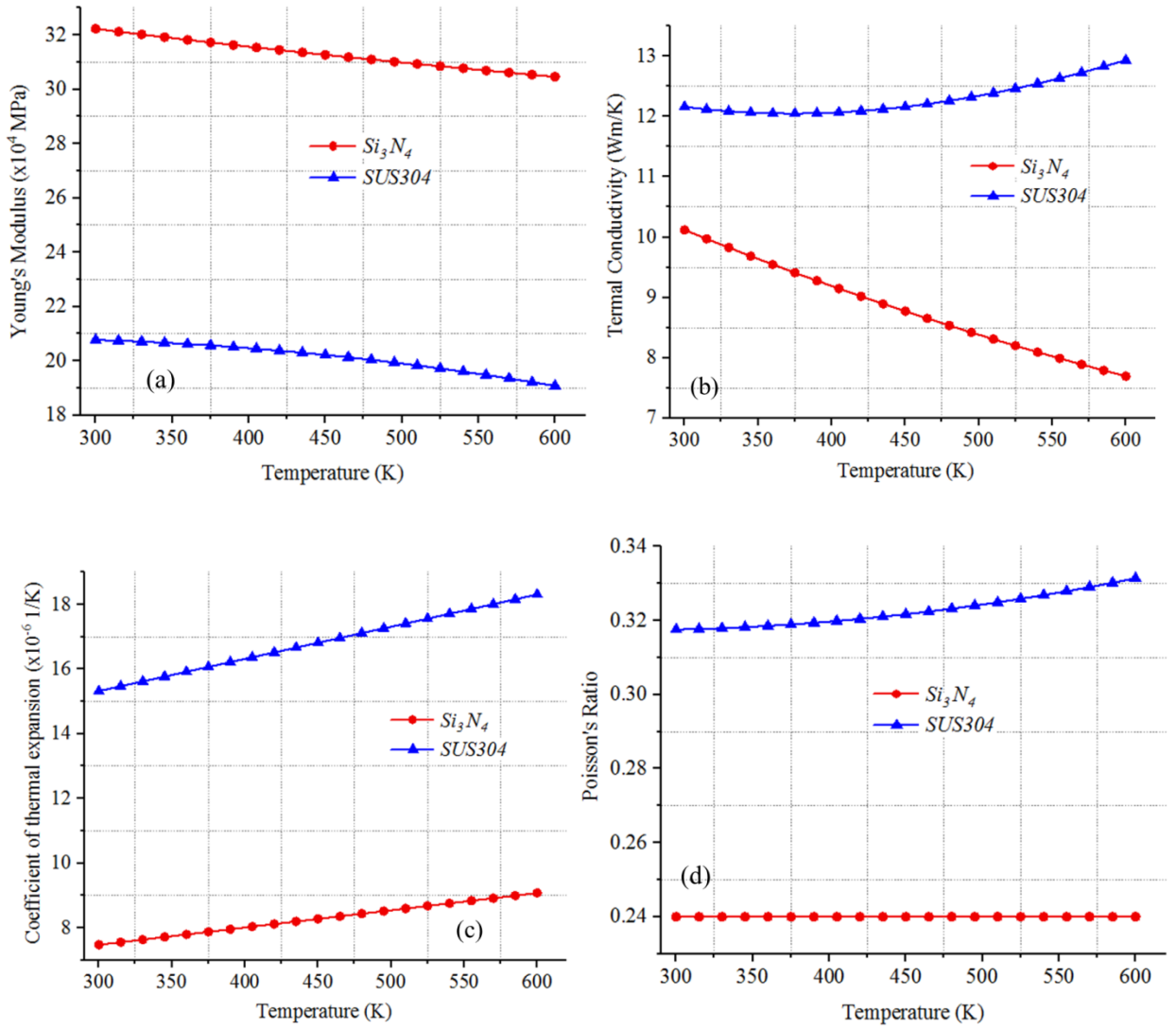

Fig. 1.7 Variation of material properties of Si_3N_4 / $SUS304$ with temperature: (a) Young's modulus, (b) thermal conductivity, (c) coefficient of thermal expansion and (d) Poisson's ration.

In order to accurately describe the effect of temperature rise across the thickness direction, the non-uniform temperature distribution is considered. The temperature distribution across the FGM shell thickness is obtained by solving the steady-state heat transfer equation and boundary conditions given by:

$$\frac{d}{dz}\left[K(z)\frac{dT}{dz}\right]=0,\quad T(z=h/2)=T_c,\quad T(z=-h/2)=T_m \tag{1.8}$$

Where $K(z)$ is the thermal conductivity. T_c and T_m denote the temperature of the ceramic-rich and metal-rich surfaces of the shell, respectively. The solution for Eq. (1.8) is given by:

$$T(z)=T_m+\Delta T\cdot\eta(z),\quad \Delta T=T_c-T_m,\quad \eta(z)=\left(\int_{-h/2}^{z}\frac{dz}{K(z)}\Big/\int_{-h/2}^{h/2}\frac{dz}{K(z)}\right) \tag{1.9}$$

In this work, integrals in Eq. (1.9), are evaluated using numerical integration. Figure 1.8, indicates the temperature distribution across the thickness of an Aluminum-Zirconia FGM plate for various values of the power low index (n).

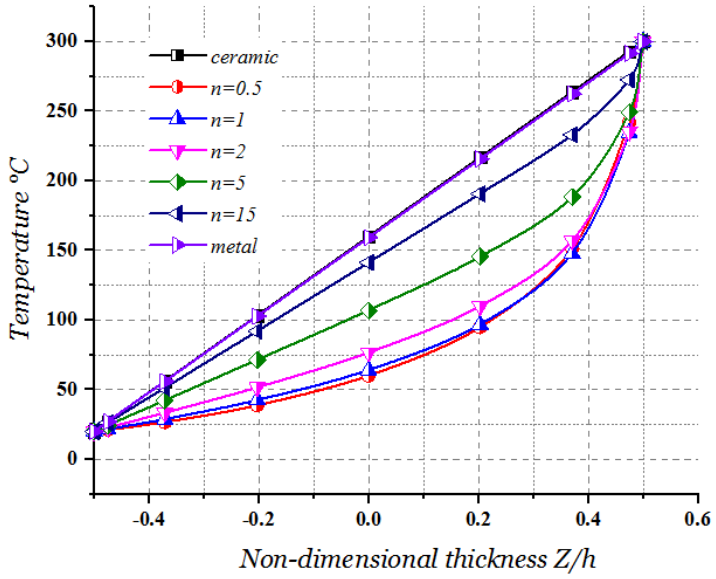

Fig. 1.8 Temperature distribution through the thickness Al/ZrO_2 FGM plate.

5. Conclusion

In this chapter, we have presented a general introduction on functionally graded materials, " the history of their development, their properties and fields of application". Then, literature review mainly deals with the work done on functionally graded plate-shell structures over the years, and finally, a brief representation that describe the effective properties of the materials. The spatial and gradual variation of the material properties makes it possible to create innovate structures that can be exploited in many areas of application in special structures in civil engineering.

6. References

[1] Shen HS. Functionally graded materials, Nonlinear analysis of plates and shells. Boca Raton, CRC Press, Taylor & Francis Group 2009; 1-3.

[2] Mahamood RM, Akinlabi ET. Functionally graded materials, Topics in mining, metallurgy and materials engineering. Springer International Publishing 2017; 1-5, doi: 10.1007/978-3-319-53756-6_1.

[3] Yin HM et al. Micromechanics-based elastic model for functionally graded materials with particle interactions. Acta Materialia 2004; 52(12):3535–3543.

[4] Reddy JN. Mechanics of laminated composite plates and shells. 2nd Edition, Boca Raton, FL: CRC Press, LLC 2004; 1-2.

[5] Genao FY, Kim J, Żur KK. Nonlinear finite element analysis of temperature-dependent functionally graded porous micro-plates under thermal and mechanical loads. Composite Structures 2021; 256:1-33.

[6] Moita JS, Correia VF, Soares CMM, Herskovis J. Higher-order finite element models for the static linear and nonlinear behaviour of functionally graded material plate-shell structures. Composite Structures 2019; 212:465-475.

[7] Mahapatra TR, Kar VR, Panda SK, Mehar K. Nonlinear thermoelastic deflection of temperature-dependent FGM curved shallow shell under nonlinear thermal loading. Journal of Thermal Stresses 2017; 40(9):1184-1199.

[8] Yamanoushi M et al. Proceedings of the first international symposium on functionally gradient materials. Japan, 1990.

[9] Koizumi M. The concept of FGM, ceramic transactions, functionally gradient materials. 1993; 34:3-10.

[10] Niino M et al. The functionally gradient materials. Journal of the Japan society for composite materials 1987; 13(1):257.

[11] Hirai T, Chen L. Recent and prospective development of functionally graded materials in Japan. Materials Science Forum 1999; 308–311:509–514.

[12] Chan S H. Performance and emissions characteristics of a partially insulated gasoline engine. International Journal of Thermal Science 2001; 40:255–261.

[13] Uemura S. The activities of FGM on new applications. Materials Science Forum 2003; 423–425:1-10.

[14] Hon D, Shiraishi W. Cellulose Chemistry; 2nd Edition, Marcel Dekker, New York 2001.

[15] Wang SS. Fracture mechanics for delamination problems in composite materials. J. Compos. Mater 1983; 17(3):210-223.

[16] Gupta A, Talha M. Recent development in modeling and analysis of functionally graded materials and structures. Progress in Aerospace Sciences 2015; 79:1-14.

[17] Müller E. et el. Functionally graded materials for sensor and energy applications. Materials Science and Engineering 2003; 17-39.

[18] Qiu J et al. Fabrication and high durability of functionally graded piezoelectric bending actuators. Smart Materials and Structures 2003; 12:115–121.

[19] Liu LS et al. The optimization design of metal = ceramic FGM armor with neural net and conjugate gradient method. Materials Science Forum 2003; 423–425:791–796.

[20] Jha D, Kant T, Singh R. A critical review of recent research on functionally graded plates. Composite Structures 2013; 96:833-849.
[21] Tornabene F, Viola E, Inman DJ. 2-D differential quadrature solution for vibration analysis of functionally graded conical, cylindrical shell and annular plate structures. Sound and Vibration 2009; 328(3):259-290.
[22] Yas MH, Shakeri M, Heshmati M, Mohammadi S. Layer-wise finite element analysis of functionally graded cylindrical shell under dynamic load. Mechanical Science and Technology 2011; 22:597-604.
[23] Jung WY, Han SC. Transient analysis of FGM and laminated composite structures using a refined 8-node ANS shell element. Composites: Part B 2014; 56:372-383.
[24] Tornabene F, Fantuzzi N, Bacciocchi M. Free vibrations of free-form doubly-curved shells made of functionally graded materials using higher-order equivalent single layer theories. Composites Part B: Engineering 2014; 67:490-509.
[25] Wali M, Hajlaoui A, Dammak F. Discrete double directors shell element for the functionally graded material shell structures analysis. Computer methods in applied mechanics and engineering 2014; 278:388-403.
[26] Asemi K, Salami SJ, Salehi M, Sadighi M. Dynamic and static analysis of FGM skew plates with 3D elasticity based graded finite element modeling. Latin American Journal of Solids and Structures 2014; 11(3):504–533.
[27] Mahmoudkhani S. Nonlinear vibration and mode shapes of FG cylindrical shells. Latin American Journal of Solids and Structures 2014; 14(3):422–440.
[28] Khan AA, Alam MN, Rahman NU, Wajid M. Finite element modelling for static and free vibration response of functionally graded beam. Latin American Journal of Solids and Structures 2016; 13(4):690–714.
[29] Jin G, Su Z, Ye T. A unified accurate solution for three-dimensional vibration analysis of functionally graded plates and cylindrical shells with general boundary conditions. Advances in Functionally Graded Materials and Structures 2016; 97-117.
[30] Frikhaa A, Wali M, Hajlaoui A, Dammak F. Dynamic response of functionally graded material shells with a discrete double directors shell element. Composite Structures 2016; 154:385-395.
[31] Hajlaoui A, Triki E, Frikha A, Wali M, Dammak F. Nonlinear dynamics analysis of FGM shell structures with a higher order shear strain enhanced solid-shell element. Latin American Journal of Solids and Structures 2017; 14(1):72–91.
[32] Mellouli H, Jrad H, Wali M, Dammak F. Free vibration analysis of FG-CNTRC shell structures using the meshfree radial point interpolation method. Computers and Mathematics with Applications 2020; 79(11):3160-3178.
[33] Moita JS, Araújo AL, Correia VF, Soares CMM. Vibrations of functionally graded material axisymmetric shells. Composite Structures 2020; 248.
[34] Hajlaoui A, Jarraya A, EL Bikri K, Dammak F. Buckling analysis of functionally graded materials structures with enhanced solid-shell elements and transverse shear correction. Composites Structures 2015; 132:87-97.
[35] Zghal S, Frikha A, Dammak F. Free vibration analysis of carbon nanotube-reinforced functionally graded composite shell structures. Applied Mathematical Modelling 2018; 53:132-155.
[36] Mallek H, Jrad H, Wali M, Kessentini A, Gamaoun F, Dammak F. Dynamic analysis of functionally graded carbon nanotube–reinforced shell structures with piezoelectric layers under

dynamic loads. Journal of Vibration and Control 2020; 26(13-14):1157-1172.
[37] Sahua NK, Biswal DK, Joseph SV, Mohanty CS. Vibration and damping analysis of doubly curved viscoelastic-FGM sandwich shell structures using FOSDT. Structures 2020; 26:24-38.
[38] Huang XL, Shen HS. Nonlinear vibration and dynamic response of functionally graded plates in thermal environments. International Journal of solids and structures 2004; 41(9-10):2403-2427.
[39] Pradyumna S, Nanda N. Geometrically nonlinear transient response of functionally graded shell panels with initial geometric imperfection. Mechanics of advanced materials and structures 2013; 20(3):217-226.
[40] Aliaga JW, Reddy JN. Nonlinear thermoelastic analysis of functionally graded plates using the third-order shear deformation theory. International journal of computational engineering science 2004; 5(4):753-779.
[41] Talha M, Singh BN. Thermo-mechanical buckling analysis of finite element modeled functionally graded ceramic-metal plates. International Journal of Applied Mechanics 2011;3(4):867-880.
[42] Tran LV, Thai CH, Nguyen-Xuan H. An isogeometric finite element formulation for thermal buckling analysis of functionally graded plates. Finite Elements in Analysis and Design 2013; 73:65-76.
[43] Bouguenina O, Belakhdar K, Tounsi A, Bedia EAA. Numerical analysis of FGM plates with variable thickness subjected to thermal buckling. Steel and Composite Structures 2015; 19(3):679-695.
[44] Hessameddin Y, Abdolhossein F, Mohammad KN, Soraya M. Thermal Buckling Analysis of Piezoelectric Functionally Graded Plates with Temperature-Dependent Properties. Mechanics of Advanced Materials and Structures 2015; 22(10): 864-875.
[45] Ahmad RK, Jabbari M, Eslami MR. Thermo-Electro-Mechanical Buckling of Shear Deformable Hybrid Circular Functionally Graded Material Plates. Mechanics of Advanced Materials and Structures 2015; 22(7): 578-590.
[46] Zhang Da-Guang. Thermal post-buckling analysis of functionally graded material elliptical plates based on high-order shear deformation theory. Mechanics of Advanced Materials and Structures 2017; 24(2):142-148.
[47] Kanishk S, Dinesh K. Nonlinear stability analysis of a perforated FGM plate under thermal load. Mechanics of Advanced Materials and Structures 2018; 25(2):100-114.
[48] Hirbod A, Amin Y. Thermal buckling analysis of moderately thick FGM plates based on the von Kármán nonlinearity and improved third order shear deformation theory. Journal of Thermal Stresses 2019; 42(11):1432-1446
[49] Singh SJ, Harsha SP. Buckling analysis of FGM plates under uniform, linear and non-linear in-plane loading. J Mech Sci Technol 2019; 33:1761-1767.
[50] Nguyen DK, Hoang TT, Nguyen DD. Nonlinear buckling and post-buckling of imperfect piezoelectric S-FGM circular cylindrical shells with metal–ceramic–metal layers in thermal environment using Reddy's third-order shear deformation shell theory. Mechanics of Advanced Materials and Structures 2019; 26(3):248-259.
[51] Zenkour AM, Radwan AF. Bending and buckling analysis of FGM plates resting on elastic foundations in hygrothermal environment. Archiv.Civ.Mech.Eng 2020; 20(112).
[52] Kumar R. Thermomechanically induced post-buckling analysis of functionally graded material plates with circular cut-outs resting on elastic foundations. J Thermoplastic Compos Mater 2020.
[53] Mojtaba F, Majid A, Erasmo C. Mechanical and thermal buckling loads of rectangular FG plates by using higher-order unified formulation. Mechanics of Advanced Materials and Structures 2021; 28(6):608-617.
[54] Shen HS. Bending, buckling and vibration of functionally graded plates and Shells. Advances in Mechanics 2004; 34:53–60.

[55] Zhang N et al. Functionally Graded Materials: An Overview of Stability, Buckling, and Free Vibration Analysis. Advances in Materials Science and Engineering 2019; 1-18.

[56] Birman V, Byrd LW. Modeling and analysis of functionally graded materials and structures. Applied Mechanics Reviews 2007; 60:195–216.

[57] Khan T, Zhang N, Akram A. State of the art review of functionally graded materials. International Conference on Computing, Mathematics and Engineering Technologies – iCoMET, 2019 **doi:** 10.1109/ICOMET.2019.8673489.

[58] Xuan HN, Tran LV, Thai CH, Thoi TN. Analysis of functionally graded plates by an efficient finite element method with node-based strain smoothing. Thin-Walled Structures 2012; 54:1-18.

[59] Chung YL, Chi SH. The residual stress of functionally graded materils. Journal of the Chinese Institute of Civil and Hydraulic Engineering. 2001; 13:1-9.

[60] Trabelsi S, Zghal S, Dammak F. Thermo-elastic buckling and post-buckling analysis of functionally graded thin plate and shell structures. J Braz. Soc. Mech. Sci. Eng. 2020; 42:1-22.

Chapter 2

Plates and shells theories

1. Introduction

Shell structures represent a particular type of structural components characterized by their curved geometry, being a three-dimensional solid whose thickness is much smaller than the other two dimensions. These elements are light weight constructions enclosing space using one or more curved surfaces. However, due to their shape, heavy loads can be sustained efficiently due to the membrane effect. The property of these elements , is that they are characterized by the stress resultants in the middle surface presenting in-plane components due to membrane behaviour and normal to the surface components due to bending behaviour. Therefore, thin shell structures, with their high mechanical performance, have been widely used in various fields of structural engineering such as " industrial, aerospace, automobiles, marine, and constructions that offer large internal space ". Thus, the capability of analysis and design of these structures, is pushed to discover more efficient and accurate solutions for economic and environmental issues.
Shell structures are becoming thinner lighter, and more flexible, so their deflections may have an important order of magnitude under either static or dynamic loads, which makes their behaviour often considered as geometrically nonlinear. The importance of performing a dynamic analysis of the shell structures, is so because often such structures are subjected to time varying loadings such as impact, explosion or seismic effects. The computational mechanics has now reached a level of maturity enabling complex simulations. However, one of the difficulties of nonlinear analysis is the fact that they are based on incremental iterative algorithms. Nevertheless, recent developments in computer technology and in computational mechanics, allow us to formulate computational models capable of delivering accurate results especially by means of the Finite Elements Method.
In this chapter we will form kinematic relation of different shell theories. These ones are established related to the mid-plane's displacement and rotations, including classical shell theory (CST), theory of first order shear strain (FSDT) and high order theories shear strain (HSDTs), since they have been widely used in shell modeling. In addition, a short presentation of the

different finite element approaches to generate shell elements is represented with focus on advantages, disadvantages, and disregarding the element formulation insights. Also, an extensive review of the literature related the development of degenerated shell element with emphasis on the work recently published. Finally, numerical integration method of the governing finite element equations derived in the next chapter is described.

2. An overview on shell theories

The specific geometry of this oriented structures encourage the use of particular kinematic instead of general kinematic of solid bodies. Shell theory is concerned with reducing the three dimensional stress problem of elasticity to two dimensions for that particular class of structures. For this purpose, governing equations are reduced, via imposing some hypothesis on the displacement field, to a set of bi-dimensional equations related to a reference surface commonly situated at mid-thickness so called the mid-surface. This objective may be realized if the deformations of any point in the shell can be uniquely described in terms of the displacements of the middle surface.

The reduction of the three dimensional problem requires the use of some kinematic assumptions, when employed together with the standard variational procedure lead to the two dimensional shell equations, which provide the basis for the finite element discretization.

2.1 Shell theories

Shell theories are commonly regarded as originating from one of three classes, classical theory, first-order shear deformation theory (FSDT) and higher-order theories. Within each class of shell theories several modified versions exist, developed to fulfill specific needs. Classical theory and first order shear deformation theory refer to the theories of Kirchhoff-Love and Mindlin-Reissner respectively. In the following each class of theories will be treated separately, emphasizing the assumptions made during the derivation of the theory and the implications of these assumptions. The development of these theories was motivated by the successful development of plate theory by [1]. This theory was based on the assumption that a normal to the undeformed mid-surface remains unstretched and normal to the deformed mid-surface.

2.1.1 Classical shell theory

The classical shell theory (CST) is based on the Kirchhoff-Love hypothesis for plates and shells, in which a linear distribution of displacements in the thickness direction [2, 3], that are an extension of the Euler-Bernoulli beam theory:

- Transverse normal to the mid-surface before deformation remain normal, straight and inextensible after deformation.
- Deformations due to transverse shear are neglected.
- Normal strains and stresses in the out-of plane direction are also considered negligible.

Thus, the deformation of the shell can be described fully from the deformation of the mid-surface whereby the theory is reduced to a two dimensional description. The displacement field of the classical theory is given as:

$$\begin{cases} u(\xi,\eta,\zeta) = u_0(\xi,\eta) - \zeta \dfrac{\partial w_0(\xi,\eta)}{\partial \xi} \\ v(\xi,\eta,\zeta) = v_0(\xi,\eta) - \zeta \dfrac{\partial w_0(\xi,\eta)}{\partial \eta} \\ w(\xi,\eta,\zeta) = w_0(\xi,\eta) \end{cases} \tag{2.1}$$

Where, u_0, v_0 and w_0 are displacements of a point on the mid-surface and ζ is the distance from the middle surface to the point considered. The displacement field in Eq. (2.1) is linear and rotations are only dependent on the transverse displacement, w_0. The displacements are represented in Figure 2.1, where the assumptions done can be observed.

One of the main advantages of the classical shell theory is its simplicity and that only depends on three variables. From the displacement field it is also obvious that the strains are functions of the second order derivative of w_0. Thus the displacement field is called C_1-continuous.

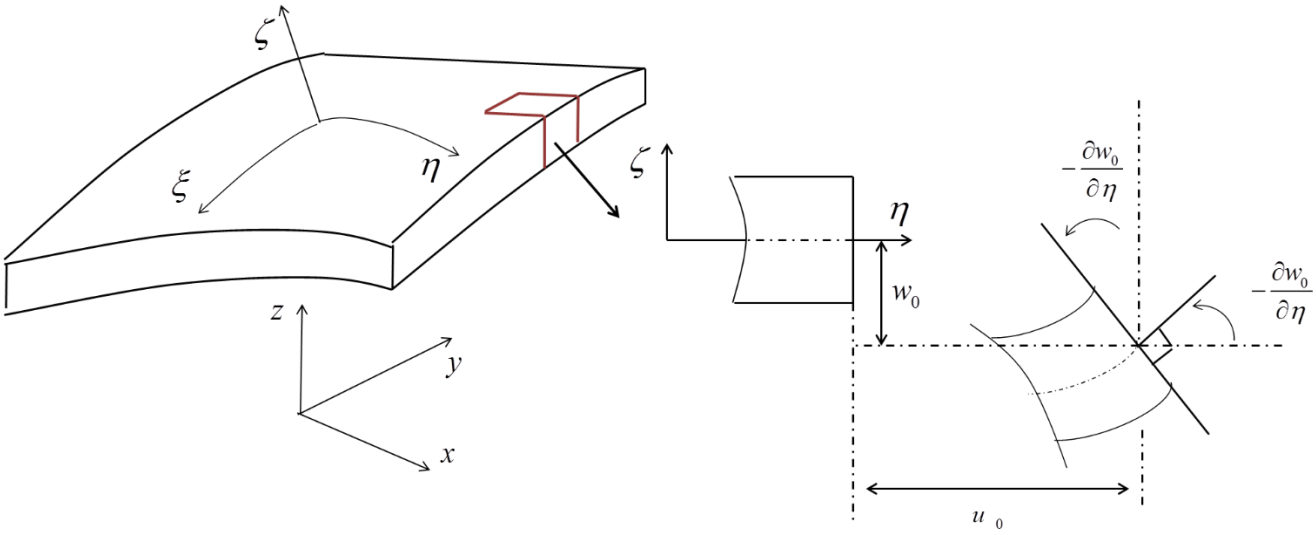

Fig. 2.1 Kirchhoff-Love assumptions represented in a deformed configuration.

The basic limitations of the classical shell theory are similar to the ones in the Euler-Bernoulli beam theory and therefore, the results are only accurate for low curvature and low thickness to in-plane dimension ratio. Regarding laminated plates/shells, the classical shell theory yields unsatisfactory results if the in-plane stiffness is significantly higher than the transverse stiffness because relatively high transverse shear strains can occur that are not accounted for in the Kirchhoff-Love assumptions.

2.1.2 Reissner-Mindlin (FSDT) shell theory

The first order shear deformation theory (FSDT) is an extension of the classical shell theory which includes some of the effects of the transverse strains neglected in CST [4, 5]. As the classical theory it disregards the effects of transverse normal strains but accounts for transverse shearing strains by allowing the normal to rotate:

- Transverse normal to the mid-surface before deformation remain inextensible after deformation.
- The transverse normal stress, $\boldsymbol{\sigma_{33}}$, is negligible.
- The transverse normal remains straight but not perpendicular to the mid-surface after having deformed.

The displacement field of the FSDT is given as in Figure 2.2:

$$\begin{cases} u(\xi,\eta,\zeta) = u_0(\xi,\eta) + \zeta \cdot \beta_\xi(\xi,\eta) \\ v(\xi,\eta,\zeta) = v_0(\xi,\eta) + \zeta \cdot \beta_\eta(\xi,\eta) \\ w(\xi,\eta,\zeta) = w_0(\xi,\eta) \end{cases} \tag{2.2}$$

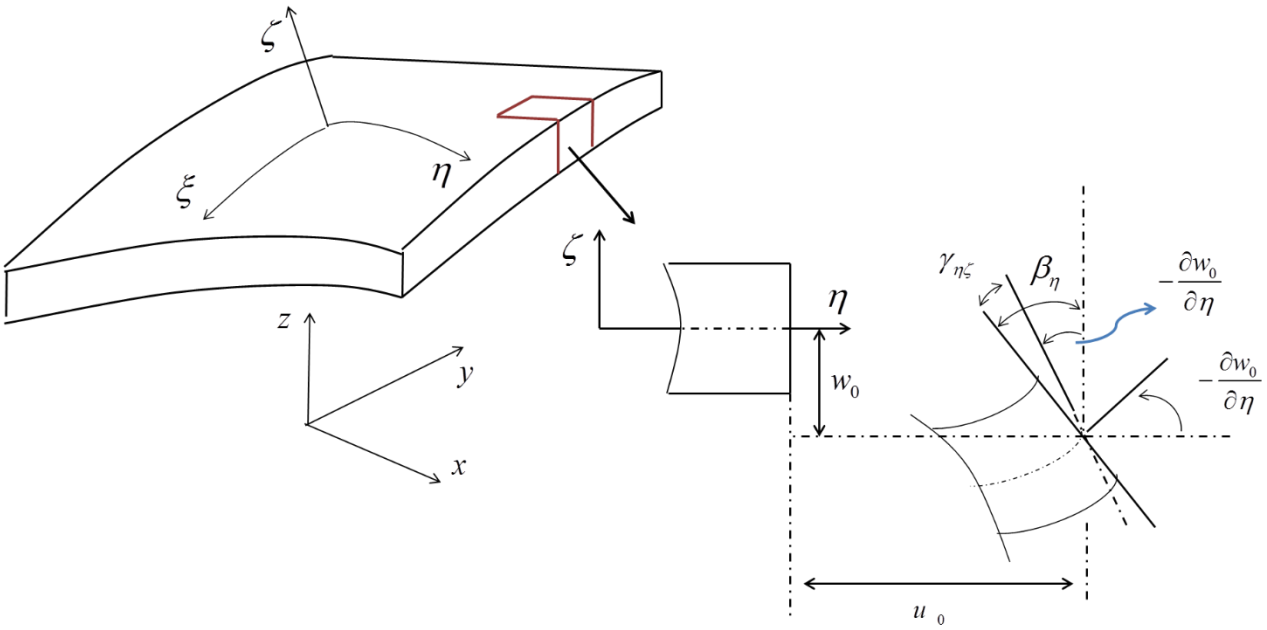

Fig. 2.2 Reissner-Mindlin assumptions represented in a deformed configuration.

Unlike the classical shell theory, the Mindlin-Reissner theory provides a good result for thin and moderately thick shells. The numerical codes that are formulated with this theory are simpler to implement because lower order derivatives are needed. Actually, the basic assumptions employed in the Mindlin-Reissner shell theory exclude the transverse normal deformation and thus they are restricted to small strain problems. From the computational point of view the main advantage compared with the Kirchhoff-Love type shell theory is the fact that only C° inter element continuity is required, which simplifies considerably the construction of finite elements.

2.1.3 Higher-order theory

Several contributors have proposed higher-order theories in order to overcome the limitations of the classical and first order shell/plate theories [6-13]. These higher-order theories are more

accurate than the first order theory. They are based on a nonlinear distribution through the thickness trying to represent the warping of transversal section in the deformed configuration. Figure 2.3.

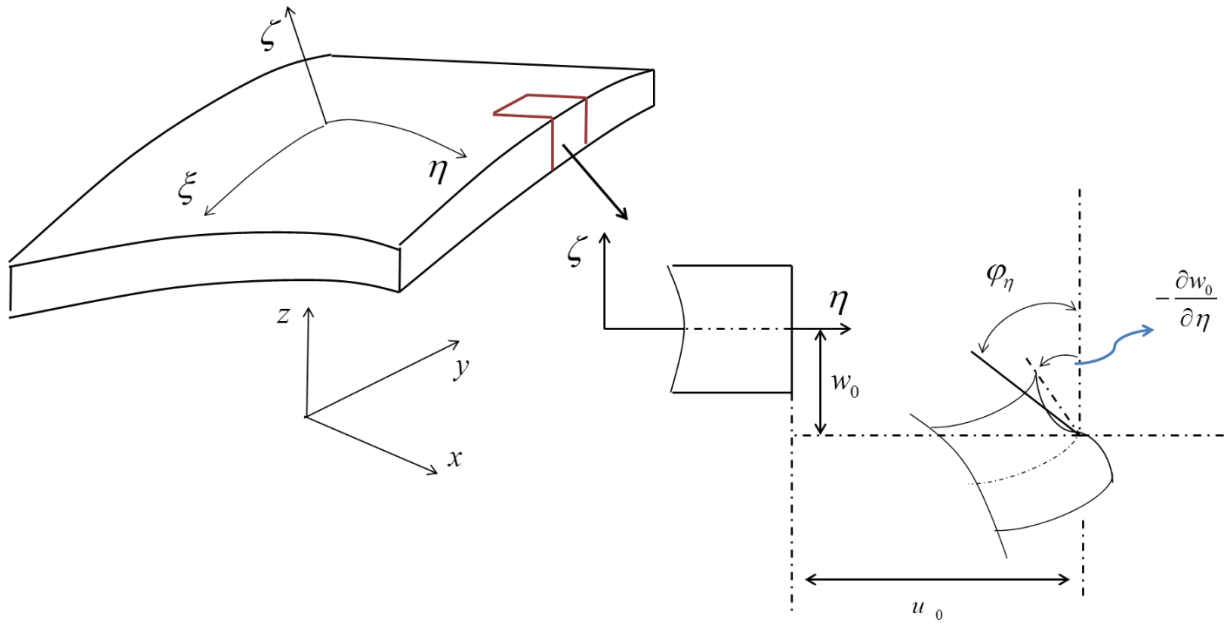

Fig. 2.3 Higher-order assumptions represented in a deformed configuration.

These higher-order theories described in the references are increasing the computational cost due to the increase in variables. Hence, the displacement field is generally written as follows:

$$\begin{cases} u(\xi,\eta,\zeta) = u_0(\xi,\eta) - \zeta \dfrac{\partial w_0(\xi,\eta)}{\partial \xi} + \psi(\zeta)\varphi_\xi(\xi,\eta) \\ v(\xi,\eta,\zeta) = v_0(\xi,\eta) - \zeta \dfrac{\partial w_0(\xi,\eta)}{\partial \eta} + \psi(\zeta)\varphi_\eta(\xi,\eta) \\ w(\xi,\eta,\zeta) = w_0(\xi,\eta) \end{cases} \tag{2.3}$$

Where, $\psi(\zeta)$ is a transverse shear function characterizing the theories corresponding. Actually, the displacements of the classical plate theory (CST) is obtained by taking $\psi(\zeta)=0$ while the first order theory (FSDT) can be obtained by $\psi(\zeta)=\zeta$.

(FSDT) remains the most widely used in engineering today for determining the gross behavior of structures in spite of its theoretical short comings.

3. Overview of shell finites elements

Curved shell structures constitute possibly the most difficult class of structures to analysis by the finite element method and the difficulties involved have lead to the development of considerable variety of approaches to the problems and a large number of element types. The following different approaches used to generate the shell elements.

3.1 Flat shell element

The geometry of these types of elements is assumed as flat. The curved geometry of shell is obtained by assembling number of flat shell elements. These elements are based on combination of membrane element and bending element that enforced Kirchhoff's hypothesis. It is important to note that the coupling of membrane and bending effects due to curvature of the shell is absent in the interior of the individual elements. Some of the major attractive features of these elements are:

- Simplicity of formulation.
- Capability of modelling rigid body motion without including strains.
- The use of these elements would still less expensive than using elements based on three dimensional continuum mechanics.

3.2 Curved shell element

Curved shell elements are symmetrical about an axis of rotation. As in case of axisymmetric plate elements, membrane forces for these elements are represented with respected to meridian direction as (u,N_z,M_θ) and in circumferential directions as (w,N_θ,M_z). However, the difficulties associated with these elements includes, difficulty in describing geometry and achieving inter-elemental compatibility. Also, the satisfaction of rigid body modes of behaviour is acute in curved shell elements.

3.3 Solid shell element

Though, use of 3D solid element is another option for analysis of shell structure, dealing with too many degrees of freedom makes it uneconomic in terms of computation time. Further, due to small thickness of shell element, the strain normal to the mid surface is associated with very large stiffness coefficients and thus makes the equations ill conditioned.

4. Shells degenerated from 3D solid elements

The appearance of the bi-dimensional shell element derived from a three- dimensional Iso-parametric element was by AHMAD [14,15]. This approach has the advantage of being independent of any particular shell theory and can be used to formulate a general shell element for geometric nonlinear dynamic analysis. Moderately thick shells can be analysed using such elements. However, selective and reduced integration techniques are necessary to use due to shear locking effects in case of thin shells. The assumptions for degenerated shell are similar to the Reissner-Mindlin assumptions.

The idea of the degeneration concept is to eliminate nodes from a solid element by imposing on it kinematic constraints and assumptions yield to shell surface element as shown in Figure 2.4. More details on the concept of degeneration procedure, can be found in chapter 3.

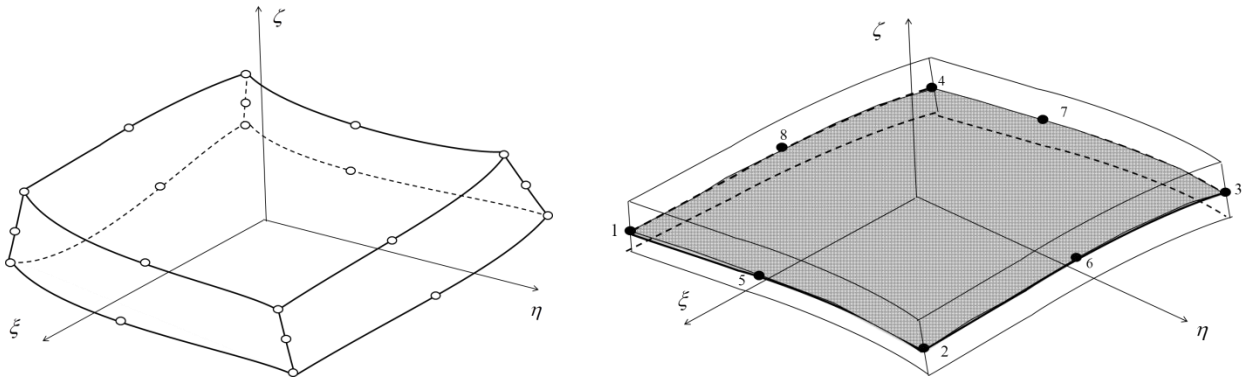

(a) 3D solid element (b) Degenerated shell element

Fig. 2.4 Degeneration of 3D element.

There is a large number of publication concerning degenerated shell element in the framework of linear, geometrically nonlinear and free vibration analyses. Bath [16] presented an insight of the formulation of a 4 and 8-node shell element using a mixed interpolation of tensorial components, for linear and nonlinear analysis in practical engineering environments.

Dvorkin and Bath [17] proposed a new 4-node quadrilateral shell element for general nonlinear geometric and material analysis. The element formulation was based on 3D continuum mechanics theory and applicable for both thin and thick shells. Swamy Naidu and Sateesh [18] developed a new 4-node bilinear degenerated shell element for analysis of shell structures. Assumed transverse shear and in-plane membrane strains, respectively were considered in the shell formulation to avoid the shear and membrane locking phenomenon. Norachan et al. [19] analysed plate and shell structures using 8-node degenerated thin-walled element based on the nonlinear co-rotational formulation in linear and geometrically nonlinear analysis. They also used the assumed natural strain (ANS) and enhanced assumed strain (EAS) to overcome locking problems. Jayasankar et al. [20] studied the free vibration behaviour of thick laminated composites shell structures using nine-node degenerated shell element, an enhanced interpolation of the transverse shear and membrane strains were introduced in the element formulation to produce shear and membrane locking free element. Tuan et al. [21] studied the free vibration analysis of stiffened laminated composite cylindrical shell using eight-noded Iso-parametric degenerated shell element based on Reissner-Mindlin assumptions which taking into account the shear deformation and rotatory effect. Patel et al. [22] performed static and dynamic instability of stiffened shell panels subjected to uniform in-plane harmonic edge loading using eight-noded degenerated shell element and a compatible three-noded curved beam was introduced to model the stiffeners. The method of Hill's infinite determinant was applied to analyse the dynamic instability regions. Lee and Han [23] investigated the free vibration analysis of plates and shells using nine-node degenerated shell element to determine the natural frequencies. The assumed natural strains were derived to alleviate the locking problems. Choi and Yoo [24] have developed an improved degenerated shell element for the analysis of the shell structures undergoing large deflection. In the formulation of the element stiffness, the combined use of three different techniques was made. They are: (1) an enhanced interpolation of transverse shear strains in the natural coordinate system to overcome the shear locking problem, (2) the reduced integration technique in in-plane strains to avoid the membrane locking behaviour, and (3) selective addition

of the nonconforming displacement modes to improve the element performances. This element was free of serious shear/membrane locking problems and undesirable compatible/commutable spurious kinematic deformation modes. Marinkovic et al. [25] offered a degenerated shell element and a simplified formulation that relies on small incremental steps for the geometrically nonlinear analysis of piezoelectric composite structures. Chen [26] used a four node quadrilateral degenerated shell element to create an elastoplastic incremental finite element computer code to simulate a circular rail drawing process of sheet metals. HosseiniKordkheili et al. [27] developed a degenerated shell element by using explicit hybrid stabilization method with a reduced order integration scheme to stabilize spurious zero energy modes from the sub-integration. This stabilization was achieved after employing appropriate contravariant higher order stress modes. The relevant finite element formulation of the piezolaminated nine nodded shell element was then derived to analyse smart structures behaviours. Lei et al. [28] developed a new isogeometric Reissner–Mindlin degenerated shell element for linear analysis. It is based on the mixed use of non-uniform rational basis spline and Lagrange basis functions in the same domain. The mid-surface of the shell was represented and discretized using non-uniform rational basis spline and the directors of the shell were discretized using Lagrange polynomials.

5. Numerical solution and obtainable results

The governing equations in the finite element method are given on integral form. Consequently, the tangent stiffness matrix, $\boldsymbol{K_T}$, the mass matrix, $\boldsymbol{M}$, and the nodal load vector $\boldsymbol{r}$ must be evaluated by integration. Thus, the integration is performed numerically.

5.1 Modified numerical integration

When full numerical integration is employed, curved degenerated shell elements might exhibit membrane/shear locking in curved/thin applications. Several techniques have been proposed to mitigate membrane and shear locking. The most commonly used are: the assumed natural strain (ANS) [29], the mixed interpolation of tensorial components (MITC) [30], and the reduced/selective integration. As our shell element is meant to nonlinear dynamic analysis, full numerical integration with ANS or MITC technics are avoided in the aim to save computational time. An efficient modified reduced (2x2) numerical integration scheme is used instead.

It is well-known that reduced/selective numerical integration produces a soft higher-order deformation modes, which increases numerical accuracy considerably as compared to full integration. However, reduced integration may possess zero energy hourglass modes. Nevertheless, a modified five-point reduced integration has been applied to membrane and shell elements successfully [31, 32].

The numerical approximation to the exact integral using the 5-point integration scheme is defined as follows:

$$I^* = w_0 \cdot f(0,0) + w_\alpha \cdot f(\pm\alpha, \pm\alpha), \quad w_\alpha = 1 - \left(\frac{w_0}{4}\right), \quad \alpha = \left(\frac{1}{3w_\alpha}\right)^{0.5} \tag{2.4}$$

Where, f is the function to be integrated, w_i is a weighting factor, and α indicates the location of integration points. The 5-point scheme converges to the 2 x 2 Gaussian scheme as $w_0 \to 0$. In this study, w_0 is taken as 0.01.

All components of the element stiffness matrix are evaluated using the modified 5-points reduced numerical integration scheme. This modified integration scheme provides a full rank stiffness matrix with no need for hourglass control, resulting in a highly efficient shell element.

6. Shear correction factor

It is well known that in the first-order shear deformation theory (FSDT), the shear distribution across the shell thickness is constant and require the introduction of shear correction factors. The computational algorithm (see Appendix *A*) for the transverse shear correction factors is presented [33, 34]. This algorithm is based on the static equilibrium and energy equivalence between the shear energy of the shell or plate and the energy from three-dimensional theory. Consider U_1 the transverse shear energy obtained for a three-dimensional stress distribution and U_2 the energy associated with the 2D shell model:

$$U_1 = \frac{1}{2}\int_{-h/2}^{h/2} \tau^T \cdot H_\tau^{-1} \cdot \tau \cdot dz \quad , \quad U_2 = \frac{1}{2} T^T \cdot H_c^{-1} \cdot T \tag{2.5}$$

Where, $\tau = \begin{bmatrix} \tau_{xz} & \tau_{yz} \end{bmatrix}^T$ is the transverse shear stress, $T = \begin{bmatrix} T_x & T_y \end{bmatrix}^T$ is the transverse shear forces and H_τ, H_c are the 2x2 reduced transverse local and global shear stiffness matrix respectively. H_c is to be calculated and for an FGM, H_τ is defined as:

$$H_\tau(z) = G(z)\begin{bmatrix} 1 & 0 \\ 0 & 1 \end{bmatrix} \quad , \quad G(z) = \frac{E(z)}{2(1+\nu(z))} \tag{2.6}$$

Where, $G(z)$ is the transverse shear modulus at location z. In the case of pure bending-shear behaviour, the in plane strain are:

$$\varepsilon = \left(F_{mf} + zF_f\right)M \tag{2.7}$$

Where, $M = \begin{bmatrix} M_x & M_y & M_{xy} \end{bmatrix}^T$ is the bending moments and

$$\begin{bmatrix} F_m & F_{mf} \\ F_{mf} & F_f \end{bmatrix} = \begin{bmatrix} H_m & H_{mf} \\ H_{mf} & H_f \end{bmatrix}^{-1} \quad , \quad \left(H_m, H_{mf}, H_f\right) = \int_{-h/2}^{h/2} \left(1, z, z^2\right) H(z)\, dz \tag{2.8}$$

Where, $H(z)$ is the 3x3 reduced in plane elasticity tensor which is given for an FGM as:

$$H(z) = \frac{E(z)}{1-\nu^2(z)}\begin{bmatrix} 1 & \nu(z) & 0 \\ \nu(z) & 1 & 0 \\ 0 & 0 & \dfrac{1-\nu(z)}{2} \end{bmatrix} \tag{2.9}$$

The following expression of the plane stresses:

$$\sigma_t(z) = H(z)\varepsilon = A(z)M \quad , \quad A(z) = H(z)\left(F_{mf} + zF_f\right) \tag{2.10}$$

The transverse shear stresses are derived classically from the homogeneous equilibrium equation which leads to:

$$\tau_{xz} = -\int_{-h/2}^{z} \left(\sigma_{xx,x} + \tau_{xy,y}\right) dz \quad , \quad \tau_{yz} = -\int_{-h/2}^{z} \left(\tau_{xy,x} + \sigma_{yy,y}\right) dz \tag{2.11}$$

The shear stresses are consequently given by:

$$\tau(z) = D_1(z)T + D_2(z)\lambda \tag{2.12}$$

Where, T , λ , $D_1(z)$ and $D_2(z)$ are given by:

$$T = \begin{bmatrix} T_x & T_y \end{bmatrix}^T = \begin{bmatrix} M_{x,x} + M_{xy,x} & M_{xy,x} + M_{y,y} \end{bmatrix}^T \tag{2.13}$$

$$\lambda = \begin{bmatrix} M_{x,x} - M_{xy,y} & M_{xy,x} - M_{y,y} & M_{y,x} & M_{x,y} \end{bmatrix}^T \tag{2.14}$$

$$D_1(z) = -\frac{1}{2}\int_{-h/2}^{z} \begin{bmatrix} A_{11} + A_{33} & A_{13} + A_{32} \\ A_{31} + A_{23} & A_{22} + A_{33} \end{bmatrix} dz \tag{2.15}$$

$$D_2(z) = -\frac{1}{2}\int_{-h/2}^{z} \begin{bmatrix} A_{11} - A_{33} & A_{13} - A_{32} & 2A_{12} & 2A_{31} \\ A_{31} - A_{23} & A_{33} - A_{22} & 2A_{32} & 2A_{21} \end{bmatrix} dz \tag{2.16}$$

With A_{ij} are the components of $A(z)$ Eq. (2.10). Hence the energy U_1, Eq. (2.5) becomes:

$$U_1 = \frac{1}{2}\begin{bmatrix} T \\ \lambda \end{bmatrix}^T \begin{bmatrix} F_{11} & F_{12} \\ F_{12}{}^T & F_{22} \end{bmatrix} \begin{bmatrix} T \\ \lambda \end{bmatrix} \tag{2.17}$$

With,

$$F_{ij} = \int_{-h/2}^{h/2} D_i{}^T H_\tau{}^{-1} D_j dz \quad i, j = 1, 2 \tag{2.18}$$

The energy equivalence between U_1 and U_2 allows us to write:

$$H_c = F_{11}{}^{-1} \tag{2.19}$$

The appropriate shear correction factors will then be obtained:

$$k_1 = (H_c)_{11} \Big/ \left(\overline{H}_c\right)_{11} \quad , \quad k_2 = (H_c)_{22} \Big/ \left(\overline{H}_c\right)_{22} \quad , \; k_{12} = (H_c)_{12} \Big/ \left(\overline{H}_c\right)_{12} \tag{2.20}$$

With, $\overline{H}_c = \int_{-h/2}^{h/2} H_\tau(z)dz$ (2.21)

For the case of homogenous isotropic material:

$$D_1(z) = -\frac{6}{h^3}\left(z^2 - \left(\frac{h}{2}\right)^2\right) I_2 \qquad F_{11} = \frac{6}{5h} H_\tau^{-1} \tag{2.22}$$

The correction factors are then:

$$k_1 = k_2 = 5/6 \quad k_{12} = 0 \tag{2.23}$$

7. Conclusion

A review of the various research carried out in the literature for stress, free vibration and geometrically nonlinear of plates/shells was presented. An effort has been made to include all major contributions in the area of current interest highlighting evidence the most relevant literature available for different elements. The use of 2D theoretical models which now seem to provide accuracy as good as 3D models should be pursued in the interest of computational cost and efficient analyses. In addition, modified reduced numerical evaluation of element matrices which results a great efficiency. Furthermore, A computational algorithm for the transverse shear correction factors is established.

8. References

[1] Kirchhoff G.Vor1esungen uber Hathematische Physik. Mechanik 1876; 1.

[2] Kirchhoff G. Uber das gleichgewicht und die bewegung einer elastischen scheibe. Journal fur reine und angewandte Mathematik 1850; 40:51-88.

[3] Love AEH. On the small vibrations and deformations of thin elastic shells, Phil. Trans. Roy. Sci. 1888; 179:491.

[4] Mindlin RD. Influence of rotatory inertia and shear on flexural motions of isotropic elastic plates. J. Appl. Mech. 1951; 18:31-38.

[5] Reissner E. The effect of transverse shear deformation on the bending of elastic plates. Journal of Applied Mechanics 1945; 12:69–76.

[6] Liberscu L. On the theory of anisotropic elastic shell and plates. Int. J. Solids. Struct. 1967; 3:53-68.

[7] Whitney JM. Shear correction factors for orthotropic laminates under static load. J. Appl. Mech. 1973; 40:302-304.
[8] Nelson RB, Lorch DR. A refined theory for laminated orthotropic plates. ASME J. Appl. Mech. 1974; 41:177-183.
[9] Reddy JN. A simple higher-order theory for laminated composite plates. J. Appl. Mech. 1984; 51: 745-752.
[10] Touratier M. An efficient standard plate theory. Engng. Sci 1991; 29(8): 901-916.
[11] Idlbi A, Karama M, Touratier M. Comparaison of various laminated plate theories. Composite Structures 1997; 37:173-784.
[12] Kant T, Swaminathan K. Analytical solutions for the static analysis of laminated composite and sandwich plates based on a higher order refined theory. Composite Structures 2002; 56:329-344.
[13] Swaminathan K, Ragounadin D. Analytical solutions using a higher-order refined theory for the static analysis of antisymmetric angle-ply composite and sandwich plates. Composite Structures 2004; 64: 405-417.
[14] Ahmad S. Curved finite element in the analysis of solid shells and plates structures. 1969 Ph.D Thesis, University of Wales, Swansea.
[15] Ahmad S, Irons BM, Zienkiewicz OC. Analysis of thick and thin shell structures by curved finite elements. Int. J. Num. Meth. Eng. 1970; 2:419-451.
[16] Bath KJ. A formulation of general shell elements-the use of mixed interpolation of tensorial components. International Journal for Numerical Methods in Engineering 1986; 22:697-722.
[17] Dvorkin EN, Bath KJ. A continuum mechanics based four-node shell element for general nonlinear analysis. Engineering Computations 1984; 1(1):77-88.
[18] Swamy Naidu NV, Sateesh B. Improved bilinear degenerated shell element. International Journal of computational methods 2015; 12(1):1-22.
[19] Norachan P, Suthasupradit S, Kim Ki-DU. A co-rotational 8-node degenerated thin-walled element with assumed natural strain and enhanced assumed strain. Finite Elements in Analysis and Design 2012; 50:70-85.
[20] Jayasankar S, Mahesh S, Narayanan S, Padmanabhan C. Dynamic analysis of layered composite shells using nine node degenerate shell elements. Journal of Sound and Vibration 2007; 299:1-11.
[21] Tuan TA, Quoc TH, Tu TM. Free vibration analysis of laminated stiffened cylindrical panels using finite element method. Journal of Science and Technology 2016; 54(5):771-784.
[22] Patel SN, Datta PK, Sheikh AH. Buckling and dynamic instability analysis of stiffened shell panels. Thin-Walled Structures 2006; 44:321-333.
[23] Lee SJ, Han SE. Free-vibration analysis of plates and shells with a nine-node assumed natural degenerated shell element. Journal of Sound and Vibration 2001; 241(4):605-633.
[24] Choi CK, Yoo SW. Geometrically nonlinear behaivor of an improved degenerated shell element. Korea Advanced Institute of Science and Technology 1991; 40(3):785-794.

[25] Marinkovic D, Koppe H, Gabbert U. Degenerated shell element for geometrically nonlinear analysis of thin-walled piezoelectric active structures. Institut fur Mechanik, Otto-von-Guericke-Universit at Magdeburg, Universitatsplatz 2, D-39106 Magdeburg, Germany 2008; 17:1-10.

[26] Chen TC. Degenerated shell element analysis of circular rail drawing of sheet metal. Department of Mechanical Engineering, National Chin-Yi University of Technology 2011; 15:360-364.

[27] HosseiniKordkheili SA, Salmani H, Afshari SSG. A stabilized piezolaminated nine-nodded shell element formulation for analyzing smart structures behaviors. Department of Aerospace Engineering, Sharif, University of Technology, Tehran, Iran 2015, 1-30.

[28] Lei Z, Gillot F, Jezequel L. An isogeometric Reissner-Mindlin shell element based on mixed grid. Advances in Mechanical Engineering 2018; 10(4):1-12.

[29] Park KC, Stanley GM. A curved C^0 shell element based on assumed natural-coordinate strains. Journal of Applied Mechanics 1986; 53(2):278-290.

[30] Dvorkin EN, Bath KJ. A continuum mechanics based four-node shell element for general non-linear analysis. Engineering Computations1984; 1(1):77-88.

[31] Boutagouga D. A new enhanced assumed strain quadrilateral membrane element with drilling degree of freedom and modified shape functions. Int. J. Numer. Meth. Engng 2017; 110(6):573-600.

[32] Groenwold AA, Stander N. An efficient 4-node 24 D.O.F thick shell finite element with 5-point quadrature. Engineering Computation 1995; 12(8):723-747.

[33] Hajlaoui et al. Buckling analysis of functionally graded materials structures with enhanced solid-shell elements and transverse shear correction. Composites Structures 2015; 132: 87-97.

[34] Nguyen T K et al. First-order shear deformation plate models for functionally graded materials. Composites Structures 2008; 83(1):25-36.

Chapter 3

Formulation of a nonlinear curved 8-node degenerated shell element in thermal environments

1. Introduction

In many engineering problems, the structural behaviour can be nonlinear. However, displacements may be so large that they can change the structure's shape, which can significantly change the stiffness and orientation of the structure. Besides, boundary conditions may change during loading. The nonlinearity structural behaviour can be either classified into geometrical nonlinear, in which the relation between strain-displacement becomes nonlinear due to the effect of large displacements and rotations on the global geometric configuration of the structure, material nonlinear and contacts nonlinear.

Structures that exhibit nonlinear behaviour are of special importance, and require special treatment. For instance, the initial state of stress commonly known as 'residual stresses' is important and requires special handling. Also, the structural behavior is remarkably non-proportional to the applied load and hence, the principle of superposition cannot be applied. Therefore, the sequence of application of loads (loading history) may be important. This is a reason for dividing loads into small increments in nonlinear FE analysis. As a consequence, nonlinear analysis is generally carried out using a method of incremental resolution. It is based upon the progressive increase of the applied forces, to obtain in an incremental way, the nonlinear response of the structure satisfying the equilibrium equations in successive discrete time increments. During each time step between time t and $t+\Delta t$, the configuration $C_{t+\Delta t}$ to be calculated, is obtained starting from the configuration C_t considered as known. Often, the analysis introduces a reference configuration, which is a particular known state of the structure at a time t_0. This known configuration is used as reference when describing the geometrical transformations undergone by the structure as it moves between two successive configurations.

In this chapter, the derivation of the degenerated curved shell element in the geometrically nonlinear formulation based on the total Lagrangian approach with regarding thermal

environment are described for analysis of shells of arbitrary shape. Curved shell element formulation is interesting both from the theoretical and practical points of view.

2. Geometrically nonlinear behaviour

In linear analysis, the change in geometry and spatial orientation of structures, are considered small enough that the change in its stiffness can be ignored. However, in large displacement analysis, the displacement induced deformations, could be a major source of nonlinearities. Structures undergoing large displacements due to load-induced deformations, can have significant changes in their overall configuration, which can cause the structure to respond nonlinearly in a stiffening and or a softening manner. In finite element analysis, the overall stiffness of a structure depends on the stiffness contribution of each of its finite elements. During large displacements, the nodal coordinates will change causing the elements to deform and to change their spatial orientations. Subsequently, the element stiffness contribution in the overall stiffness will also change.

There are two common formulations for the description of structural behavior [1,2]. A description of the solid body movement is called:

- Total Lagrangian Description (TLD): in which the initial un-deformed configuration is the reference geometry to which strains and stresses are referred. In this formulation, the strains are Green strains and the corresponding work-conjugate stresses are second Piola–Kirchhoff stresses.
- Updated Lagrangian Description (ULD): in which the reference system is the current configuration to which the strains (Almansi strains) and the corresponding stresses (Cauchy stresses, often termed true stresses) are referred.
- Co-rotational Lagrangian Description (CLD): if the reference configuration is replaced by a very close un-deformed configuration. This co-rotational un-deformed configuration is much easier to handle.

2.1 Total Lagrangian formulation

The 'TLD' uses the initial un-deformed configuration as a reference. In this formulation, all quantities "displacements, strains and stresses" that describe the response of the structure are expressed with respect to the initial un-deformed configuration. Consequently, to obtain the exact nonlinear solution, the nonlinear Green-Lagrange strain tensor must be complete "no terms neglected". The Green-Lagrange second order terms imply second derivatives of all the components of the displacement vector.

3. Measurement of strains and stresses

In nonlinear mechanics, the method of measuring strain and stress becomes more difficult. Many measures of strain and stress can be defined [3,4]. A stress definition must be energetically conjugate to the strain adopted, the integral of the product of the stress and the strain for a volume would correctly represent the deformation energy in the same volume. In geometrically nonlinear analysis, "Green-Lagrange and Cauchy strain tensors" with their conjugate stress "2nd Piola-Kirchhoff and Cauchy stress tensors" must be introduced.

4. Formulation of the degenerated shell element

General three-dimensional elasticity theory does not benefit from the simplifications intrinsic to shell theory, such as the inextensible straight normal and zero normal stress. These assumptions can be adequately introduced in the formulation of solid elements to yield the so-called "degenerated shell elements". Once again, the motivation for the development of a degenerated shell finite element is mainly due to the computational difficulties associated with three-dimensional models for thin plate and shell structures on the one hand, and complex mathematical hypotheses and expressions shell theories on the other hand. These complexities could be avoided by using a degenerate three-dimensional Iso-parametric solid element (reduced) to a surface shell element having only nodal variables of typical surface area. Curved shell element should be capable to model complex curved shell geometries and also account for both membrane and flexural effects [5]. The measure of the transverse shear deformation, is permitted since the mid-surface normal are not necessarily to be kept normal during deformation. Therefore, degenerated shell elements give good results for thick shells. Moreover, It should be

able to satisfy the rigid body and constant strain patch tests, be free of membrane and shear locking as well as of spurious internal mechanisms. Unfortunately, fully integrated stiffness matrix overestimates the stiffness of the shell as its thickness decreases "the shear-locking problem". The satisfaction of all these conditions is still a major and, to some extent, unsolved challenge.

In a degenerated shell model, the numbers of unknowns present are five per node (three mid-surface displacements and two director rotations). However, these elements can be considered as a generalization of Reissner-Mindlin shell theory regarding the non– orthogonal of the surface normal and, therefore, they suffer from transverse shear locking. In their curved shapes they can also suffer from membrane locking. Shear and membrane locking in degenerated shell elements can be eliminated by using selective/reduced integration or assumed strain fields [6]. The degenerated shell elements are in general cheap in computational cost due to the reduced number of DOF and using coarse mesh.

4.1 Basic concepts

In the formulation of degenerated shell element, a three-dimensional solid element is degenerated (reduced) to a shell element having only mid-surface nodal variables. The process of creating degenerated shell elements, consists to eliminate nodes by imposing different constraints on the behaviour of the element [7]. Figure 3.1 shows a 20-noded quadratic hexahedron and the corresponding degenerated shell element. The top, middle and bottom surfaces are curved whereas the transverse sections are limited by straight lines (fibres). The degeneration procedure implies the definition of a *reference surface* (generally coinciding with the shell middle surface) with respect to which all displacements of the shell points are defined. The displacement field is specified assuming that the fibres remain straight and inextensible after deformation [6]. In addition, the stress normal to the reference surface is ignored (plane stress condition). The first assumption introduces transverse shear deformation and it also allows using a C^0 continuous interpolation for all the kinematic variables (displacement and rotations). It is interesting that this formulation is identical to Reissner-Mindlin theory.

The reference surface is discretized into C^0 continuous curved shell elements with n nodes. Each node typically has five DOFs " three Cartesian displacements and two rotations defining the motion of the normal to the shell surface ".

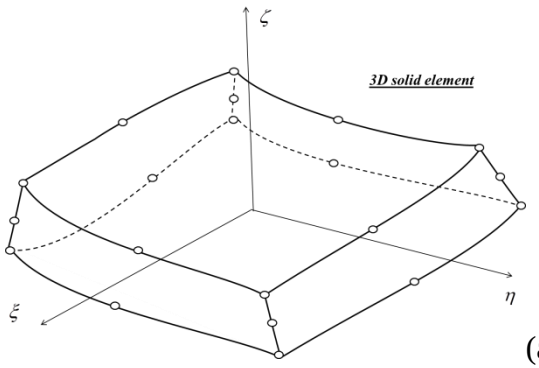

(a)

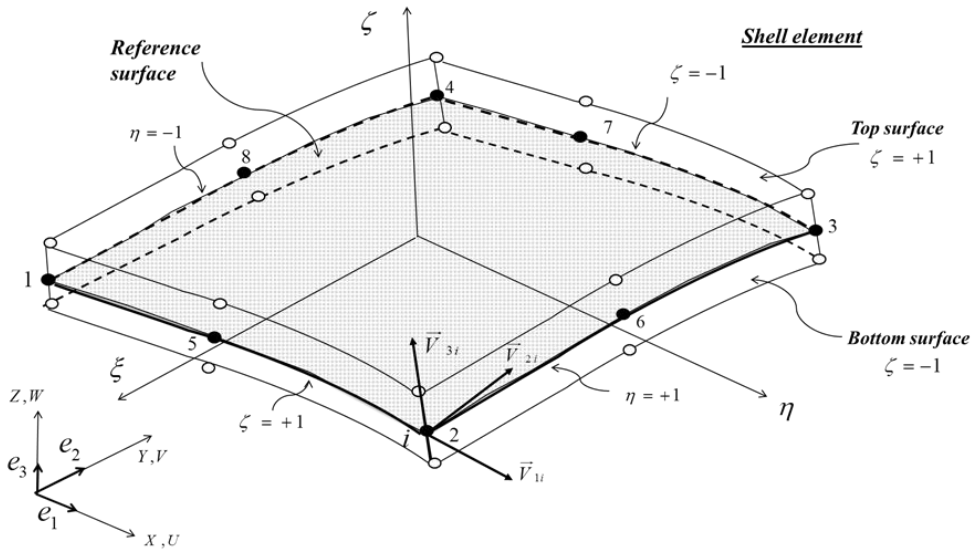

(b)

Fig. 3.1 Degeneration process of (a) 20-noded hexahedron into (b) a 8-noded degenerated shell element. Global, nodal and curvilinear coordinate systems.

Before proceeding any further, we will define the different coordinate systems necessary for the shell formulation.

5. Coordinate systems and bases

Different coordinate systems and space bases are needed in the formulation of the 8-node curved shell element, they are used to properly define the features that characterize the shell element and its enhancements. The relation within coordinate systems varies depending on which field is being transformed. When dealing with positions or displacements they can be graphically represented by a vector. Therefore, their expression in another coordinate system

requires the use of a rotation matrix. If we seek the relation between the strain or stress quantities in one coordinate system and the same quantity is expressed in another coordinate system, the transformation becomes more complex. In order to formulate the shell element of this work the following coordinate systems and bases are needed [8]:

- Cartesian 3D coordinate system. Global coordinate system $\{X,Y,Z\}$.
- Curvilinear coordinate system. Natural element mapping $\{\xi,\eta,\zeta\}$.
- Nodal coordinate system $\vec{v}_{1i},\vec{v}_{2i},\vec{v}_{3i}$.
- Covariant coordinate system (g_1,g_2,g_3).
- Local coordinate system x',y',z'.

Each of the previously listed coordinate systems has some properties that make them being defined in a specific manner and gives them useful features to be used while performing calculations on the finite element. These are described in the following subsections [6].

5.1 Cartesian 3D coordinate system

The geometry of the shell is defined with respect to a global Cartesian coordinate system X,Y,Z with associated unit vectors e_1,e_2,e_3, see Figure 3.1. This system defines the directions for the global displacements u,v,w associated with the axes X,Y,Z respectively.

5.2 Curvilinear coordinate system

A normalized curvilinear system ξ,η,ζ is defined such that ζ is a linear coordinate in the thickness direction at each point on the reference surface as defined in Figures 3.1 and 3.2. ζ takes the values $+1$ and -1 at the top and bottom surfaces, respectively and zero at the middle surface. The thickness direction at a point is obtained by standard interpolation of the nodal thickness (fibre) directions.

Clearly, the direction of ζ coincides with that of V_{3i} at each node. A thickness coordinate $\bar{z}$ in the direction of ζ is defined as:

$$\bar{z}_i = (\zeta - \zeta_0)\frac{h_i}{2} \tag{3.1}$$

Where, h_i is the shell thickness and ζ_0 is the value of ζ at the reference surface (ζ_0 = 0 if the reference surface coincides with the shell middle surface, as usually happens). Coordinate measures the distance of a point to the reference surface along the thickness direction.

Such reference system is defined by attaching the axes of coordinates to the middle point of both element edges. The transversal axis is defined as normal to the surface in the element centre (see Figure 3.3).

5.3 Nodal coordinate system

A Cartesian coordinate system formed by unit vectors $\vec{v}_{1i}, \vec{v}_{2i}, \vec{v}_{3i}$ is defined at each node on the reference surface (Figure 3.1). This system is used to define the nodal rotations. The fibre (or pseudo-normal) vector $\vec{v}_{3i}$ can be derived by the following way:

It is simpler to define V_{3i} as a vector in the normal direction at node *i* with a modulus equal to the shell thickness.

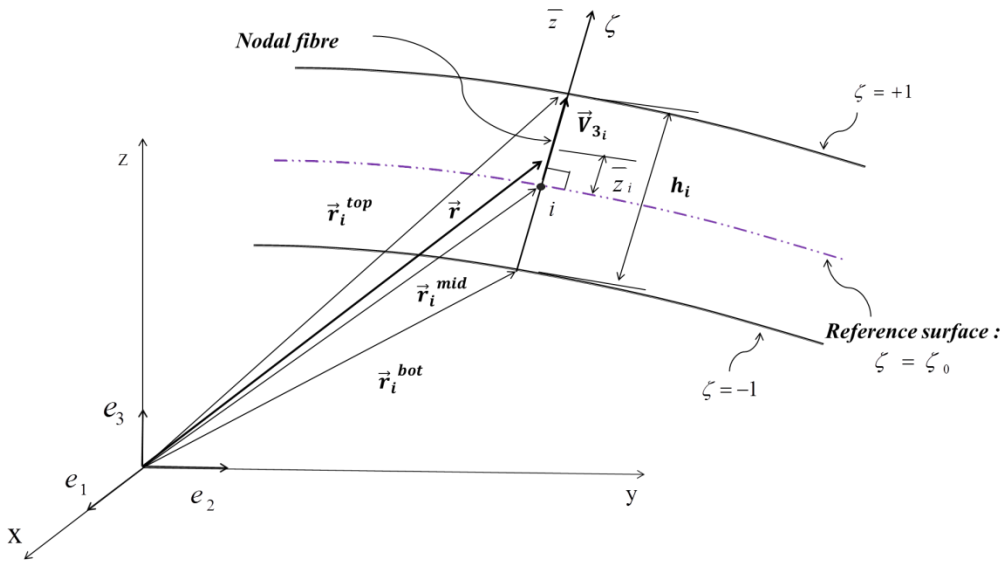

Fig. 3.2 Definition of the fibre vector V_{3i}.

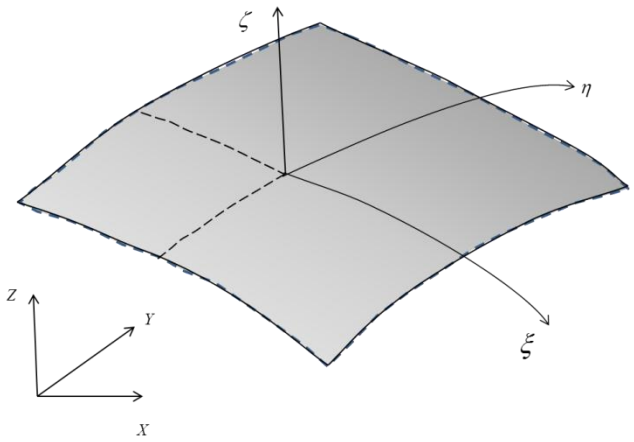

Fig. 3.3 Degenerated shell element with the global coordinates X, Y, Z and the convective curvilinear coordinates ξ, η, ζ.

The nodal normal vector at node (*i*) can be obtained by the cross product of two vectors that are tangent to the reference surface at (*i*):

$$V_{3i} = \sum_{j=1}^{n} \left(\frac{\partial N_j(\xi_i, \eta_i)}{\partial \xi} r_{0j} \wedge \frac{\partial N_j(\xi_i, \eta_i)}{\partial \eta} r_{0j} \right) \tag{3.2}$$

Where, $\boldsymbol{r}_{0j}$ defines the position vector of a point on the reference surface as shown in Figure 3.2 and $N_j(\xi_i, \eta_i)$ is the 2D shape function of node *j* (see Appendix *B*). Then, the director vector is given by: $\boldsymbol{v}_{3i} = \dfrac{\boldsymbol{V}_{3i}}{\|\boldsymbol{V}_{3i}\|}$.

5.4 Covariant coordinate system

Additional coordinate systems is usually defined for shell analysis (Figure 3.4). The *covariant* system g_1, g_2, g_3 where $g_1 = dr/d\xi$ and $g_2 = dr/d\eta$ are vectors tangent to the lines ξ = constant and η = constant, respectively and g_3 is the normal vector.

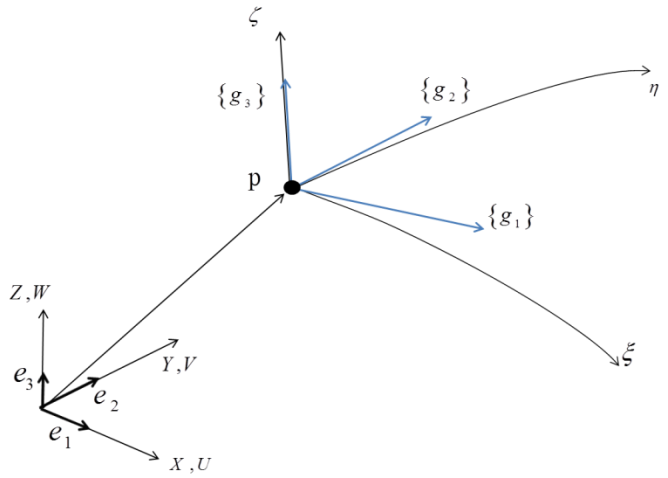

Fig. 3.4 Curvilinear coordinates ξ, η, ζ and its covariant base g_1, g_2, g_3 in the current configuration.

The covariant systems is used these coordinate systems to formulate curved shell elements such as the definition of the strain fields.

5.5 Local Coordinate System

A Cartesian coordinate system x', y', z' is chosen at each shell point defining the direction for the local displacement u', v', w' (Figure 1.5). The so called *lamina (or local) coordinate system* changes from point to point in the shell. The local system is used for defining and computing the local strain and stress fields.

The unit vectors associated to directions x', y', z' are l, m, n respectively. The normal vector z' is obtained as the cross product of two tangent vectors to the curves ξ = constant and η = constant at each point:

$$z' = \left\{\frac{\partial r}{\partial \xi}\right\} \wedge \left\{\frac{\partial r}{\partial \eta}\right\} \tag{3.3}$$

Where, $r = \{X, Y, Z\}^T$ is the position vector of a shell point (Figure 3.2).

The unit normal vector n is obtained as:

$$n = \frac{z'}{|z'|} \tag{3.4}$$

The direction of x' is taken as tangent to the curvilinear coordinate ξ = constant at each point, Thus:

$$x' = \left\{ \frac{\partial r}{\partial \xi} \right\} = \left\{ \frac{\partial X}{\partial \xi}, \frac{\partial Y}{\partial \xi}, \frac{\partial Z}{\partial \xi} \right\}^T \tag{3.5}$$

and the associated unit vector is $l = x' / |x'|$.

The unit vector m' associated to y' is obtained by the cross product of vectors n and l, $m = n \wedge l$.

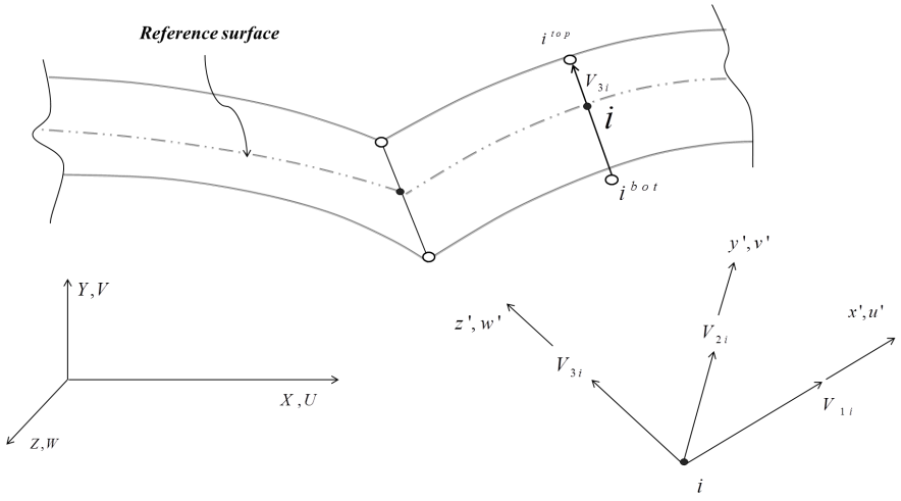

Fig. 3.5 Local and global coordinates.

6. Formulation of element matrices

In the following, the interpolation matrix N, the strain-displacement matrix B, and the tangent stiffness matrix K_T, are determined for the degenerated shell element.

6.1 Geometry and kinematics of shell

The position vector of an arbitrary point " p " within an element is determined by the Iso-parametric interpolation of the nodal coordinates as [9]:

$$r = \sum_{i=1}^{n} N_i(\xi,\eta) \frac{1+\zeta}{2} r_i^{top} + \sum_{i=1}^{n} N_i(\xi,\eta) \frac{1-\zeta}{2} r_i^{bot} \tag{3.6}$$

Where, r_i^{top} and r_i^{bot} are the position vectors for the top and bottom surfaces at each node *i*, see Figure 3.2. ζ defines the position of the point in the thickness direction and *n* is the number of

element nodes. The above expression can be rewritten in terms of a vector connecting the top and bottom points of shell as:

$$\begin{Bmatrix} x \\ y \\ z \end{Bmatrix} = \sum_{i=1}^{n} N_i(\xi,\eta) \left\{ \frac{1}{2} \left\{ \begin{Bmatrix} x_i \\ y_i \\ z_i \end{Bmatrix}_{top} + \begin{Bmatrix} x_i \\ y_i \\ z_i \end{Bmatrix}_{bottom} \right\} + \frac{\zeta}{2} \left\{ \begin{Bmatrix} x_i \\ y_i \\ z_i \end{Bmatrix}_{top} - \begin{Bmatrix} x_i \\ y_i \\ z_i \end{Bmatrix}_{bottom} \right\} \right\} \tag{3.7}$$

Or,

$$\begin{Bmatrix} x \\ y \\ z \end{Bmatrix} = \sum_{i=1}^{n} N_i(\xi,\eta) \left(\begin{Bmatrix} x_i \\ y_i \\ z_i \end{Bmatrix}_{mid} + \frac{1}{2}\zeta \mathrm{V}_{3i} \right) \tag{3.8}$$

Where,

$$\begin{Bmatrix} x_i \\ y_i \\ z_i \end{Bmatrix} = \frac{1}{2} \left(\begin{Bmatrix} x_i \\ y_i \\ z_i \end{Bmatrix}_{top} + \begin{Bmatrix} x_i \\ y_i \\ z_i \end{Bmatrix}_{bottom} \right) \quad \text{and} \quad \mathrm{V}_{3i} = \begin{Bmatrix} x_i \\ y_i \\ z_i \end{Bmatrix}_{top} - \begin{Bmatrix} x_i \\ y_i \\ z_i \end{Bmatrix}_{bottom} \tag{3.9}$$

For relatively thin shells, it is convenient to replace the vector V_{3i} by a unit vector v_{3i} in the direction normal to the mid-surface:

$$\begin{Bmatrix} x \\ y \\ z \end{Bmatrix} = \sum_{i=1}^{n} N_i(\xi,\eta) \left(\begin{Bmatrix} x_i \\ y_i \\ z_i \end{Bmatrix}_{mid} + \frac{1}{2}\zeta h_i v_{3i} \right) \tag{3.10}$$

Eq. (3.10) can be rewritten in standard formula as:

$${}^{t}x(\xi,\eta,\zeta) = \sum_{i=1}^{n} N_i(\xi,\eta)\,{}^{t}r_i + \frac{\zeta}{2} h_i \sum_{i=1}^{n} N_i(\xi,\eta)\,{}^{t}v_{3i} \tag{3.11}$$

Where ${}^{t}r_i$ denotes the Cartesian coordinates of nodal points at a time " t ", h_i is the shell thickness at node i and $v_{3i} = \begin{bmatrix} l_3 & m_3 & n_3 \end{bmatrix}$ where, l_{3i} , m_{3i} and n_{3i} are the unit vectors with respect to a global Cartesian coordinate system *X, Y, Z*.

Form Eq. (3.11), the global coordinate of an arbitrary point within an element at time " t " is determined by the interpolation of the global coordinates and the direction cosines of the normal vectors of all nodes of the element using shape functions by Eq. (3.11). Once the interpolation of

the position has been derived, the last step in order to obtain the kinematics of the degenerated element is to interpolate the nodal displacements. The displacement can be expressed as the difference between the position of the point after and before deformation, then using the geometry interpolation in Eq. (3.11), the displacement vector $\boldsymbol{u}$ from the initial configuration to the configuration at a time " t " is [10]:

$$\boldsymbol{u}(\xi,\eta,\zeta) = {}^{t}\boldsymbol{x}(\xi,\eta,\zeta) - {}^{0}\boldsymbol{x}(\xi,\eta,\zeta) \tag{3.12}$$

Where, the superscript ${}^{0}(.)$ and ${}^{t}(.)$ denotes, the initial configuration and the configuration at time " t " respectively. Substituting Eq. (3.11) in Eq. (3.12) yields:

$$\boldsymbol{u}(\xi,\eta,\zeta) = \sum_{i=1}^{n} N_i(\xi,\eta)u_i + \frac{\zeta}{2}h_i\sum_{i=1}^{n} N_i(\xi,\eta)\left({}^{t}\boldsymbol{v}_{3i} - {}^{0}\boldsymbol{v}_{3i}\right) \tag{3.13}$$

The next step is expressing the difference between the node directors in Eq. (3.13) in a more "useful" way for the analysis. In the above equation, two orthogonal unit vector ${}^{t}\boldsymbol{v}_{1i}$ and ${}^{t}\boldsymbol{v}_{2i}$ are introduced to express the director vector in terms of α_i and β_i, where, α_i and β_i are the incremental rotation angles of the director vector ${}^{t}\boldsymbol{v}_{3i}$ about the tangent vectors ${}^{t}\boldsymbol{v}_{1i}$ and ${}^{t}\boldsymbol{v}_{2i}$ respectively. Note that ${}^{t}\boldsymbol{v}_{1i}$ and ${}^{t}\boldsymbol{v}_{2i}$ are also orthogonal to ${}^{t}\boldsymbol{v}_{3i}$. Thus, the displacement becomes:

$${}^{t}\boldsymbol{v}_{3i} - {}^{0}\boldsymbol{v}_{3i} = -\alpha_i\,{}^{t}\boldsymbol{v}_{2i} + \beta_i\,{}^{t}\boldsymbol{v}_{1i} \tag{3.14}$$

By using the Eqs. (3.13) and (3.14), the incremental displacement vector of an arbitrary point " p " inside the element " e " can be found from the following relation:

$$\boldsymbol{u}(\xi,\eta,\zeta) = \sum_{i=1}^{n} N_i(\xi,\eta)u_i + \frac{\zeta}{2}h_i\sum_{i=1}^{n} N_i(\xi,\eta)\begin{bmatrix} -{}^{t}\boldsymbol{v}_{2i} & {}^{t}\boldsymbol{v}_{1i}\end{bmatrix}\begin{Bmatrix}\alpha_i\\ \beta_i\end{Bmatrix} \tag{3.15}$$

Hence, each node has three global displacements and two rotations about the local in-plane axis respectively $\hat{\boldsymbol{u}} = \begin{Bmatrix} u & v & w & \theta_x & \theta_y\end{Bmatrix}^{T}$. Form the displacement interpolation in Eq. (3.15), the interpolation matrix can be determined by collecting terms and forming a matrix equation as:

$$N = \left[\cdots \left| \begin{matrix} N_i & 0 & 0 & -N_i h_z l_2 & N_i h_z l_1 \\ 0 & N_i & 0 & -N_i h_z m_2 & N_i h_z m_1 \\ 0 & 0 & N_i & -N_i h_z n_2 & N_i h_z n_1 \end{matrix} \right| \cdots \right] \tag{3.16}$$

Where, $h_z = 1/2 \cdot h_i \cdot \zeta$.

The interpolation matrix is also used when the strain-displacement matrix is defined.

6.2 Strain-displacement matrix

To define strain, we first consider the concept of deformation since strain is the " change in displacement". The displacement from *0* to time *t* of a point " *P* " in a body is described by the displacement vector ***u***, defined naturally as the difference between the position vector ***v*** of point " *P* " at time *0* and time *t* respectively. $u = {}_t v - {}_0 v$ where we note that ${}_t v = {}_0 v + u$. In differential terms this may be expressed using the " change in displacement" analogy:

$$\varepsilon = \frac{\partial {}_t v}{\partial x} - \frac{\partial {}_0 v}{\partial x} = \frac{\partial u}{\partial x} \tag{3.17}$$

The strain expression in Eq. (3.17) is the normal strain definition (change in longitudinal displacement) and does not account for angular deformation, shearing strains. From a geometric consideration the shearing strain for the plane case can be shown to be:

$$\gamma_{12} = \frac{\partial u_2}{\partial x} + \frac{\partial u_1}{\partial y} \tag{3.18}$$

The out-of-plane shearing strains can also be defined naturally from this expression. Using Eqs. (3.17) and (3.18) we easily arrive at the well-known linear strain definition:

$$\varepsilon_{ij} = \frac{1}{2}\left(\frac{\partial u_j}{\partial x_i} + \frac{\partial u_i}{\partial x_j} \right) \tag{3.19}$$

The total strain definition containing both linear and non-linear terms can be expressed as:

$$\varepsilon_{ij} = \frac{1}{2}\left(\frac{\partial u}{\partial x_j} + \frac{\partial u}{\partial x_i} + \frac{\partial u}{\partial x_i}\frac{\partial u}{\partial x_j} \right) \tag{3.20}$$

In the formulation of shell elements, it is more convenient to use a local covariant base to express displacement and strain. The covariant base vectors of the shell's coordinate system are denoted as $\boldsymbol{g}_i$. They are obtained by partial derivatives of the position vectors with respect to convective coordinates:

$$ {}^{t}\boldsymbol{g}_i = \frac{\partial {}^{t}\boldsymbol{x}}{\partial \xi_i}, \quad {}^{0}\boldsymbol{g}_i = \frac{\partial {}^{0}\boldsymbol{x}}{\partial \xi_i} \tag{3.21} $$

In which $\xi_i = (\xi, \eta, \zeta)$ for (i = 1, 2, 3). Likewise, the contravariant base vectors are denoted as $\boldsymbol{g}^i$. They are defined by: $\boldsymbol{g}_i \cdot \boldsymbol{g}^j = \delta_{ij}$. In the global Cartesian coordinate system, the displacement vector $\boldsymbol{u}$ satisfies:

$$ {}^{t}\boldsymbol{g}_i = {}^{0}\boldsymbol{g}_i + \frac{\partial \boldsymbol{u}}{\partial \xi_i} \tag{3.22} $$

The Green-Lagrange strain in the configuration at time " t " with respect to the reference configuration, can be written in terms of the covariant components as:

$$ {}_{0}^{t}\tilde{\boldsymbol{\varepsilon}}_{ij} = \frac{1}{2}\left({}^{t}\boldsymbol{g}_i \cdot {}^{t}\boldsymbol{g}_j - {}^{0}\boldsymbol{g}_i \cdot {}^{0}\boldsymbol{g}_j \right) \tag{3.23} $$

The incremental covariant Green-Lagrange strain components are:

$$ {}_{0}\tilde{\boldsymbol{\varepsilon}}_{ij} = {}_{0}^{t+\Delta t}\tilde{\boldsymbol{\varepsilon}}_{ij} - {}_{0}^{t}\tilde{\boldsymbol{\varepsilon}}_{ij} = \frac{1}{2}\left(\frac{\partial \boldsymbol{u}}{\partial \xi_i} {}^{t}\boldsymbol{g}_j + {}^{t}\boldsymbol{g}_i \frac{\partial \boldsymbol{u}}{\partial \xi_j} + \frac{\partial \boldsymbol{u}}{\partial \xi_i} \frac{\partial \boldsymbol{u}}{\partial \xi_j} \right) \tag{3.24} $$

It is frequently used in finite element analysis to decompose the strains into linear and nonlinear parts as:

$$ {}_{0}\tilde{\boldsymbol{\varepsilon}}_{ij} = {}_{0}\tilde{\boldsymbol{e}}_{ij} + {}_{0}\tilde{\boldsymbol{\eta}}_{ij} \tag{3.25} $$

With, ${}_{0}\tilde{\boldsymbol{e}}_{ij} = \frac{1}{2}\left(\frac{\partial \boldsymbol{u}}{\partial \xi_i} {}^{t}\boldsymbol{g}_j + {}^{t}\boldsymbol{g}_i \frac{\partial \boldsymbol{u}}{\partial \xi_j} \right)$ stands for the linear part, while ${}_{0}\tilde{\boldsymbol{\eta}}_{ij} = \frac{1}{2}\left(\frac{\partial \boldsymbol{u}}{\partial \xi_i} \frac{\partial \boldsymbol{u}}{\partial \xi_j} \right)$ presents the nonlinear part.

Furthermore, Green–Lagrangian strain components in the global Cartesian system $\boldsymbol{\varepsilon}_{ij}$ can be expressed in terms of covariant Green–Lagrangian strain components $\tilde{\boldsymbol{\varepsilon}}_{ij}$ using the relation:

$$\boldsymbol{\varepsilon}_{ij}\boldsymbol{e}_i\boldsymbol{e}_j = \tilde{\boldsymbol{\varepsilon}}_{ij}\boldsymbol{g}^i\boldsymbol{g}^j \tag{3.26}$$

In which, $\boldsymbol{e}_i$ denotes Cartesian system base vectors, while $\boldsymbol{g}^i$ denotes the contravariant base vectors. Yet, the contravariant base vectors can be expressed in terms of the Cartesian system base vectors as: $\boldsymbol{g}^i = \boldsymbol{Q}_{ij}\boldsymbol{e}_j$.

Substituting in Eq. (3.26), we get:

$$\boldsymbol{\varepsilon}_{ij} = \boldsymbol{Q}^{ki}\boldsymbol{Q}^{lj}\tilde{\boldsymbol{\varepsilon}}_{kl} \tag{3.27}$$

With, $\boldsymbol{Q}_{ij} = \boldsymbol{g}^i\boldsymbol{e}_j$. Using Voight notation, Eq. (3.27) yields:

$$\boldsymbol{\varepsilon} = \boldsymbol{Q}\tilde{\boldsymbol{\varepsilon}} \tag{3.28}$$

With, $\boldsymbol{\varepsilon} = \{\varepsilon_{11} \quad \varepsilon_{22} \quad \varepsilon_{33} \quad \varepsilon_{12} \quad \varepsilon_{13} \quad \varepsilon_{23}\}^T$, $\tilde{\boldsymbol{\varepsilon}} = \{\tilde{\varepsilon}_{11} \quad \tilde{\varepsilon}_{22} \quad \tilde{\varepsilon}_{33} \quad \tilde{\varepsilon}_{12} \quad \tilde{\varepsilon}_{13} \quad \tilde{\varepsilon}_{23}\}^T$ and $\boldsymbol{Q}$ is the transformation matrix:

$$\boldsymbol{Q} = \left[\begin{array}{ccc:ccc} l_1^2 & m_1^2 & n_1^2 & l_1m_1 & m_1n_1 & n_1l_1 \\ l_2^2 & m_2^2 & n_2^2 & l_2m_2 & m_2n_2 & n_2l_2 \\ l_3^2 & m_3^2 & n_3^2 & l_3m_3 & m_3n_3 & n_3l_3 \\ \hdashline 2l_1l_2 & 2m_1m_2 & 2n_1n_2 & l_1m_2+l_2m_1 & m_1n_2+m_2n_1 & n_1l_2+n_2l_1 \\ 2l_2l_3 & 2m_2m_3 & 2n_2n_3 & l_2m_3+l_3m_2 & m_2n_3+m_3n_2 & n_2l_3+n_3l_2 \\ 2l_3l_1 & 2m_3m_1 & 2n_3n_1 & l_3m_1+l_1m_3 & m_3n_1+m_1n_3 & n_3l_1+n_1l_3 \end{array}\right] \tag{3.29}$$

Green–Lagrangian strain, in the global Cartesian system, can be written in terms of displacements as:

$$\tilde{\boldsymbol{\varepsilon}}_{ij} = \frac{1}{2}\left(\frac{\partial \boldsymbol{u}_i}{\partial \boldsymbol{x}_j} + \frac{\partial \boldsymbol{u}_j}{\partial \boldsymbol{x}_i} + \frac{\partial \boldsymbol{u}_k}{\partial \boldsymbol{x}_i}\frac{\partial \boldsymbol{u}_k}{\partial \boldsymbol{x}_j}\right) \tag{3.30}$$

The linear strain is written as:

$$\boldsymbol{e}_{ij} = \frac{1}{2}\left(\frac{\partial \boldsymbol{u}_i}{\partial \boldsymbol{x}_j} + \frac{\partial \boldsymbol{u}_j}{\partial \boldsymbol{x}_i} \right) \tag{3.31}$$

And the non-linear strain, in Cartesian coordinates, is:

$$\boldsymbol{\eta}_{ij} = \frac{1}{2}\left(\frac{\partial \boldsymbol{u}_k}{\partial \boldsymbol{x}_i} \frac{\partial \boldsymbol{u}_k}{\partial \boldsymbol{x}_j} \right) \tag{3.32}$$

By inserting the displacement interpolations in Eq. (3.31) it is possible to derive a discretized expression for the linear strains. However, since the displacements are derived with respect to the global coordinates and the displacement interpolations are functions of the natural coordinates. The global Cartesian derivatives of the vector $\boldsymbol{\varepsilon}$ are next expressed in terms of the curvilinear derivatives of the displacement by:

$$\begin{bmatrix} \frac{\partial u}{\partial x} & \frac{\partial v}{\partial x} & \frac{\partial w}{\partial x} \\ \frac{\partial u}{\partial y} & \frac{\partial v}{\partial y} & \frac{\partial w}{\partial y} \\ \frac{\partial u}{\partial z} & \frac{\partial v}{\partial z} & \frac{\partial w}{\partial z} \end{bmatrix} = J^{-1} \begin{bmatrix} \frac{\partial u}{\partial \xi} & \frac{\partial v}{\partial \xi} & \frac{\partial w}{\partial \xi} \\ \frac{\partial u}{\partial \eta} & \frac{\partial v}{\partial \eta} & \frac{\partial w}{\partial \eta} \\ \frac{\partial u}{\partial \zeta} & \frac{\partial v}{\partial \zeta} & \frac{\partial w}{\partial \zeta} \end{bmatrix} \tag{3.33}$$

Where, $\boldsymbol{J}$ is the Jacobian matrix formed as:

$$J = \begin{bmatrix} \frac{\partial x}{\partial \xi} & \frac{\partial y}{\partial \xi} & \frac{\partial z}{\partial \xi} \\ \frac{\partial x}{\partial \eta} & \frac{\partial y}{\partial \eta} & \frac{\partial z}{\partial \eta} \\ \frac{\partial x}{\partial \zeta} & \frac{\partial y}{\partial \zeta} & \frac{\partial z}{\partial \zeta} \end{bmatrix} \tag{3.34}$$

The derivatives of the displacement with respect to the natural coordinates can be determined directly from the displacement interpolation in Eq. (3.15) which yields the following relation:

$$\begin{cases} \dfrac{\partial u}{\partial \xi} = \left\{ \dfrac{\partial u}{\partial \xi}, \dfrac{\partial v}{\partial \xi}, \dfrac{\partial w}{\partial \xi} \right\}^T = \displaystyle\sum_{i=1}^{n} \frac{\partial N_i}{\partial \xi} \left[I, \bar{z}_i A_i \right] \{\hat{\boldsymbol{u}}\}^e \\ \dfrac{\partial u}{\partial \eta} = \left\{ \dfrac{\partial u}{\partial \eta}, \dfrac{\partial v}{\partial \eta}, \dfrac{\partial w}{\partial \eta} \right\}^T = \displaystyle\sum_{i=1}^{n} \frac{\partial N_i}{\partial \eta} \left[I, \bar{z}_i A_i \right] \{\hat{\boldsymbol{u}}\}^e \\ \dfrac{\partial u}{\partial \zeta} = \left\{ \dfrac{\partial u}{\partial \zeta}, \dfrac{\partial v}{\partial \zeta}, \dfrac{\partial w}{\partial \zeta} \right\}^T = \displaystyle\sum_{i=1}^{n} N_i \left[0, \frac{h_i}{2} A_i \right] \{\hat{\boldsymbol{u}}\}^e \end{cases} \tag{3.35}$$

Where, $\hat{\boldsymbol{u}} = \{u \quad v \quad w \quad \theta_x \quad \theta_y\}^T$ stands for the vector of nodal degrees of freedom, I is unit matrix, $A_i = [-v_{2i} \quad v_{1i}]$ and $\bar{z}_i = \zeta h_i / 2$.

Proceeding the process and computing the terms in $\boldsymbol{J}$ matrix in Eq. (3.34) from Eq. (3.11) as:

$$\begin{cases} \dfrac{\partial r}{\partial \zeta} = \left\{ \dfrac{\partial x}{\partial \xi}, \dfrac{\partial y}{\partial \xi}, \dfrac{\partial z}{\partial \xi} \right\}^T = \displaystyle\sum_{i=1}^{n} \frac{\partial N_i}{\partial \xi} \left[r_i + \bar{z}_i v_{3i} \right] \\ \dfrac{\partial r}{\partial \eta} = \left\{ \dfrac{\partial x}{\partial \eta}, \dfrac{\partial y}{\partial \eta}, \dfrac{\partial z}{\partial \eta} \right\}^T = \displaystyle\sum_{i=1}^{n} \frac{\partial N_i}{\partial \eta} \left[r_i + \bar{z}_i v_{3i} \right] \\ \dfrac{\partial r}{\partial \zeta} = \left\{ \dfrac{\partial x}{\partial \zeta}, \dfrac{\partial y}{\partial \zeta}, \dfrac{\partial z}{\partial \zeta} \right\}^T = \displaystyle\sum_{i=1}^{n} N_i \frac{h_i}{2} v_{3i} \end{cases} \tag{3.36}$$

In which $r_i = [x_i, y_i, z_i]$.

The derivatives of the displacements with respect to the global coordinate can be found. Practically, this is done by multiplying the inverse Jacobian matrix with the derivative of the displacements in (3.35). Thereby an expression for the derivatives of the displacements with respect to the global coordinates is obtained:

$$\frac{\partial u}{\partial x} = \left(j_{11}^{-1} \sum_{i=1}^{n} \frac{\partial N_i}{\partial \xi} + j_{12}^{-1} \sum_{i=1}^{n} \frac{\partial N_i}{\partial \eta} \right) u_i + \left[R + j_{13}^{-1} \sum_{i=1}^{n} N_i \frac{h_i}{2} \right] l_{1i} \theta_{yi} - \left[R + j_{13}^{-1} \sum_{i=1}^{n} N_i \frac{h_i}{2} \right] l_{2i} \theta_{xi} \tag{3.37}$$

Where, $R = \left(j_{11}^{-1} \sum_{i=1}^{n} \frac{\partial N_i}{\partial \xi} + j_{12}^{-1} \sum_{i=1}^{n} \frac{\partial N_i}{\partial \eta} \right) \bar{z}_i$ and j_{ij}^{-1} is the element *ij* of the inverse of the Jacobian $\boldsymbol{J}$.

Performing similarly for all the derivatives of the displacements with respect to the global coordinates yield to the global strain vector in terms of global displacements well-defined as:

$$
\begin{cases}
\varepsilon_{11} = \sum_{i=1}^{n} \dfrac{\partial N_i}{\partial x} u_i - \dfrac{\partial g}{\partial x} l_{2i}\theta_{xi} + \dfrac{\partial g}{\partial x} l_{1i}\theta_{yi} \\
\varepsilon_{22} = \sum_{i=1}^{n} \dfrac{\partial N_i}{\partial y} v_i - \dfrac{\partial g}{\partial y} m_{2i}\theta_{xi} + \dfrac{\partial g}{\partial y} m_{1i}\theta_{yi} \\
\varepsilon_{33} = \sum_{i=1}^{n} \dfrac{\partial N_i}{\partial z} w_i - \dfrac{\partial g}{\partial z} n_{2i}\theta_{xi} + \dfrac{\partial g}{\partial z} n_{1i}\theta_{yi} \\
\gamma_{12} = \dfrac{\partial u}{\partial y} + \dfrac{\partial v}{\partial x} = \sum_{i=1}^{n} \dfrac{\partial N_i}{\partial x} v_i - \dfrac{\partial g}{\partial x} m_{2i}\theta_{xi} + \dfrac{\partial g}{\partial x} m_{1i}\theta_{yi} + \sum_{i=1}^{n} \dfrac{\partial N_i}{\partial y} u_i + \dfrac{\partial g}{\partial y} l_{1i}\theta_{yi} - \dfrac{\partial g}{\partial y} l_{2i}\theta_{xi} \\
\gamma_{23} = \dfrac{\partial w}{\partial y} + \dfrac{\partial v}{\partial z} = \sum_{i=1}^{n} \dfrac{\partial N_i}{\partial y} w_i + \dfrac{\partial g}{\partial y} n_{1i}\theta_{yi} - \dfrac{\partial g}{\partial y} n_{2i}\theta_{xi} + \sum_{i=1}^{n} \dfrac{\partial N_i}{\partial z} v_i - \dfrac{\partial g}{\partial z} m_{2i}\theta_{xi} + \dfrac{\partial g}{\partial z} m_{1i}\theta_{yi} \\
\gamma_{13} = \dfrac{\partial w}{\partial x} + \dfrac{\partial u}{\partial z} = \sum_{i=1}^{n} \dfrac{\partial N_i}{\partial x} w_i + \dfrac{\partial g}{\partial x} n_{1i}\theta_{yi} - \dfrac{\partial g}{\partial x} n_{2i}\theta_{xi} + \sum_{i=1}^{n} \dfrac{\partial N_i}{\partial z} u_i + \dfrac{\partial g}{\partial z} l_{1i}\theta_{yi} - \dfrac{\partial g}{\partial z} l_{2i}\theta_{xi}
\end{cases}
\tag{3.38}
$$

Where,

$$
\begin{cases}
\dfrac{\partial g}{\partial x} = \left[\sum_{i=1}^{n} \dfrac{\partial N_i}{\partial x} \bar{z}_i + \sum_{i=1}^{n} N_i \dfrac{\partial \bar{z}_i}{\partial x} \right] \\
\dfrac{\partial g}{\partial y} = \left[\sum_{i=1}^{n} \dfrac{\partial N_i}{\partial y} \bar{z}_i + \sum_{i=1}^{n} N_i \dfrac{\partial \bar{z}_i}{\partial y} \right] \\
\dfrac{\partial g}{\partial z} = \left[\sum_{i=1}^{n} \dfrac{\partial N_i}{\partial z} \bar{z}_i + \sum_{i=1}^{n} N_i \dfrac{\partial \bar{z}_i}{\partial z} \right]
\end{cases}
\tag{3.39}
$$

Hence, The linear strain vector can be expressed as: $\boldsymbol{e} = \boldsymbol{B}_0 \hat{\boldsymbol{u}}$, where the $\boldsymbol{B}_0$ is the linear strain-displacement matrix, $\boldsymbol{B}_0$ is given as:

$$
B_0 = \left[\cdots\cdots \left| \begin{array}{ccccc}
\dfrac{\partial N_i}{\partial x} & 0 & 0 & -\dfrac{\partial g}{\partial x} l_{2i} & \dfrac{\partial g}{\partial x} l_{1i} \\
0 & \dfrac{\partial N_i}{\partial y} & 0 & -\dfrac{\partial g}{\partial y} m_{2i} & \dfrac{\partial g}{\partial y} m_{1i} \\
0 & 0 & \dfrac{\partial N_i}{\partial z} & -\dfrac{\partial g}{\partial z} n_{2i} & \dfrac{\partial g}{\partial z} n_{1i} \\
\dfrac{\partial N_i}{\partial y} & \dfrac{\partial N_i}{\partial x} & 0 & -\left(\dfrac{\partial g}{\partial x} m_{2i} + \dfrac{\partial g}{\partial y} l_{2i} \right) & \left(\dfrac{\partial g}{\partial x} m_{1i} + \dfrac{\partial g}{\partial y} l_{1i} \right) \\
0 & \dfrac{\partial N_i}{\partial z} & \dfrac{\partial N_i}{\partial y} & -\left(\dfrac{\partial g}{\partial y} n_{2i} + \dfrac{\partial g}{\partial z} m_{2i} \right) & \left(\dfrac{\partial g}{\partial y} n_{1i} + \dfrac{\partial g}{\partial z} m_{1i} \right) \\
\dfrac{\partial N_i}{\partial z} & 0 & \dfrac{\partial N_i}{\partial x} & -\left(\dfrac{\partial g}{\partial x} n_{2i} + \dfrac{\partial g}{\partial z} l_{2i} \right) & \left(\dfrac{\partial g}{\partial x} n_{1i} + \dfrac{\partial g}{\partial z} l_{1i} \right)
\end{array} \right| \cdots\cdots \right]
\tag{3.40}
$$

As can be seen the expression in Eq. (3.40) is independent of the displacements which is due to the distinction between linear and non-linear terms made in Eq. (3.25). Consequently, the variation of the linear strain vector is simply $\delta \boldsymbol{e} = \boldsymbol{B}_0 \, \delta \hat{\boldsymbol{u}}$.

When determining the non-linear strain-displacement matrix from the variation $\delta \boldsymbol{\eta}$ we consider the variation of the non-linear part of the strain vector as given from the strain definition in Eq. (3.25), stated again as:

$$\boldsymbol{\eta}_{ij} = \frac{1}{2}\left(\frac{\partial \boldsymbol{u}_k}{\partial \boldsymbol{x}_i} \frac{\partial \boldsymbol{u}_k}{\partial \boldsymbol{x}_j} \right) \tag{3.41}$$

When expressing the variation of the non-linear strain vector, it proves convenient to define an auxiliary matrix, $\boldsymbol{A}$, whereby Eq. (3.41) is written as:

$$\boldsymbol{\eta} = \frac{1}{2} \boldsymbol{A} \theta \tag{3.42}$$

With,

$$\boldsymbol{A} = \begin{bmatrix} \psi_x & 0 & 0 \\ 0 & \psi_y & 0 \\ 0 & 0 & \psi_z \\ \psi_y & \psi_x & 0 \\ 0 & \psi_z & \psi_y \\ \psi_z & 0 & \psi_x \end{bmatrix}, \quad \psi_i = \left\{ \frac{\partial u}{\partial x_i} \quad \frac{\partial v}{\partial x_i} \quad \frac{\partial w}{\partial x_i} \right\}, \text{ and } 0 = \{0 \quad 0 \quad 0\} \, .$$

The vector $\boldsymbol{\theta}$ is given as: $\theta = \left\{ \psi_x \quad \psi_y \quad \psi_z \right\}^T$.

However, taking the variation of $\boldsymbol{\eta}$ in Eq. (3.42) yields the following expression:

$$\delta \boldsymbol{\eta} = \frac{1}{2} \delta \boldsymbol{A} \theta + \frac{1}{2} \boldsymbol{A} \delta \theta \tag{3.43}$$

Since both $\boldsymbol{A}$ and $\boldsymbol{\theta}$ are functions of the nodal displacements. In order to obtain the variation of $\boldsymbol{A}$, an interesting property of the matrix is used. By inserting the expressions for $\boldsymbol{\theta}$ and $\boldsymbol{A}$ in Eq. (3.43) it is easily shown that the variation can be written as $\boldsymbol{\delta A \theta} = \boldsymbol{A \delta \theta}$. Thereby Eq. (3.43) can be written simply as $\boldsymbol{\delta \eta} = \boldsymbol{A \delta \theta}$. The matrix $\boldsymbol{A}$ is not suitable as a strain-displacement relation since $\boldsymbol{\eta}$ must be a direct function of the nodal displacements. Therefore, another expression is needed and to this end an auxiliary matrix is again introduced. Consequently, the vector $\boldsymbol{\theta}$ is

written as a product of the matrix $\boldsymbol{G}$ and the nodal displacements, $\theta = \boldsymbol{G}\hat{\boldsymbol{u}}$. The matrix $\boldsymbol{G}$ is the auxiliary matrix determined directly from Eq. (3.37) due to the definition of $\boldsymbol{\theta}$:

$$G = \left[\begin{array}{c|ccccc|c} \cdots\cdots & \frac{\partial N_i}{\partial x} & 0 & 0 & -\frac{\partial g}{\partial x} l_{2i} & \frac{\partial g}{\partial x} l_{1i} & \\ & 0 & \frac{\partial N_i}{\partial x} & 0 & -\frac{\partial g}{\partial x} m_{2i} & \frac{\partial g}{\partial x} m_{1i} & \\ & 0 & 0 & \frac{\partial N_i}{\partial x} & -\frac{\partial g}{\partial x} n_{2i} & -\frac{\partial g}{\partial x} n_{1i} & \\ & \frac{\partial N_i}{\partial y} & 0 & 0 & -\frac{\partial g}{\partial y} l_{2i} & \frac{\partial g}{\partial y} l_{1i} & \\ & 0 & \frac{\partial N_i}{\partial y} & 0 & -\frac{\partial g}{\partial y} m_{2i} & \frac{\partial g}{\partial y} m_{1i} & \cdots\cdots \\ & 0 & 0 & \frac{\partial N_i}{\partial y} & -\frac{\partial g}{\partial y} n_{2i} & -\frac{\partial g}{\partial y} n_{1i} & \\ & \frac{\partial N_i}{\partial z} & 0 & 0 & -\frac{\partial g}{\partial z} l_{2i} & \frac{\partial g}{\partial z} l_{1i} & \\ & 0 & \frac{\partial N_i}{\partial z} & 0 & -\frac{\partial g}{\partial z} m_{2i} & \frac{\partial g}{\partial z} m_{1i} & \\ & 0 & 0 & \frac{\partial N_i}{\partial z} & -\frac{\partial g}{\partial z} n_{2i} & \frac{\partial g}{\partial z} n_{1i} & \end{array} \right] \tag{3.44}$$

Inserting the expression for $\boldsymbol{\theta}$ in $\boldsymbol{\eta}$ yields $\boldsymbol{\delta\eta} = \boldsymbol{AG\delta\hat{u}}$, whereby the nonlinear strain-displacement matrix can be determined as $\boldsymbol{B_{NL}} = \boldsymbol{AG}$.

Now, both the linear and non-linear strain-displacement matrices have been determined and the overall strain-displacement matrix can be found as $\boldsymbol{B} = \boldsymbol{B_0}+\boldsymbol{B_{NL}}$. From $\boldsymbol{B}$ the tangent stiffness matrix can be determined.

6.3 Constitutive relation

Once the strain tensor has been defined, stresses are related to strains and hence displacements through a constitutive relation which for linear material behaviour is Hook's general law. Regarding thermal effect, the thermal strain ε^{th} in the global system coordinates, using Voight notation, can be calculated as follows:

$$\boldsymbol{\varepsilon}^{th} = -\alpha(T,z)\Delta T(z)\cdot\begin{bmatrix}1 & 1 & 1 & 0 & 0 & 0\end{bmatrix}^T \tag{3.45}$$

In which, $\Delta T(z)$ is the temperature change and $\alpha(T,z)$ is the effective thermal expansion coefficient. Note that $\alpha(T,z)$ is variable with the thickness coordinate and temperature. The temperature change ΔT is defined as:

$$\Delta T(z) = T(z) - T_0 \tag{3.46}$$

Where, T_0 is the reference temperature.

The Voight form of the stress tensor in global Cartesian coordinates is determined by the following relation:

$$\begin{Bmatrix}\sigma_{11}\\ \sigma_{22}\\ \sigma_{33}\\ \sigma_{12}\\ \sigma_{13}\\ \sigma_{23}\end{Bmatrix} = [\boldsymbol{C}]\left(\begin{Bmatrix}\varepsilon_{11}^m\\ \varepsilon_{22}^m\\ \varepsilon_{33}^m\\ 2\varepsilon_{12}^m\\ 2\varepsilon_{13}^m\\ 2\varepsilon_{23}^m\end{Bmatrix} - \begin{Bmatrix}\varepsilon_{11}^{th}\\ \varepsilon_{22}^{th}\\ \varepsilon_{33}^{th}\\ 2\varepsilon_{12}^{th}\\ 2\varepsilon_{13}^{th}\\ 2\varepsilon_{23}^{th}\end{Bmatrix}\right) \tag{3.47}$$

According to shell assumptions, the strain energy associated with the stresses along the thickness direction is neglected. Then, since the normal stress and strain along the thickness direction is ignored in the local convected coordinates, the following vector of stresses is obtained in local coordinates:

$$\tilde{\boldsymbol{\sigma}} = \begin{Bmatrix}\sigma_{11} & \sigma_{22} & 0 & \sigma_{12} & \sigma_{13} & \sigma_{23}\end{Bmatrix}^T \tag{3.48}$$

Accordingly, the linear constitutive matrix is expressed in the local coordinates by:

$$\tilde{\boldsymbol{C}} = \begin{bmatrix} C_{11} & C_{12} & 0 & 0 & 0 & 0\\ C_{12} & C_{11} & 0 & 0 & 0 & 0\\ 0 & 0 & 0 & 0 & 0 & 0\\ 0 & 0 & 0 & C_{44} & 0 & 0\\ 0 & 0 & 0 & 0 & C_{55} & 0\\ 0 & 0 & 0 & 0 & 0 & C_{66}\end{bmatrix} \tag{3.49}$$

Where,

$$C_{11}=\frac{E(T,z)}{1-\nu^2(T,z)},\quad C_{12}=\nu(T,z)C_{11},\quad C_{44}=C_{55}=C_{66}=k_s\left(\frac{1-\nu(T,z)}{2}\right) \tag{3.50}$$

The elastic modulus $E(T,z)$ and the Poisson's ratio $\nu(T,z)$ vary with the thickness and temperature. The shear correction factor k_s, is introduced to improve the shear distribution across the shell thickness. The constitutive matrix $\boldsymbol{C}$ in the global coordinates can be obtained by using the following transformation:

$$\boldsymbol{C}=\boldsymbol{Q}^T\tilde{\boldsymbol{C}}\,\boldsymbol{Q} \tag{3.51}$$

where $\boldsymbol{Q}$ stands for the transformation matrix in Eq. (3.29).

6.4 Incremental equilibrium governing equations

The basis of this incremental formulation is the use of the virtual work principle. Considering the equilibrium of the body at a time ($t+\Delta t$), the principle of virtual displacements is written referred to the initial configuration at a time ($t = 0$) in the following form:

$$\int_{{}^0V}{}_0^{t+\Delta t}S_{ij}\,\delta\,{}_0^{t+\Delta t}\varepsilon_{ij}\,d\,{}^0V={}^{t+\Delta t}W \tag{3.52}$$

Where, ${}_0^{t+\Delta t}S_{ij}$ and ${}_0^{t+\Delta t}\varepsilon_{ij}$ denote the second Piola-Kirchhoff stress tensor and the incremental Green-Lagrange strain tensor at ($t+\Delta t$) referred to the configuration at a time ($t = 0$). The quantity ${}^{t+\Delta t}W$ represents the external virtual work. In dynamic analysis, the incremental total external virtual work is given by:

$${}^{t+\Delta t}W=\int_{{}^0V}{}_0^{t+\Delta t}t_k\,\delta u_k\,d\,{}^0A+\int_{{}^0V}{}_0^{t+\Delta t}f_k\,\delta u_k\,d\,{}^0V \tag{3.53}$$

Where, ${}_0^{t+\Delta t}t_k$ denotes surface traction, and ${}_0^{t+\Delta t}f_k$ stands for body forces. In dynamic analysis, body forces arise from mass inertia and acceleration.

For the incremental solution, the stresses and strains are decomposed into known quantities ${}_0^tS_{ij}$ and ${}_0^t\varepsilon_{ij}$, and unknown increments ${}_0S_{ij}$ and ${}_0\varepsilon_{ij}$, so that:

$$\begin{cases}{}_0^{t+\Delta t}\varepsilon_{ij}={}_0^t\varepsilon_{ij}+{}_0\varepsilon_{ij}\\ {}_0^{t+\Delta t}S_{ij}={}_0^tS_{ij}+{}_0S_{ij}\end{cases} \tag{3.54}$$

By considering thermal stresses, stress and incremental stress tensors are given by:

$$\begin{cases} {}_0^tS_{ij} = {}_0^tS_{ij}^m + {}_0^tS_{ij}^{th} \\ {}_0S_{ij} = {}_0S_{ij}^m + {}_0S_{ij}^{th} \end{cases} \tag{3.55}$$

Where, the subscripts (*m*) and (*th*) stands for mechanical and thermal quantities respectively.

After splitting the strain increment into linear and nonlinear parts ${}_0\varepsilon_{ij} = {}_0e_{ij} + {}_0\eta_{ij}$ and using the linearized expression ${}_0S_{ij} = {}_0C_{ijkl}\,{}_0e_{kl}$, the incremental stress can be written as:

$${}_0S_{ij} = {}_0C_{ijkl}\left({}_0e_{kl}^m + {}_0e_{kl}^{th}\right) \tag{3.56}$$

Then, by substituting from (3.54) to (3.56) into (3.52) and linearizing the principle of virtual work in the configuration at time $(t+\Delta t)$ about the known configuration at time (*t*), the following total Lagrangian formulation is obtained:

$$\begin{aligned} &\int_{{}_0V} {}_0C_{ijkl}\,{}_0e_{kl}\delta\,{}_0e_{kl}\,d\,{}^0V + \int_{{}_0V} {}_0^tS_{ij}^m\delta\,{}_0\eta_{ij}\,d\,{}^0V + \int_{{}_0V} {}_0^tS_{ij}^{th}\delta\,{}_0\eta_{ij}\,d\,{}^0V \\ &\quad = {}^{t+\Delta t}W - \int_{{}_0V} {}_0^tS_{ij}^m\delta\,{}_0e_{ij}\,d\,{}^0V - \int_{{}_0V} {}_0^tS_{ij}^{th}\delta\,{}_0e_{ij}\,d\,{}^0V \end{aligned} \tag{3.57}$$

This equation is the basic equilibrium relation employed to develop the governing finite element matrices and vectors. For the actual solution of problems, it is frequently important to use equilibrium iterations (Newton-Raphson method).

Introducing finite element discretization [11], Eq. (3.57) can be written in the following matrix form:

$$\begin{aligned} &\delta U_e^T\left(\int_{{}_0V} B^TCB\,d\,{}^0V + \int_{{}_0V}[G]^T\,H^m[G]\,d\,{}^0V + \int_{{}_0V}[G]^T\,H^{th}[G]\,d\,{}^0V\right) \\ &\quad = {}^{t+\Delta t}W - \delta U_e^T\left(\int_{{}_0V} B^TS^m\,d\,{}^0V - \int_{{}_0V} B^TS^{th}\,d\,{}^0V\right) \end{aligned} \tag{3.58}$$

Finally, we obtain the incremental equilibrium equation written in condensed form as:

$$M\ddot{U} + C\dot{U} + {}^tK_TU = {}^{t+\Delta t}F_{ext} - {}^t f_{int}^m - {}^t f_{int}^{th} \tag{3.59}$$

Where, *U* is the incremental displacement vector, and K_T is the tangent matrix defined as:

$$K_T = (K + K_{\sigma m} + K_{\sigma th}) \tag{3.60}$$

With,

$$K = \int_{0_V} B^T C B \, d\,{}^0V\,, \quad K_{\sigma m} = \int_{0_V} G^T H^{m} G \, d\,{}^0V\,, \quad K_{\sigma th} = \int_{0_V} G^T H^{th} G \, d\,{}^0V \tag{3.61}$$

The matrix *B*, represents the overall strain-displacement matrix with $B = B_0 + B_{NL}$. The external, internal and thermal nodal force vectors are described as follows:

$$F_{ext} = \int_{0_V} tU \, d\,{}^0V\,, \quad f_{int}^{m} = \int_{0_V} B^T S^m \, d\,{}^0V\,, \quad f_{int}^{th} = \int_{0_V} B^T S^{th} \, d\,{}^0V \tag{3.62}$$

Mechanical and thermal stress H^m and H^{th} are:

$$H^m = \begin{bmatrix} \sigma_x \cdot I & \tau_{xy} \cdot I & \tau_{xz} \cdot I \\ \tau_{xy} \cdot I & \sigma_y \cdot I & \tau_{yz} \cdot I \\ \tau_{xz} \cdot I & \tau_{yz} \cdot I & \sigma_z \cdot I \end{bmatrix}, \quad H^{th} = \begin{bmatrix} \sigma_x^{\,th} \cdot I & \tau_{xy}^{\,th} \cdot I & \tau_{xz}^{\,th} \cdot I \\ \tau_{xy}^{\,th} \cdot I & \sigma_y^{\,th} \cdot I & \tau_{yz}^{\,th} \cdot I \\ \tau_{xz}^{\,th} \cdot I & \tau_{yz}^{\,th} \cdot I & \sigma_z^{\,th} \cdot I \end{bmatrix}, \quad I = \begin{bmatrix} 1 & 0 & 0 \\ 0 & 1 & 0 \\ 0 & 0 & 1 \end{bmatrix} \tag{3.63}$$

7. Numerical methods for nonlinear problems

The finite element discretization of the equations governing the geometric nonlinear behaviour presented in this chapter, leads to a set of non-linear algebraic equations called "equations of residual forces". The numerical solution of this resulting nonlinear system of equations usually counts on incremental algorithms. They have become standard methods for nonlinear structural analysis. Most of these algorithms is based on the iterative Newton-Raphson method. The aim of the iterative procedure is to minimize the out-of-balance residual forces till equilibrium is achieved. For this purpose, several techniques of path-following methods, based on different approaches, have been proposed. Actually an effective path-following solution method should be able to trace the entire static load-displacement curve, which may include load limit points, turning points, and possibly bifurcation points. Basically, iterative methods add a constraint equation to the original non-linear governing equations, and then solve the extended system of equations by incremental-iterative procedures such as Newton-Raphson, or modified Newton Raphson to obtain the solution in discrete points along the equilibrium path. The additional constraint equation could be linear [12] or quadratic [13, 14]. Also, these algorithms differ in efficiency, and ability to handle different types of nonlinear behaviour.

7.1 Load-displacement equilibrium path

In general, static behaviour of structural systems can be characterized by a load-displacement curve, this response is plotted in a two dimensions coordinate system. The curve drawn in the load displacement diagram is called the *equilibrium path*. There exist a wide variety of methods of numerical resolution that are used to get the equilibrium path. The most common are iterative methods, they are based on the minimization of a residual imbalanced force after constructing a sequence of approximate solutions. Incremental solution methods can be classified as:

7.1.1 Incremental-Iterative method

Also called predictor-corrector methods. Unlike the pure incremental method, in which, no equilibrium check is performed, a predictor step is followed by a corrective iterations step. Its purpose is to eliminate the residual forces. The residual forces are the differences between the internal forces due existing internal strains, and the externally applied loads. By minimizing the residual unbalanced forces, the solution is more accurate, and the computational time is reduced when compared to the pure incremental method.

The incremental-iterative methods consist of two parts: the increment part and the iteration part. The iteration part, is based on the minimization of the out of balance residue by the use of an iterative process for each load increment. Once convergence is achieved, the next solution step is applied. The correction of balance minimization of a residue, can be done in many iterative methods. They differ from each other mainly by the nature of the matrix used for the correction. These methods include:

7.1.1.1 Newton-Raphson method

It requires the computation of the tangent stiffness matrix at every iteration, and hence, the convergence is fast, but the computer time required for each iteration is extensive. This method is well suited for analyzing highly nonlinear problems, Figure 3.6.

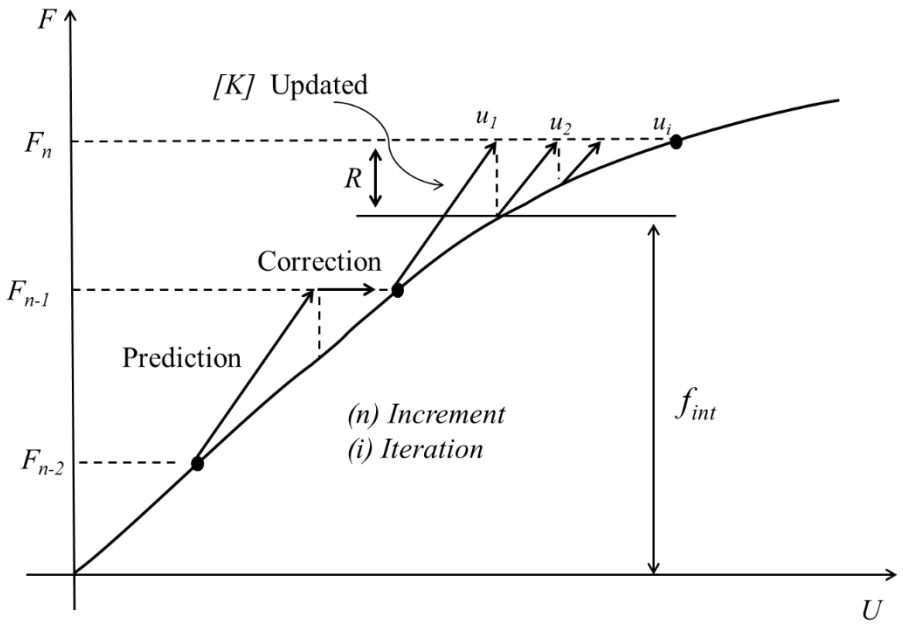

Fig. 3.6 Newton-Raphson method.

7.2 Incremental-Iterative procedure

An incremental iterative method has four essential aspects:

- *Parameterization*: The solution path is parameterized using a general scalar equation or an auxiliary surface. The aim is to find its intersection with the equation of equilibrium.
- *Prediction*: During the prediction phase, a linear estimation for the next point on the equilibrium path is established from a known converged solution on the equilibrium path.
- *Corrector*: Newton-Raphson iterations are employed during the correction phase to find a new point on the equilibrium curve.
- *Convergence criterion*.

7.2.1 Prediction

In the predictor phase, informations determined from the point previously computed (the last known geometry) are used to compute a suitable starting value for the corrector phase.

Considering an external forces load increment $\{\Delta P\}$, the corresponding elastic solution is given by:

$$\{\Delta U\} = [K]^{-1}\{\Delta P\} \tag{3.64}$$

For each finite element, this solution corresponds to a strain increment such as:

$$\{\Delta \varepsilon\} = [B]\ \{\Delta u\} \tag{3.65}$$

By assembling the elementary vectors, we define an equivalent nodal force vector $\{\Delta Q\}$ corresponds to the stress state calculated from the constitutive laws. Thus, the residue is defined by:

$$\{R\} = \{\Delta P\} - \{\Delta Q\} \tag{3.66}$$

If the residual is zero, this corresponds to a linear load increment, elsewhere, we must iterate seeking for a new solution of the equation $\{\Delta U\} = [K]^{-1}\{\Delta P\}$, till the residue is sufficiently close to zero. This is the purpose of the correction phase.

7.2.2 Correction of equilibrium

Newton-Raphson method is based on writing, at each iteration, the residue around the preceding iteration:

$$\left\{R^{(i+1)}\right\} = \left\{R^{(i)}\right\} + \left[K^{(i)}\right]\left\{\Delta U^{(i)}\right\} \tag{3.67}$$

Where, $\left\{\Delta U^{(i)}\right\} = \left\{U^{(i+1)}\right\} - \left\{U^{(i)}\right\}$ presents the correction applied to the solution at the current iteration. The correction is then, found by minimizing the residue till it falls under a specified value determined by the convergence criterion. This is thru solving the following system of linear equations:

$$\left\{R^{(i)}\right\} + \left[K^{(i)}\right]\left\{\Delta U^{(i)}\right\} = \{0\} \tag{3.68}$$

$\left[K^{(i)}\right]$ is the considered stiffness matrix.

In the conventional Newton-Raphson method, the tangent stiffness matrix is reformed ‘updated’ at every iteration, while for the modified Newton-Raphson method, the tangent stiffness matrix is only formed in the first iteration, and is kept constant in the subsequent iterations of each load increment. It may then be advantageous sometimes to replace the Newton-Raphson method by one of its variants, the “Modified Newton-Raphson” or the “Secant Newton-Raphson”.

The iterative process stops when satisfies the convergence criterion, which is chosen based on residual forces, or other variables (displacement, energy, strain...).

7.2.3 Parameterization

The incremental method is based on considering the known equilibrium configuration C_t defined at time *t*, and seek for the unknown configuration $C_{t+\Delta t}$ which is in equilibrium with the external applied loads at time $t+\Delta t$. A proportional loading with a load factor λ is assumed. Thus, the discrete equilibrium equation is $\{Q(\{q\})\} = \{P_{ext}(\{q\},\lambda)\}$ where the internal forces $\{Q\}$ are a function of the displacements $\{q\}$, and $\{P_{ext}\}$ is a function of $\{q\}$ and λ.

If the external and internal forces are not in equilibrium in any deformed configuration, a residual vector remains. The equation governing the nonlinear equilibrium of a structure is discretized by finite elements to the following form:

$$R(\{q\},\lambda) = \{P_{ext}(\{q\},\lambda)\} - \{Q(\{q\})\} = 0 \tag{3.69}$$

In case, when external forces are dependent on the deformed shape of a structure (exp: hydrostatic load), the contribution of the follower forces stiffness matrix is essential. In the other case, when external forces do not depend on the deformation of the structure, follower forces stiffness matrix is zero (the case of our study), Eq. (3.69) is written:

$$R(\{q\},\lambda) = \lambda\{P_{ext}\} - \{Q(\{q\})\} = 0 \tag{3.70}$$

$\{P_{ext}\}$: is the fixed external loading vector.

λ : loading level parameter that multiplies $\{P_{ext}\}$.

$\{q\}$: nodal displacement vector.

$Q(\{q\})$: internal force vector.

$\lambda\{P_{ext}\}$: the applied load level.

The iterative Newton-Raphson procedure, constructs a sequence of approximations of the equilibrium configuration trying to find a solution that satisfies the Eq. (3.69). At each incremental step, a series of iterations is performed until convergence is achieved.

We denote here, the increment by the subscript ***n***, and the iteration by the superscript (*i)*. The incremental-iterative procedure is given by:

$$\left[K_n^{(i)}\right]\left\{\Delta q_n^{(i+1)}\right\} = \Delta\lambda_n^{(i+1)}\left\{P_{ext}\right\} + \left\{R_n^{(i)}\right\} \tag{3.71}$$

Where, $\left\{R_n^{(i)}\right\} = \left\{R_n^{(i)}\left(\left\{q_n^{(i)}\right\}, \lambda_n^{(i)}\right)\right\}$ and $\left[K_n^{(i)}\right]$ is the tangent stiffness matrix.

The displacements and load factor, are computed through additive contributions from each Iteration:

$$\left\{q_n^{(i+1)}\right\} = \left\{q_n^{(i)}\right\} + \left\{\Delta q_n^{(i+1)}\right\} \tag{3.72}$$

$$\lambda_n^{(i+1)} = \lambda_n^{(i)} + \Delta\lambda_n^{(i+1)} \tag{3.73}$$

In the (i^{th}) iteration of the $\boldsymbol{n}^{\text{th}}$ increment, the load factor is incremented by $\Delta\lambda_n^{(i+1)}$, and the resulting displacement increment $\left\{\Delta q_n^{(i+1)}\right\}$ is found. Then, the total displacement and total load factor are updated according to Eq. (3.72) and Eq. (3.73) respectively. The residual in Eq. (3.70) is given by:

$$\left\{R_n^{(i)}\right\} = \lambda_n^{(i)}\left\{P_{ext}\right\} - \left\{Q_n^{(i)}\left(q_n^{(i)}\right)\right\} \tag{3.74}$$

The displacement vector $\{q\}$ contains (p) unknown degrees of freedom. Thus, the total number of unknowns is ($p+1$): p degrees of freedom $\{q\}$, and a load factor λ. Therefore, in addition to the n equilibrium equations of Eq. (3.70), a scalar constraint equation called the "control" or the "parameterization" equation is required. In general, it has the following form:

$$f\left(\{q\}, \lambda\right) = C - \overline{C} = 0 \tag{3.75}$$

This equation is used to set the incremental parameter to be imposed.

7.2.4 Convergence criterion

The iterative processes will continues as long as residual forces exists, until they become negligible. A convergence criterion is therefore necessary and should be pre-determined to check the equilibrium and terminate the iterations process. Thus, the equilibrium is satisfied when the norm of the residual is sufficiently small compared to a given tolerance $\boldsymbol{\varepsilon}$.

- *Residual force Criterion:*

$$\frac{\left\|R_n^1\right\|}{\left\|R_n^i\right\|} \leq \varepsilon_r \tag{3.76}$$

$\left\|R_n^1\right\|$, $\left\|R_n^i\right\|$ are respectively the residue at the iteration (*1*), and the residue at the iteration (*i*).

- *Displacement criterion:*

$$\frac{\left\|\Delta q_n^{(i)}\right\|}{\left\|q_n^{(i)} - q_{n-1}\right\|} \leq \varepsilon_d \tag{3.77}$$

$\left\{\Delta q_n^{(i)}\right\}$: incremental displacement at the considered iteration (*i*).

$\left\{q_n^{(i)}\right\}$: the current displacement (solution to be checked).

$\left\{q_{n-1}\right\}$: the last converged solution (at increment *n-1*).

- *Energy Criterion:*

The above two criteria could be combined to give an energy based criteria: The norm to be used for the residue or the displacement criteria can be selected from any one of the classic norms (Absolute, Euclidean, or maximum). Also, a maximum number of iterations is usually set. If the convergence criterion is not satisfied after this number, the process stops, and the solution is considered as diverged.

8. Conclusion

The aim of this chapter is to derive the governing finite element equations of structural mechanics for nonlinear static analysis with thermal effects. From the principle of virtual work, the governing equations are derived, which upon discretization results in the nonlinear finite element equilibrium equations. The use of Newton-Raphson method is adequate for solving equations governing the geometric nonlinear behaviour. Moreover, the formulation of degenerated shell elements is then extended in the next chapter as a specialization of the developments above to nonlinear transient dynamic analysis.

9. References

[1] Bathe KJ. Finite element procedures in engineering analysis. Prentice-Hall, Englewood Cliffs, New Jersey. 1982.

[2] Washizu K. Variational methods in elasticity & plasticity. (3rd Edition), Pergaraon Press. 1982.

[3] Chevalier L. Mécanique des systèmes et des milieux déformables. Ellipses / Edition Marketing S.A. 1996.

[4] Forest S, Amestoy M, Cantournet S, Damamme G, Kruch S. Mécanique des milieux Continues. Ecole des Mines de Paris. 2006.

[5] Djamel B, Contribution to Linear and Nonlinear Static and Dynamic Analysis of Thin Shells by Triangular and Quadrilateral Flat Shell Finite Elements with Drilling Rotational Degree of Freedom; 2015.

[6] Eugenio O, Structural Analysis with the Finite Element Method Linear Statics; Volume 2. Beams, Plates and Shells. First edition, 2013; 178-212.

[7] Sohrabuddin A et al, Analysis of Thick and Thin Shell Structures by Curved Finite Elements; Volume 2. International Journal of Numerical Mathematics, 1970; 419-451.

[8] Pau C, Guillem G. An enhanced 4-node shell element for laminated composites; Department of Materials and Production, Aalborg University, Master's Thesis, 2018.

[9] Trinh AT et al. Free vibration analysis of laminated stiffened cylindrical panels using finite element method. Journal of Science and Technology; 2016.

[10] Fathelrahman MA et al. Degenerated four nodes shell element with drilling degree of freedom. IOSR Journal of Engineering (IOSRJEN) 2013; 3(8).

[11] Moita JS et al. Buckling behavior of composite and functionally graded material plates. European Journal of Mechanics / A Solid 2019; 80:1-26.

[12] Riks E. An incremental approach to the solution of snapping and buckling problems. Int. J. Solids. Struct 1979; 15:529-551.

[13] Crisfield MA. A fast incremental/iterative solution procedure that handles snap-through. Comput. Struct 1981; 13:55-62.

[14] Ramm E. Strategies for tracing the nonlinear response near limit points. In Nonlinear Finite Element Analysis in Structural Mechanics (Edited by Wunderlich et al.), Springer 1981, NY. 63-89.

Chapter 4

Direct time integration dynamic analysis

1. Introduction

Structural analysis is primarily concerned with finding out the behaviour of a physical structure when subjected to load. This action can be in the form load due to the weight of things such as wind and snow, etc. Or some other kind of excitation such as an earthquake, impact and explosions, etc. In essence, all these loads are dynamic, which are of considerable importance in the safety studies. The distinction is made between the dynamic and the static analysis, when the external loads and displacements are applied very slowly, the inertia forces can be ignored and a static analysis which is a simplified approach of the problem can be justified. However, if a body is in motion, the inertia forces, from Newton's second law, are equal to the mass times the acceleration, then at any instant of time *(t)*, Newton's law of motion implies that the sum of all forces must be equal to the inertial force. Therefore, the governing equations lead to a dynamical problem.

In general, if the loading varies over time with frequencies higher than the Eigen frequencies of the structure, a dynamic analysis will be required. Structural dynamics are a type of structural analysis, which covers the behaviour of a structure subjected to dynamic (actions having high acceleration) loading. Dynamic analysis is the most general case that can be considered as it takes into account all the forces acting on it, also it used to find dynamic displacements, time history, and modal analysis. In dynamic analysis, to solve transient structural problems numerically, the equations of motion are first discretized in space, this procedure is called a semi discretization and will reduce the problem to a system of ordinary differential equations in time, which in turn must be integrated to complete the solution process.

In this chapter, the nonlinear dynamic response of FGM shells in a thermal environment with temperature-dependent properties is obtained using direct time integration scheme which include Newmark and composite implicit time integration methods respectively in which they are the

most widely used for solving discrete equations of motion that represent dynamic analysis of structural problems.

2. Governing equations for structural dynamics

It is assumed that a known equilibrium configuration exists at time t, and the solution at time $t+\Delta t$ has to be computed.

The governing semi-discrete equations of motion are obtained by considering the static equilibrium at time t, which includes the effect of acceleration dependent inertia forces and velocity dependent damping forces in addition to the externally applied discretized forces and the internal nodal forces of the structure, and may be written as:

$$F_I(t)+F_D(t)+F_{int}(t)=F_{ext}(t) \tag{4.1}$$

Where, $F_I(t)$ are the inertia forces, $F_D(t)$ are the damping forces, $F_{int}(t)$ are the internal (nodal) forces, including forces due to initial stresses in the system and $F_{ext}(t)$ are the external forces, all of them being time dependent.

Eq. (4.1), is valid for both linear and nonlinear systems if equilibrium is formulated with respect to the deformed (current) geometry of the structure. The equation of equilibrium governing the dynamic response of shell structures at a time $t+\Delta t$ is approximated to the following set of second-order, nonlinear, differential equations, written in matrix form as:

$$M\,{}^{t+\Delta t}\ddot{u}+C\,{}^{t+\Delta t}\dot{u}+{}^{t+\Delta t}f(u)={}^{t+\Delta t}F_{ext} \tag{4.2}$$

Where, M and C are the mass and damping matrices. F_{ext}, u, $\dot{u}$ and $\ddot{u}$ are the nodal external force, displacement, velocity and acceleration vectors, respectively. $f(u)$: is the nonlinear internal nodal force vector, with:

$$f(u)=K_T(u)u+f_{\text{int}}^{m}(u)+f_{\text{int}}^{th}(u,T) \tag{4.3}$$

Where, T stands for temperature.

The initial value problem for Eq. (4.2), consists of finding the time history response of a system, and the initial conditions:

$$\begin{cases} u(0) = u_0 \\ \dot{u}(0) = \dot{u}_0 \end{cases} \tag{4.4}$$

Where, u_0 and $\dot{u}_0$ are the given initial displacement and velocity data, substituting Eq. (4.4) and Eq. (4.5) into Eq. (4.2), we get:

$$\ddot{u}_0 = M^{-1}\left(F_{Ext}(0) - C\dot{u}_0 - Ku_0\right) \tag{4.5}$$

In principle, the equilibrium equations may be solved by any standard numerical integration scheme for both linear and nonlinear systems.

3. Methods of integration

Eq. (4.2), represent a system of nonlinear differential equations of second order. The standard procedures for the solution of differential equations can be very expensive. Therefore, there exist several different methods of integration to solve the dynamic equilibrium problem. Each method has advantages and disadvantages that depend on the type of structure and loading, these methods of analysis are commonly used such as mode superposition analysis [1, 2], response spectra analysis and direct time integration analysis.

3.1 Direct time integration methods

Direct time integration is a more general method for dynamic analysis, which treats the entire frequency content of the load imposed on the structure. It nevertheless remains very time consuming calculation. It is an incremental method performs a step by step integration of the equations of motion Eq. (4.2). This involves, after the solution is defined at time zero, the attempt to satisfy dynamic equilibrium at discrete points in time. Most methods use equal time intervals ($t+\Delta t$), ($t+2\Delta t$)…, ($t+n\Delta t$). There are a large number of different incremental solution methods. In general, they involve a solution of the complete set of equilibrium equations at each time increment.

With direct integration, the governing ordinary second order differential equations in time, resulting from the semi discretization of the structural system (by means of finite element methods), given by Eq. (4.2), is integrated using a numerical step by step procedure. The term ‘direct’ means that the equations are solved in their original form with no transformation into a different form prior to the numerical integration process. In essence, direct numerical integration

is based on two ideas, firstly the dynamic equilibrium Eq. (4.2), is satisfied at time steps ' at discrete times with intervals Δt '. This means that, basically, (static) equilibrium, which includes the effect of inertia and damping forces, is required at discrete time points within the interval of the solution. Secondly, a particular variation of displacements, velocities and accelerations within each time interval Δt is assumed.

Different forms of these assumed variations give rise to different direct integration schemes [3-11], each of which have different accuracy, stability and cost. The available direct integration can be subdivided into explicit and implicit methods, each with distinct advantages and disadvantages. The critical parameter in the use of each of these methods is generally the largest value of the time step which can be used to provide sufficiently accurate results. Explicit methods employs finite difference methods and is particularly efficient for short duration dynamical problems or wave propagation problems (high frequency structural modes), in which the solution at time $t+\Delta t$ is obtained by considering the equilibrium conditions at time t, and such integration schemes do not require factorization of the effective stiffness matrix in the step by step solution. However, explicit time integration schemes are only conditionally stable and generally require small time steps to be employed to ensure numerical stability. Typically, most used explicit methods include: central difference method [12], Runge-Kutta method [13, 14], and the Newmark method with ($\beta = 0, \gamma = 1/2$).

Generally, implicit algorithms are most effective for structural dynamics problems (in which the response is controlled by a relatively small number of low frequency modes), where the equations for displacements at the current time step involve the velocities and accelerations at the current step itself, $t+\Delta t$. The most implicit methods are unconditionally stable, typical most used implicit methods include: Newmark method [4], Houbolt method [3], and Wilson- θ method [5]. In principle, it had been shown in many works [15-17], that the classical Newmark and Wilson- θ [18] fails to produce stable and accurate solutions in severe nonlinear problems, especially when nonlinear dynamics problems must be integrated for a long time steps [19, 20]. Hughes et al. [21] proposed the constraint energy method by extending the trapezoidal rule [4] with the constraint of energy conservation via the method of Lagrange multipliers. However, Kuhl and Ramm [22] had observed that this algorithm conserves the total energy perfectly, but leads to final failure in the Newton-Raphson iteration of equilibrium. Simo et al. [20, 23-24]

introduced the energy-momentum method where the average of the strains was used to exactly enforce energy conservation. However, these methods are computationally costly that solve a scalar variable either at the integration point or over each element in an averaged sense and may result in non-symmetric tangent stiffness matrices. Hence, to obtain stable and accurate solutions for a long time nonlinear problems, an efficient conservative and/or decaying scheme is required.

Bath and Baig [17] proposed a composite implicit time integration scheme method, which basis in the work of Bank et al. [25] for solving first order equations arising in the simulation of silicon devices and circuits. This method is a simple combination of the trapezoidal rule and the three-point Euler backward method that displays some numerical damping in the time integration process. Their success to manage stability in the geometrically nonlinear dynamic regime is mainly due to their ability to offer the minimal numerical damping for low-frequency responses and the maximal numerical damping for parasitic high-frequency modes.

Some facts with the algorithm for the solution of linear and nonlinear structural dynamics and wave propagation problems had been presented in [17, 26-30], this problem motivated the development of many algorithms, based on the idea of conserving or decaying the system energy [15, 17, 22, 31-32]. In this work, composite implicit time integration and Newmark methods are adopted, in which they are the most widely used for solving discrete equations of motion that represent dynamic analysis of structural problems.

3.1.1 Newmark method

Newmark [4], presented a family of single step by step integration methods, this algorithm is the most widely used implicit methods of direct time integration for solving semi discrete equations of equilibrium, it has been applied to the dynamic analysis of many practical engineering structures.

Let us assume that a known solution of dynamic equilibrium equations exists at time t. The solution of this nonlinear dynamic equilibrium equations at time $t+\Delta t$ is to be calculated, Eq. (4.2), is considered at time $t+\Delta t$ as:

$$M\,{}^{t+\Delta t}\ddot{u} + C\,{}^{t+\Delta t}\dot{u} + {}^{t+\Delta t}f\left(u\right) = {}^{t+\Delta t}F_{ext} \tag{4.6}$$

Where, ${}^{t+\Delta t}u$, ${}^{t+\Delta t}\dot{u}$ and ${}^{t+\Delta t}\ddot{u}$ are respectively, the approximations at time $t+\Delta t$.

In Newmark acceleration method, to begin the iterative process the Eq. (4.5), must be initialized. Hence, Taylor's series displays an accurate approach to obtain the following two additional equations:

$$\begin{cases} {}^{t+\Delta t}u = {}^{t}u + \Delta t \cdot {}^{t}\dot{u} + \dfrac{\Delta t^2}{2} \cdot {}^{t}\ddot{u} + \dfrac{\Delta t^3}{6} \cdot {}^{t}\dddot{u} + ... \\ {}^{t+\Delta t}\dot{u} = {}^{t}\dot{u} + \Delta t \cdot {}^{t}\ddot{u} + \dfrac{\Delta t^2}{2} \cdot {}^{t}\dddot{u} + ... \end{cases} \tag{4.7}$$

Newmark, reduced these equations and expressed them in the following form:

$$\begin{cases} {}^{t+\Delta t}u = {}^{t}u + \Delta t \cdot {}^{t}\dot{u} + \dfrac{\Delta t^2}{2} \cdot {}^{t}\ddot{u} + \beta \cdot \Delta t^3 \cdot \dddot{u} \\ {}^{t+\Delta t}\dot{u} = {}^{t}\dot{u} + \Delta t \cdot {}^{t}\ddot{u} + \gamma \cdot \Delta t^2 \cdot \dddot{u} \end{cases} \tag{4.8}$$

Assuming the acceleration to be linear within the time step, the term $\dddot{u}$ could be written as:

$$\dddot{u} = \frac{\left({}^{t+\Delta t}\ddot{u} - {}^{t}\ddot{u}\right)}{\Delta t} \tag{4.9}$$

The substitution of Eq. (4.9) into Eq. (4.8), provides Newmark's equations in standard form:

$$\begin{cases} {}^{t+\Delta t}u = {}^{t}u + \Delta t \cdot {}^{t}\dot{u} + \left[\dfrac{1}{2} - \beta\right]\Delta t^2 \cdot {}^{t}\ddot{u} + \beta \cdot \Delta t^2 \cdot {}^{t+\Delta t}\ddot{u} \\ {}^{t+\Delta t}\dot{u} = {}^{t}\dot{u} + \left[1 - \gamma\right]\Delta t \cdot {}^{t}\ddot{u} + \gamma \cdot \Delta t^2 \cdot {}^{t+\Delta t}\ddot{u} \end{cases} \tag{4.10}$$

Newmark used Eq. (4.10) and Eq. (4.6) iteratively, for each time step. Later, Wilson formulated Newmark's method in matrix notation, added stiffness and mass proportional damping, and eliminated the need for iteration by introducing the direct solution of equations at each time step, this requires that Eq. (4.10) be rewritten in the following form:

$$\begin{cases} {}^{t+\Delta t}\ddot{u} = b_1\left[{}^{t+\Delta t}u - {}^{t}u\right] + b_2\,{}^{t}\dot{u} + b_3\,{}^{t}\ddot{u} \\ {}^{t+\Delta t}\dot{u} = b_4\left[{}^{t+\Delta t}u - {}^{t}u\right] + b_5\,{}^{t}\dot{u} + b_6\,{}^{t}\ddot{u} \end{cases} \tag{4.11}$$

The substitution of Eq. (4.11) into Eq. (4.6), allows the dynamic equilibrium of the system at time $t + \Delta t$ to be written in terms of the unknown node displacements ${}^{t+\Delta t}u$ as:

$$\left[b_1 M + b_4 C + K_T\right]{}^{t+\Delta t}u = {}^{t+\Delta t}R + M\left[b_1\,{}^{t}u - b_2\,{}^{t}\dot{u} - b_3\,{}^{t}\ddot{u}\right] + C\left[b_4\,{}^{t}u - b_5\,{}^{t}\dot{u} - b_6\,{}^{t}\ddot{u}\right] \tag{4.12}$$

Where, the constants b_1 to b_6 are defined as:

$$\begin{cases} b_1 = \dfrac{1}{\beta \Delta t^2},\ b_2 = \dfrac{-1}{\beta \Delta t},\ b_3 = \left[1 - \dfrac{1}{2\beta}\right] \\ b_4 = \gamma \cdot \Delta t \cdot b_1,\ b_5 = 1 + \gamma \cdot \Delta t \cdot b_2,\ b_6 = \Delta t\left[1 + \gamma \cdot b_3 - \gamma\right] \end{cases} \tag{4.13}$$

β and γ are parameters that control the stability and accuracy of the algorithm. Newmark, had originally proposed an unconditionally stable scheme with constant acceleration over the time step, in this case: $\gamma = 1/2$ and $\beta = 1/4$. Note that the constants b_i need to be calculated only once for both linear and nonlinear analysis. The matrix $\overline{K} = K_T + b_1 M + b_4 C$ is usually considered as the effective stiffness matrix, where M, C and K_T are time invariant mass, damping and tangent stiffness matrices.

In the other hand, the effective load vector is taken to be:

$${}^{t+\Delta t}R = {}^{t+\Delta t}R + M\left[b_1\, {}^{t}u - b_2\, {}^{t}\dot{u} - b_3\, {}^{t}\ddot{u}\right] + C\left[b_4\, {}^{t}u - b_5\, {}^{t}\dot{u} - b_6\, {}^{t}\ddot{u}\right] \tag{4.14}$$

Where, $R = F_{ext} - f_{int}^{m} - f_{int}^{th}$.

Common forms of the Newmark's method are: Newmark average acceleration: $\beta = 1/4$, $\gamma = 1/2$, Newmark linear acceleration: $\beta = 1/6$, $\gamma = 1/2$, Newmark central difference: $\beta = 0$, $\gamma = 1/2$. The average acceleration form appears to be the most popular one and it is used exclusively in this study.

It is possible to form the damping matrix based on mass proportional and/or stiffness proportional damping as follows [33]:

$$C = a \cdot M + b \cdot K \tag{4.15}$$

Where, α and β are the damping coefficients, they are determined experimentally.

The recurrence scheme of Newmark method is presented in *appendix C*.

3.1.2 Composite implicit time integration scheme

The time integration method for the nonlinear dynamics should keep the energy (and momentum) conserving and / or decaying to guarantee the stability [27]. The composite implicit

time integration scheme proposed by [26], which is also called Bath method, for solving nonlinear dynamics shows good stability and fully implicit second-order accurate method. This approach is used to calculate the unknown displacements, velocities and accelerations by considering the complete time step Δt is subdivided into two equal sub-steps, therefore the method is a 'composite scheme'. For the first sub step solution, the well-known trapezoidal rule is used, and for the second sub step solution, the well-known 3-point Euler backward formula is employed with resulting equations:

$$\begin{cases} {}^{t+\frac{\Delta t}{2}}\ddot{u} = \dfrac{16}{\Delta t^2}\left({}^{t+\frac{\Delta t}{2}}u - {}^{t}u \right) - \dfrac{8}{\Delta t}\,{}^{t}\dot{u} - {}^{t}\ddot{u} \\ {}^{t+\frac{\Delta t}{2}}\dot{u} = \dfrac{4}{\Delta t}\left({}^{t+\frac{\Delta t}{2}}u - {}^{t}u \right) - {}^{t}\dot{u} \end{cases} \tag{4.16-1}$$

$$\begin{cases} {}^{t+\Delta t}\dot{u} = \dfrac{1}{\Delta t}\,{}^{t}u - \dfrac{4}{\Delta t}\,{}^{t+\frac{\Delta t}{2}}u + \dfrac{3}{\Delta t}\,{}^{t+\Delta t}u \\ {}^{t+\Delta t}\ddot{u} = \dfrac{1}{\Delta t}\,{}^{t}\dot{u} - \dfrac{4}{\Delta t}\,{}^{t+\frac{\Delta t}{2}}\dot{u} + \dfrac{3}{\Delta t}\,{}^{t+\Delta t}\dot{u} \end{cases} \tag{4.16-2}$$

Applying the equation of equilibrium Eq. (4.6) at time $t+\Delta t/2$ and $t+\Delta t$ respectively yields:

$$\begin{cases} M\,{}^{t+\frac{\Delta t}{2}}\ddot{u} + C\,{}^{t+\frac{\Delta t}{2}}\dot{u} + {}^{t+\frac{\Delta t}{2}}f(u) = {}^{t+\frac{\Delta t}{2}}F_{ext} \\ M\,{}^{t+\Delta t}\ddot{u} + C\,{}^{t+\Delta t}\dot{u} + {}^{t+\Delta t}f(u) = {}^{t+\Delta t}F_{ext} \end{cases} \tag{4.17}$$

Substituting Eqs. (4.16-1) and (4.16-2) into Eq. (17) yields:

$$\begin{cases} \widehat{K}_1\,{}^{t+\frac{\Delta t}{2}}u = \widehat{R}_1 \\ \widehat{K}_2\,{}^{t+\Delta t}u = \widehat{R}_2 \end{cases} \tag{4.18}$$

In which:

$$\begin{cases} \widehat{K}_1 = \dfrac{16}{\Delta t^2}M + \dfrac{4}{\Delta t}C + {}^{t+\Delta t/2}K_T \\ \widehat{K}_2 = \dfrac{9}{\Delta t^2}M + \dfrac{3}{\Delta t}C + {}^{t+\Delta t}K_T \end{cases} \tag{4.19}$$

$$\begin{cases} \widehat{f}_1 = M\,\dfrac{16}{\Delta t^2}\,{}^{t+\Delta t/2}u + C\,\dfrac{4}{\Delta t}\,{}^{t+\Delta t/2}\dot{u} + {}^{t+\Delta t/2}f_{int}^{m} + {}^{t+\Delta t/2}f_{int}^{th} \\ \widehat{f}_2 = M\,\dfrac{9}{\Delta t^2}\,{}^{t+\Delta t}u + C\,\dfrac{3}{\Delta t}\,{}^{t+\Delta t}\dot{u} + {}^{t+\Delta t}f_{int}^{m} + {}^{t+\Delta t}f_{int}^{th} \end{cases} \tag{4.20}$$

$$\begin{cases} \widehat{R}_1 = {}^{t+\Delta t/2}R + M\left(\dfrac{16}{\Delta t^2}\,{}^{t}u + \dfrac{8}{\Delta t}\,{}^{t}\dot{u} + {}^{t}\ddot{u}\right) + C\left(\dfrac{4}{\Delta t}\,{}^{t}u + {}^{t}\dot{u}\right) \\ \widehat{R}_2 = {}^{t+\Delta t}R + M\left(\dfrac{12}{\Delta t^2}\,{}^{t+\Delta t/2}u - \dfrac{3}{\Delta t^2}\,{}^{t}u + \dfrac{4}{\Delta t}\,{}^{t+\Delta t/2}\dot{u} - \dfrac{1}{\Delta t}\,{}^{t}\dot{u}\right) + C\left(\dfrac{4}{\Delta t}\,{}^{t+\Delta t/2}u - \dfrac{1}{\Delta t}\,{}^{t}u\right) \end{cases} \tag{4.21}$$

With, $K_T = K + K_\sigma^m + K_\sigma^{th}$ denotes the tangent stiffness matrix, and $R = F_{ext} - f_{int}^m - f_{int}^{th}$ denotes the residue. With the initial conditions corresponding to time (t_0), the Newton-Raphson algorithm is employed for iterating within each time sub-step increment until equilibrium is achieved over the complete time domain. The recurrence scheme of Bathe method is presented in *appendix D*.

4. Mass matrix

The extension of a finite element from static analysis to dynamic analysis implies the construction of mass matrix, to consider the effect of rotational inertia, the formulation and use of the consistent mass matrix are required.

Generally, the consistent mass element matrix is derived from the kinetic energy expression using the virtual work principle including translational and rotary inertia effects. It is given by using interpolation functions:

$$M = \int_{{}^0V} S^T \rho\, S\; d\,{}^0V \tag{4.22}$$

Where, ***S*** stands for the displacement matrix, and ***ρ*** is the density matrix.

4.1 Mass matrix formulation of the degenerated shell element

The consistent mass matrix for an iso-parametric element can be computed using numerical integration. So, for the degenerated shell element, the mass matrix is given by:

$$M^e = \int S^T \rho\, S \cdot J \cdot d\xi \cdot d\eta \cdot d\zeta = \sum_{i=1}^{n} S^T \rho\, S \cdot J \cdot W_i \cdot W_j \tag{4.23}$$

Where, the matrix S that contain the displacement interpolation vector defined as:

$$\boldsymbol{S} = \begin{bmatrix} \boldsymbol{S}^1 & \boldsymbol{S}^2 & \ldots & \boldsymbol{S}^8 \end{bmatrix} \tag{4.24}$$

$$\boldsymbol{S}^i = \begin{bmatrix} N_i & 0 & 0 & -\frac{\zeta}{2} hN_i l_{2i} & \frac{\zeta}{2} hN_i l_{1i} \\ 0 & N_i & 0 & -\frac{\zeta}{2} hN_i m_{2i} & \frac{\zeta}{2} hN_i m_{1i} \\ 0 & 0 & N_i & -\frac{\zeta}{2} hN_i n_{2i} & \frac{\zeta}{2} hN_i n_{1i} \\ 0 & 0 & 0 & N_i & 0 \\ 0 & 0 & 0 & 0 & N_i \end{bmatrix} \tag{4.25}$$

$$\boldsymbol{\rho} = \begin{bmatrix} \rho & 0 & 0 & \rho h/2 & 0 \\ 0 & \rho & 0 & 0 & \rho h/2 \\ 0 & 0 & \rho & 0 & 0 \\ \rho h/2 & 0 & 0 & \rho h^2/4 & 0 \\ 0 & \rho h/2 & 0 & 0 & \rho h^2/4 \end{bmatrix} \tag{4.26}$$

5. Conclusion

Implicit time integration schemes are used in this work, to obtain the nonlinear dynamic response of FGM shells in a thermal environment with temperature-dependent properties. However, the classical Newmark scheme fail to produce stable and accurate solutions in severe nonlinear problems, especially when nonlinear dynamics problems must be integrated for a long time period. Hence, to obtain stable and accurate solutions for a long time nonlinear problems, an efficient conservative and/or decaying scheme is required.

6. References

[1] Khudada AE, Geschwindner LF. Nonlinear dynamic analysis of steel frames by modal superposition. Journal of structural engineering 1997; 123(11):1519-1527.

[2] Villaverde R, Hanna NM. Efficient mode superposition algorithm for seismic analysis of nonlinear structures. Earthquake Engineering and Structural Dynamics 1992; 21(10):849-858.

[3] Houbolt JC. A recurrence matrix solution for the dynamics response of elastic aircraft. Journal of the Aeronautical Sciences 1950; 17:540-550.

[4] Newmark NM. A method of computational for structural dynamics. Journal of Engineering Mechanics Division 1959; 8:67-94.

[5] Wilson EL et al. Nonlinear dynamics analysis of complex structures. International Journal of Earthquake Engineering and Structural Dynamics 1973; 1:241-252.

[6] Hilber HM et al. Improved numerical dissipation for time integration algorithms in structural dynamics. Earthquake Engineering and Structural Dynamics 1977; 5:283-292.

[7] Hilber HM, Hughes TJR. Dissipation and 'overshoot' for time integration schemes in structural dynamics. Earthquake Engineering and Structural Dynamics 1978; 6:99-118.

[8] Wood WL et al. An alpha modification of Newmark's method. Int. J. Num. Meth. Eng 1980; 15:1562-1566.

[9] Zienkiewicz OC et al. An alternative single step algorithm for dynamics Problems. Earthquake Engineering and Structural Dynamics 1980; 8:31-40.

[10] Bazzi G, Anderheggen E. The p- family of algorithms for time step integration with improved numerical dissipation. Earthquake Engineering and Structural Dynamics 1982; 10:537-550.

[11] Senjanovic I. Harmonic acceleration method for dynamic structural analysis. Computer and Structures 1984; 18:71-80.

[12] Javanmardi MR, Anvar SA. Implicit and Explicit time integration methods for nonlinear structural dynamics. 9th International congress on civil engineering 2012; 1-8.

[13] Runge C, Muthematische A. Uber die numerische Auflosung von Differentialgleichungen. 1895; 46: 167-178.

[14] Kutta W. Zeitschrift fur Mathematik und Physik, Beitrag zur naherungsweisen Integration totaler Differentialgleichungen. 1901; 46:435-453.

[15] Kuhl D, Crisfield MA. Energy-conserving and decaying algorithms in non-linear structural dynamics. International Journal for Numerical Methods in Engineering 1999; 45(5):569–599.

[16] Simo JC, Tarnow N. The discrete energy-momentum method. Conserving algorithms for nonlinear elastodynamics. Zeitschrift für angewandte Mathematik und Physik ZAMP 1992; 43(5):757–792.

[17] Bathe KJ, Baig MMI. On a composite implicit time integration procedure for nonlinear dynamics. Computers and Structures 2005; 83(31-32):2513–2524.

[18] Bathe KJ, Wilson EL. Stability and accuracy analysis of direct integration methods. Earthquake Engineering and Structural Dynamics 1973; 1(3):283–291.

[19] Crisfield MA, Shi J. A co-rotational element/time-integration strategy for non-linear dynamics. Int. J. Num. Meth. Eng 1994; 37(11):1897-1913.

[20] Simo JC, Tarnow N. A new energy and momentum conserving algorithm for the nonlinear dynamics of shells. Int. J. Num. Meth. Eng 1994; 37:2527-2549.

[21] Hughes TJR et al. Finite-element methods for nonlinear elasto-dynamics which conserve energy. Journal of Applied Mechanics 1978; 45(2):366–370.

[22] Kuhl D, Ramm E. Constraint energy momentum algorithm and its application to non-linear dynamics of shells. Computer Methods in Applied Mechanics and Engineering 1996; 136(3-4):293–315.

[23] Simo JC et al. On a stress resultant geometrically exact shell model. Part VI: conserving algorithms for non-linear dynamics. International Journal for Numerical Methods in Engineering 1992; 34(1):117–164.

[24] Simo JC et al. Exact energy-momentum conserving algorithms and symplectic schemes for nonlinear dynamics. Computer Methods in Applied Mechanics and Engineering 1992; 100(1):63–116.

[25] Bank RE et al. Transient simulation of silicon devices and circuits. IEEE Transactions on Computer-aided Design of Integrated Circuits and Systems 1985; 4(4):436–451.

[26] Bathe KJ. Conserving energy and momentum in nonlinear dynamics: a simple implicit time integration scheme. Computers and Structures 2007; 85(7-8):437–445.

[27] Bathe KJ, Noh G. Insight into an implicit time integration scheme for structural dynamics. Computers and Structures 2012; 98-99:1-6.

[28] Kazancı Z, Bathe KJ. Crushing and crashing of tubes with implicit time integration. International Journal of Impact Engineering 2012; 42:80–88.

[29] Noh G et al. Performance of an implicit time integration scheme in the analysis of wave propagations. Computers and Structures 2013; 123:93–105.

[30] Chandrashekhar M, Ganguli R. Large deformation dynamic finite element analysis of delaminated composite plates using contact–impact conditions. Computers and Structures 2014; 144:92–102.

[31] Chung J, Hulbert G. A time integration algorithm for structural dynamics with improved numerical dissipation: the generalized alpha method. J. Appl. Mech. 1993; 60:371-375.

[32] Ibrahimbegovic A, Mamouri S. Energy conserving/decaying implicit time-stepping scheme for nonlinear dynamics of three-dimensional beams undergoing finite rotations. Comp. Meth. Appl. Mech. Eng. 2002; 191:4241-4258.

[33] Bathe KJ. Finite Element Procedures in Engineering Analysis. Prentice-Hall, Englewood Cliffs, New Jersey, 1982.

Chapter 5

Results and discussion

1. Introduction

In this chapter, the nonlinear static and dynamic response of FGM shells with temperature-dependent material properties under thermo-mechanical loading is investigated. The nonlinear dynamic-buckling and post-buckling behaviour of functionally graded cylindrical and spherical shells in thermal environment is also considered using the implicit conservative time integration scheme. Before proceeding to the dynamic thermal buckling characteristics of FGM cases, the efficacy of the formulation is tested for the problems for which the analytical solutions are available in the literature.

Numerical comparisons are drawn between the developed finite element formulation and the existing solutions available in literature. These comparisons demonstrate the validity and reliability of the present element, and the ability of the present shell element to describe the nonlinear static and dynamic responses of FGM structures. For convenience, material properties are assumed to be independent of temperature in some examples. The temperature is assumed to be uniform on any surface lies between the top and bottom surfaces and can be varied through the thickness direction only as a nonlinear function.

In all tested examples herein, for the geometrically nonlinear analysis, a displacement convergence criteria is used where the precision criteria is taken to be: $\varepsilon = 0.001$. In the frame of this research work, the data-processing developments enabled us to have a finite elements program developed in *MATLAB* platform, which runs on a personal computer, devoted to the geometrically nonlinear static and dynamic analysis of FGM shell structures. The presented shell finite element was implemented in the above mentioned *MATLAB* program.

2. Numerical results

2.1 Eigen-values analysis

Here, we start with the eigenvalue analyses of an arbitrary single element. The eigenvalue analyses are performed to check for the presence of spurious zero-energy modes. The stiffness matrix is integrated by using the modified reduced numerical integration. The numerical results of the eigenvalue analysis confirm that the stiffness matrix has no rank deficiency.

2.2 Cantilever Plate

The nonlinear static response of an FGM plate subjected to a distributed end shear load F without temperature effect as shown in Figure 5.1, is investigated. The geometry, boundary conditions and load are also described. Zirconia and Aluminium ceramic-metal are considered, the material properties of each constituent (computed at temperature T = 300 K) are listed in Table 5.1. The lower surface of the plate is assumed to be metal rich and the top surface is assumed to be ceramic. The mesh consists of 8x1 elements.

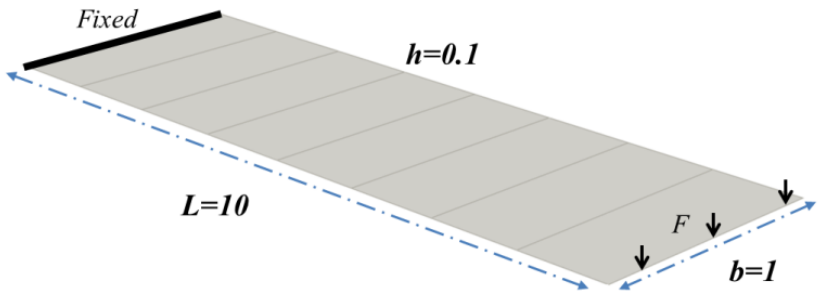

Fig. 5.1 Cantilever plate.

Table 5.1: Material properties of *Aluminium* and *Zirconia* [1]

Materials	***E** (GPa)*	***ν***	***ρ** (Kg/m^3)*	***α*** **(*1/C*)**	***κ*** **(*W/m K*)**
Zirconia	151	0.3	3000	10.10^{-6}	2.09
Aluminium	70	0.3	2707	23.10^{-6}	204

Figure 5.2, shows the effect of volume fraction index *n*, on the nonlinear response of FGM plate. It can be seen that the plate deflections are increased by increasing the volume fraction index *n*. The deflection of metallic plate is greater than ceramic due to the high bending stiffness of ceramic plate.

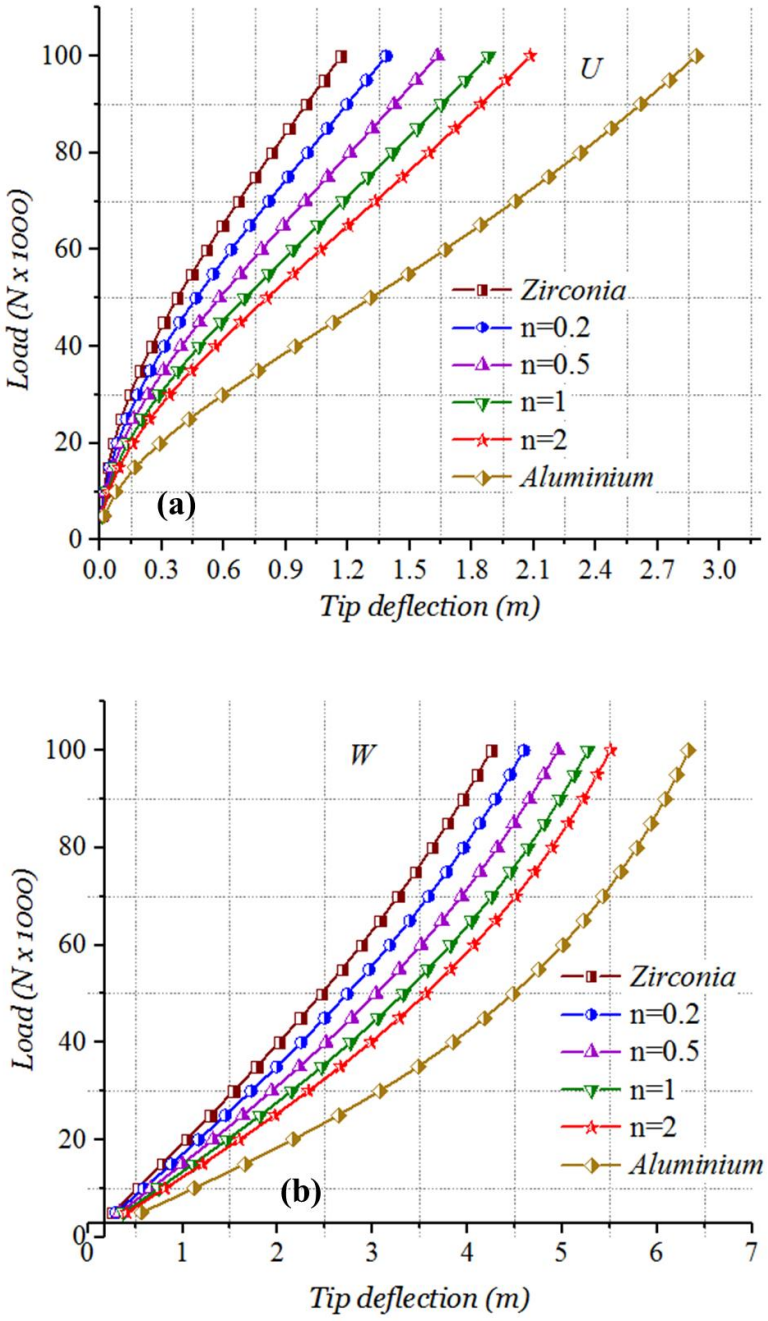

Fig. 5.2 Tip deflection of FGM cantilever plate versus shear load: (a) In-plane and (b) Out of plane deflection.

2.3 Square plate

The nonlinear forced vibration is performed, on a square plate of side length L= 0.2 m, thickness h= 0.01 m. Then, uniform pressure load applied suddenly of intensity equal to, $p(t) = -10^6$ *Pa*, as illustrated in Figure 5.3. The FGM square plate is simply supported on all its edges and made of Aluminium and Zirconia, their material properties defined in Table 5.1. The dimensionless parameters are centre deflection, $w = \left(\bar{w}E_m h / q_0 L^2\right)$, and time $\bar{t} = t\sqrt{E_m / L^2 \rho_m}$. Only one-quarter of the square plate is modelled. The mesh consists of 4x4 elements and the material properties are assumed to be independent of temperature. A time step of 10^{-5} s was used in the computations.

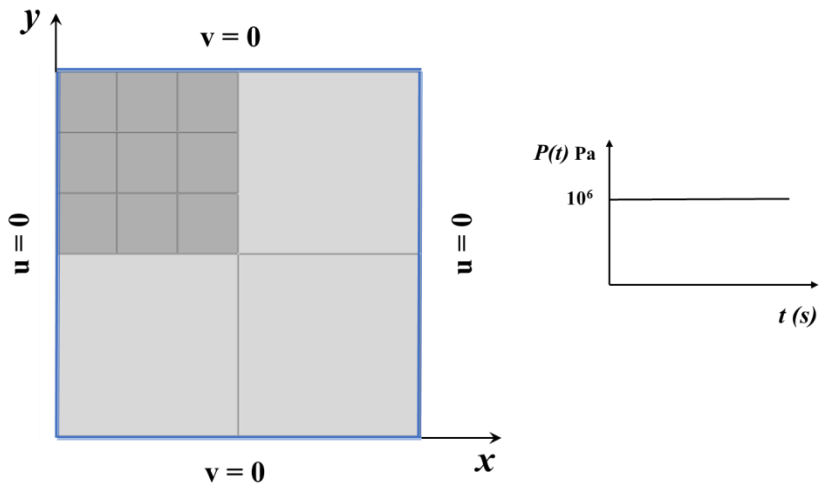

Fig. 5.3 Simply supported square plate.

Figure 5.4 shows the non-dimensional central deflection as function of non-dimensional time for an FGM square plate subjected to a suddenly applied uniform load. The dynamic response of the graded plate is intermediate to that of the metal and ceramic plates. However, the amplitude of vibration is the maximum for the metallic plate and a minimum for the ceramic one. It is seen that the amplitude of vibration increases smoothly as the amount of metal in the plate increases. Hence, the higher the bending rigidity, the lower the magnitude of deflection. Also, it is clear that the frequency of vibration of the ceramic plates is much higher than that of the metallic plates.

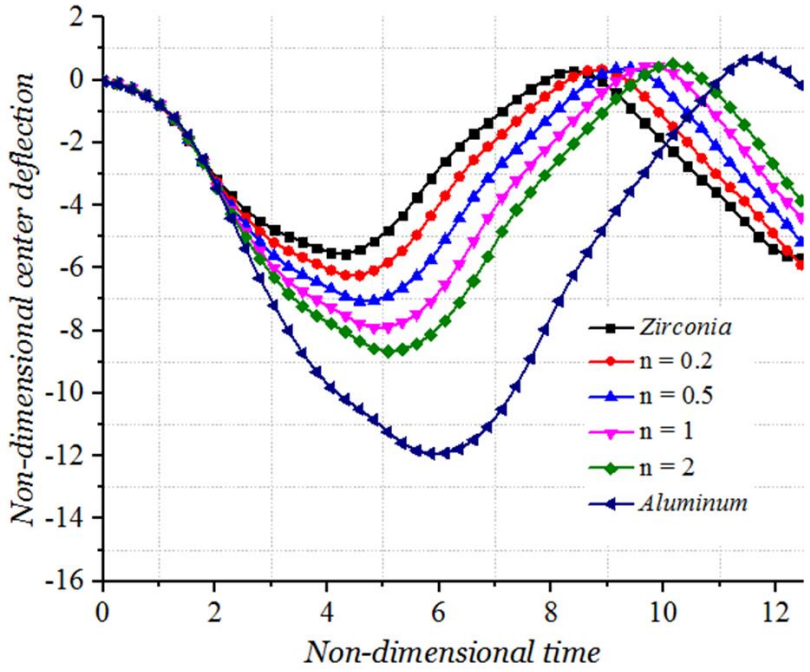

Fig. 5.4 Temporal variation of centre deflection of simply supported FGM square plate.

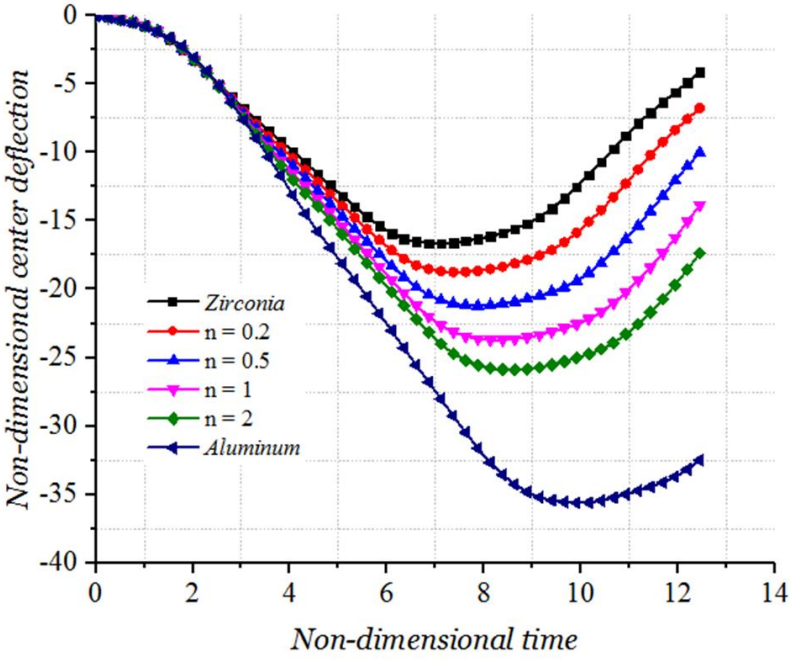

Fig. 5.5 Temporal variation of centre deflection of clamped FGM square plate.

Thus, the gradients in material properties play an important role in determining the response of the FGM plates. The computational domain for the dynamic analysis with clamped boundary conditions is the same as that of Figure 5.4. The analysis was performed for the two material combinations. Figure 5.5 shows the clamped FGM plates is much lower than the simply supported case. The effective stiffness of clamped plate is higher than the simply supported plates.

2.4 A square plate under thermo-mechanical loading

In this example, we investigated the nonlinear static and dynamic response of an FGM plate subjected to a uniformly distributed load in a thermal environment. The geometrically nonlinear behaviour of the plate was presented in [1], while an analytical solution for geometrically nonlinear dynamic analysis of an FGM plate with temperature-dependent material properties is presented in [2].

2.4.1 Static analysis

In this static analysis assessment, we investigated the behaviour of an FGM square plate of side length $a = 0.2\ m$ and thickness $h = 0.01\ m$ subjected to a thermo-mechanical loading. As illustrated in Figure 5.3, the plate is simply supported on all its edges.

The thermal load consists of applying a through-thickness temperature field by holding the bottom surface temperature at $T_m = 20°C$ while the top surface temperature is held at $T_c = 300\ °C$ in the first case, and 600 $°C$ in the second case, with the subscripts (c) and (m), denote, Zirconia and Aluminium respectively. The mechanical load consists of applying a uniformly distributed load, statically increased from 0 up to $q = -10^7\ N/m^2$. The plate's FGM is composed of Aluminium and Zirconia (Al/ZrO_2). In order to compare the obtained results against the solution presented in [1], the materiel proprieties are considered as independent of temperature. The material properties (computed at temperature $T = 300\ K$) are listed in Table 5.1. Due to the double symmetry of geometry, loading and boundary conditions, only one-quarter of the plate is modelled. The mesh of the one-quarter of the plate consists of 3×3 square elements. For convenience, the non-dimensional parameters used in the analysis, are the non-dimensional central deflection $\bar{w} = w/h$ and the load parameter $\bar{q} = q_0 a^4 / E_m h^4$, respectively.

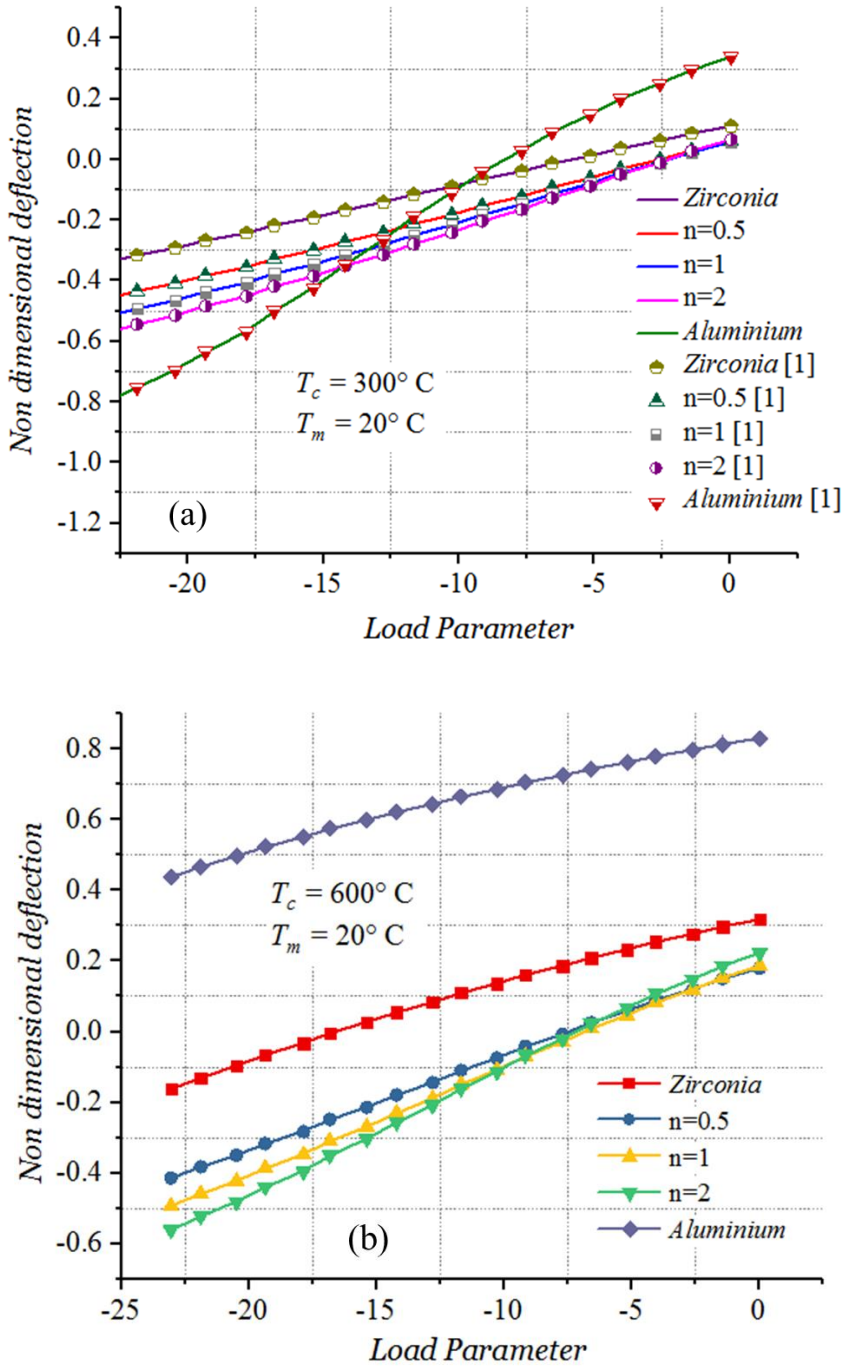

Fig. 5.6 Non-dimensional central deflection of the FGM square plate under thermo-mechanical loading: (*a*) T_c=*300 °C* and (*b*) T_c=*600 °C*.

Figure 5.6(a), shows the obtained thermo-mechanical non-dimensional load-deflection curves. An excellent agreement with the reference solution presented in [1] is observed for different power-law indexes. During the thermal loading, the plates result in upward deflections. This is

because the high temperature at the top surface causes higher thermal expansion than that of the bottom surface. One can notice that in the second load case, in which the top surface temperature is T_c = 600 °*C*, the behaviour of the isotropic plates becomes quasi-linear because of the higher curvature due to the thermal loading.

In contrast, the behaviour of the FGM plate with index $n=2$ becomes highly nonlinear. It can be easily seen from Figures 5.6(a) and 5.6(b), that the maximum deflection of the FGM plates is less sensitive to the thermal effect than that of isotropic plates.

2.4.2 Dynamic analysis

The presented formulation is deployed to carry out the nonlinear dynamic response of the FGM plate in a thermal environment with temperature-dependent material properties. In this time history analysis, the simply supported plate studied in [2], with no in-plane displacements is subjected to the thermal loading, then a uniform load equal to q (t) = -50 *MPa*, shown in Figure 5.7 is suddenly applied. In this dynamic analysis, the thickness of the plate is h = 0.025 *m*, and the time step is taken as Δt = 2 μs. Two different material mixtures are considered, the first one is zirconium oxide and titanium alloy referred to as (ZrO_2 / Ti-6A1-4V), and the second one is silicon nitride and stainless steel referred to as ($Si_3N_4 / SUS304$). The materials "mechanical and thermo-physical" properties are taken as temperature-dependent as listed in Table 5.2.

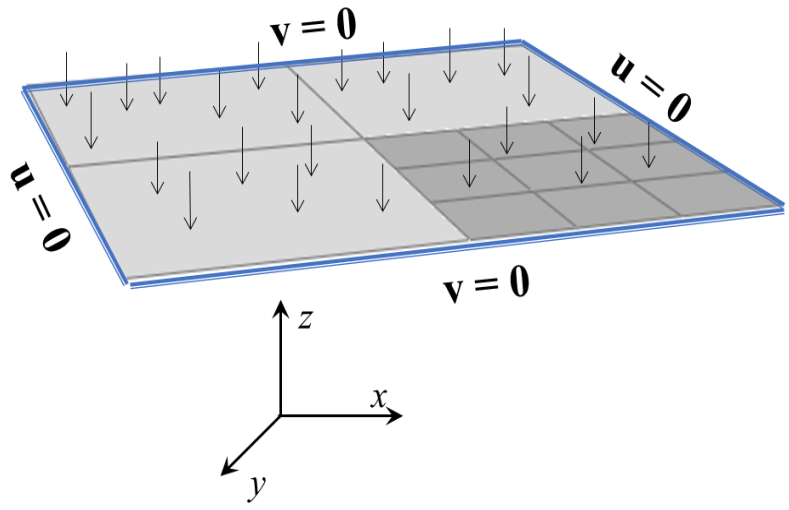

Fig. 5.7 Square plate under suddenly applied dynamic uniform load.

Table 5.2: Temperature-dependents material properties of metal and ceramic [3]

Materials	*Properties*	P_0	P_{-1}	P_1	P_2	P_3
Silicon Nitride (Si_3N_4)	*E (Pa)*	348.43×10^{9}	0	-3.070×10^{-4}	2.160×10^{-7}	-8.946×10^{-11}
	N	0.24	0	0	0	0
	ρ (Kg/m³)	2370	0	0	0	0
	α (K^{-1})	5.8723×10^{-6}	0	9.095×10^{-4}	0	0
	K ($Wm^{-1} K^{-1}$)	13.723	0	-1.032×10^{-3}	5.466×10^{-7}	-7.876×10^{-11}
Stainless Steel (SUS304)	*E (Pa)*	201.04×10^{9}	0	3.079×10^{-4}	-6.534×10^{-7}	0
	v	0.3262	0	-2.002×10^{-4}	3.797×10^{-7}	0
	ρ (Kg/m³)	8166	0	0	0	0
	α (K^{-1})	12.330×10^{-6}	0	8.086×10^{-4}	0	0
	K ($Wm^{-1} K^{-1}$)	15.379	0	-1.264×10^{-3}	2.092×10^{-6}	-7.223×10^{-10}
Zirconium Oxide (ZrO_2)	*E (Pa)*	244.27×10^{9}	0	-1.371×10^{-3}	1.214×10^{-6}	-3.681×10^{-10}
	v	0.2882	0	1.133×10^{-4}	0	0
	ρ (Kg/m³)	3000	0	0	0	0
	α (K^{-1})	12.766×10^{-6}	0	-1.491×10^{-3}	1.006×10^{-5}	-6.778×10^{-11}
	K ($Wm^{-1} K^{-1}$)	1.7	0	1.276×10^{-4}	6.648×10^{-8}	0
Titanium Alloy (Ti-6AL-4V)	*E (Pa)*	122.56×10^{9}	0	-4.586×10^{-4}	0	0
	v	0.2884	0	1.121×10^{-4}	0	0
	ρ (Kg/m³)	4429	0	0	0	0
	α (K^{-1})	7.578×10^{-6}	0	6.638×10^{-4}	-3.147×10^{-6}	0
	K ($Wm^{-1} K^{-1}$)	1	0	1.704×10^{-2}	0	0

In this dynamic analysis assessment, a temperature field is applied by holding the bottom surface temperature at T_m = 300 K while for the top surface temperature, three cases are considered: (T_c = 300 K, T_c = 400 K and T_c = 600 K). The temperature-deflection is evaluated by considering geometric nonlinearity, see Figure 5.8, then the uniform load q is suddenly applied.

The obtained results shown in Figures 5.9 and 5.10 are in good agreement with the reference solution presented in [2], in which, the equations of motion are solved analytically by using an improved perturbation technique to determine the nonlinear frequencies and dynamic responses of FGM plates. Temperature-dependent material properties are taken into account. The excellent

agreements between the present results and those of the reference demonstrate the accuracy and effectiveness of the presented formulation.

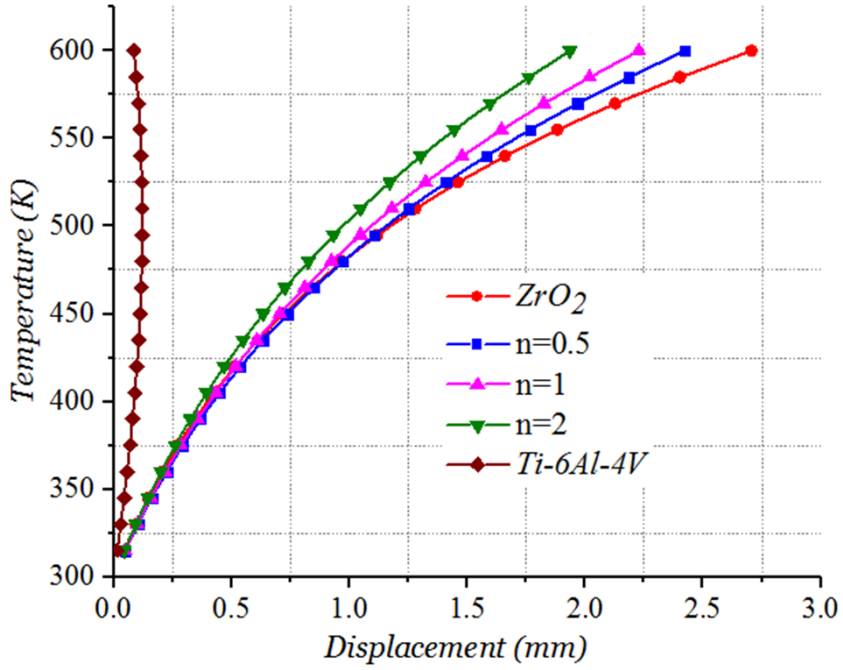

Fig. 5.8 Temperature vs. displacement curve of (ZrO_2 / Ti - 6A1 - 4V) material.

The effect of the power-law index n and the effect of thermal conditions on the dynamic response of the FGM plate are exhibited in Figures 5.9 and 5.10 for the (ZrO_2/Ti-6A1-4V) and (Si_3N_4/SUS304) respectively. Figures 5.9(a) and 5.10(a) show the obtained time history responses of the first load case for different power-law indexes using temperature-dependent material properties. Figures 5.9(b-c-d) and 5.10(b-c-d) show the obtained responses for the three thermal loading cases (T_c = 300 K, T_c = 400 K, T_c = 600 K) for a power-law index (n = 2), Zirconia/ Titanium alloy and Silicon Nitride/Stainless Steel respectively. In these figures the responses for temperature-dependent and temperature-independent properties for each constituent are shown together for comparison.

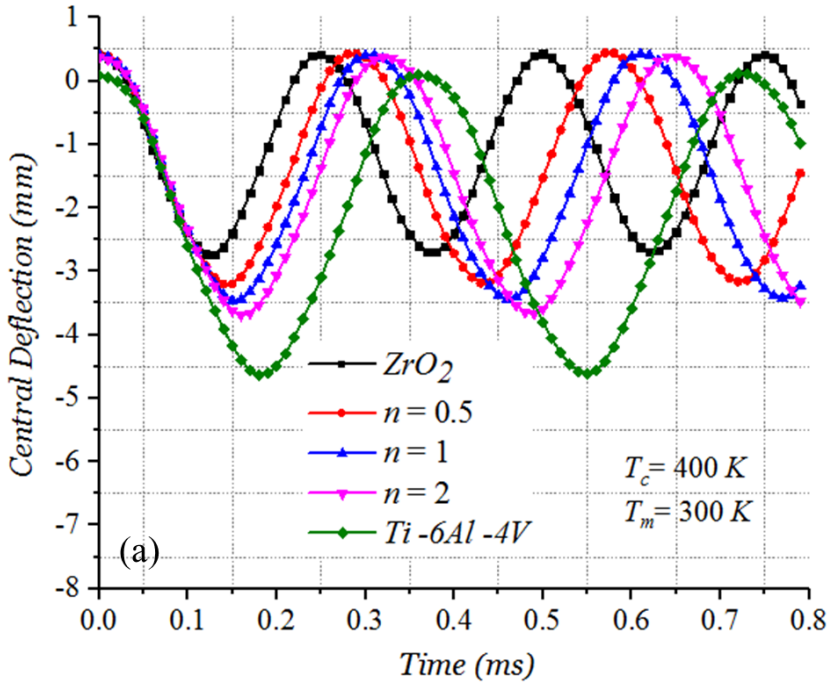
Central Deflection (mm)
Time (ms)
ZrO_2
$n = 0.5$
$n = 1$
$n = 2$
Ti -6Al -4V
T_c= 400 K
T_m= 300 K
(a)

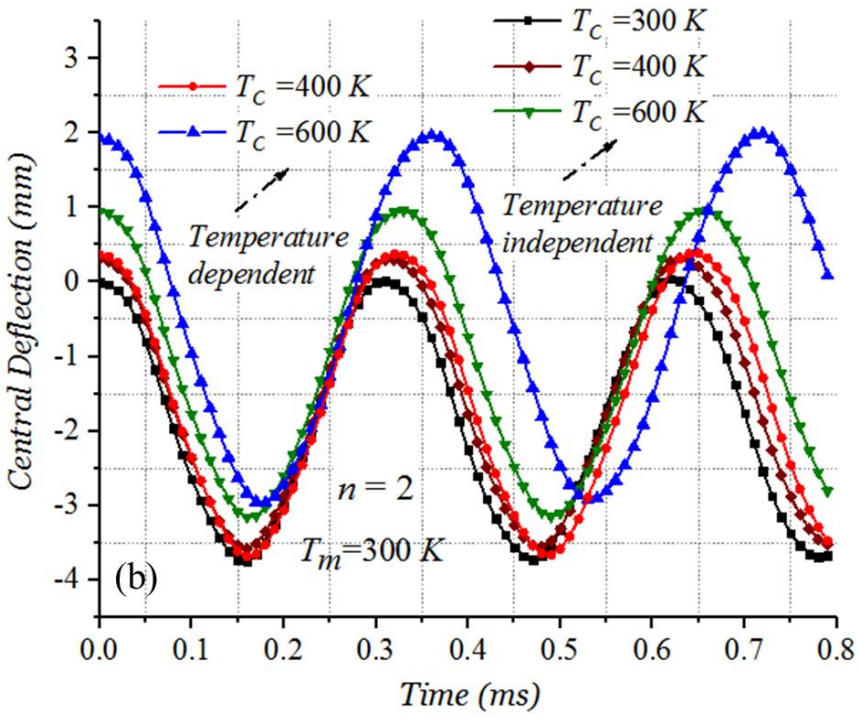
Central Deflection (mm)
Time (ms)
T_C =300 K
T_C =400 K
T_C =600 K
T_C =400 K
T_C =600 K
Temperature dependent
Temperature independent
$n = 2$
T_m=300 K
(b)

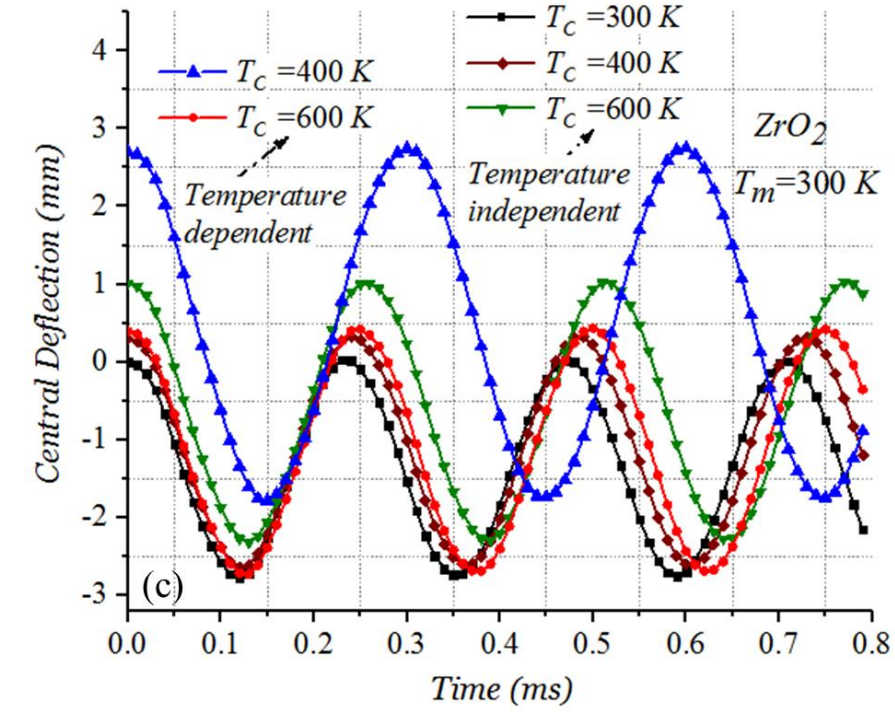
T_C =300 K
T_C =400 K
T_C =600 K
T_C =400 K
T_C =600 K
Temperature dependent
Temperature independent
ZrO_2
T_m=300 K
Central Deflection (mm)
Time (ms)
(c)

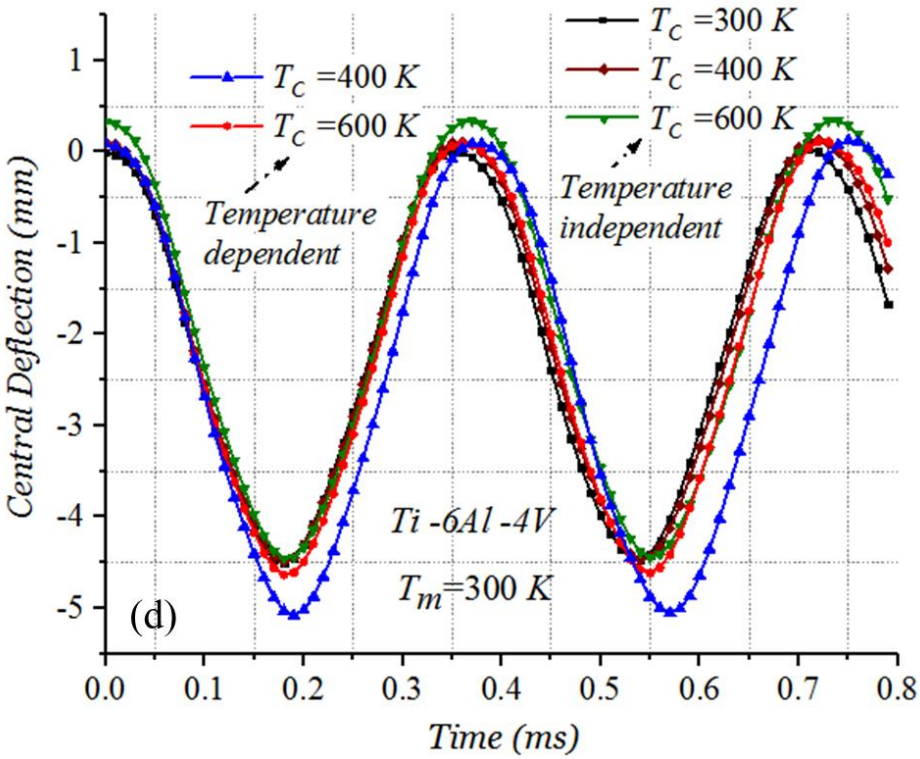
T_C =300 K
T_C =400 K
T_C =600 K
T_C =400 K
T_C =600 K
Temperature dependent
Temperature independent
Ti -6Al -4V
T_m=300 K
Central Deflection (mm)
Time (ms)
(d)

Fig. 5.9 Effect of the power-law index *n* and temperature field on the dynamic response of square plate: (a) ZrO_2 / *Ti* - 6*A*1 - 4*V* : T_c=*400 K*, (b) ZrO_2 / *Ti* - 6*A*1 - 4*V* : *n=2*, T_c=*300*, *400* and *600 K*, (c) ZrO_2, T_c=*300*, *400* and *600 K*, (d) *Ti* - 6*A*1 - 4*V* , T_c=*300*, *400* and *600 K*.

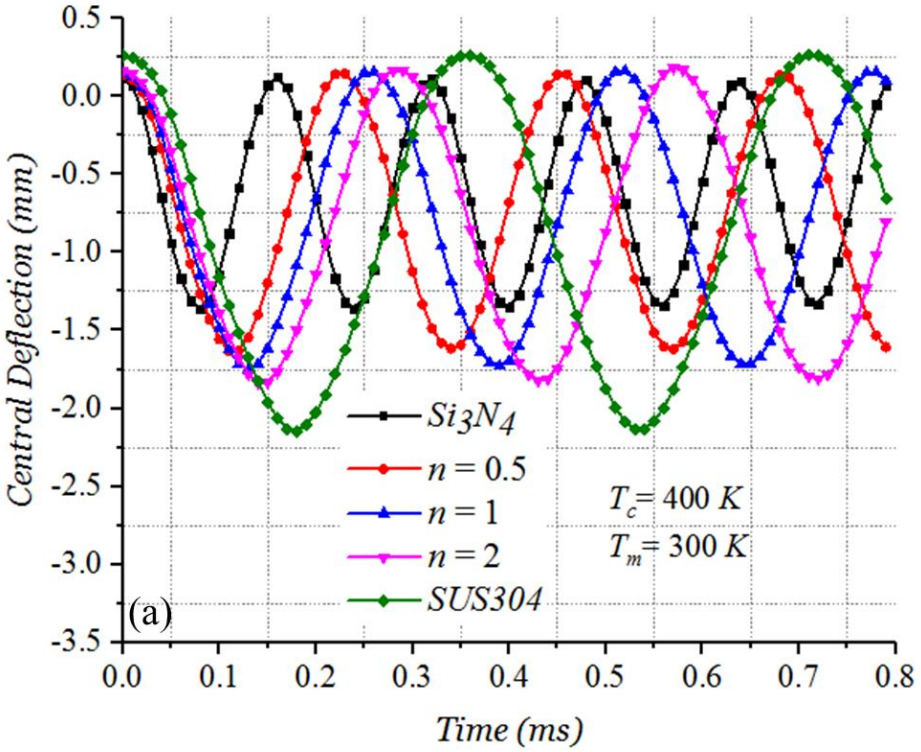

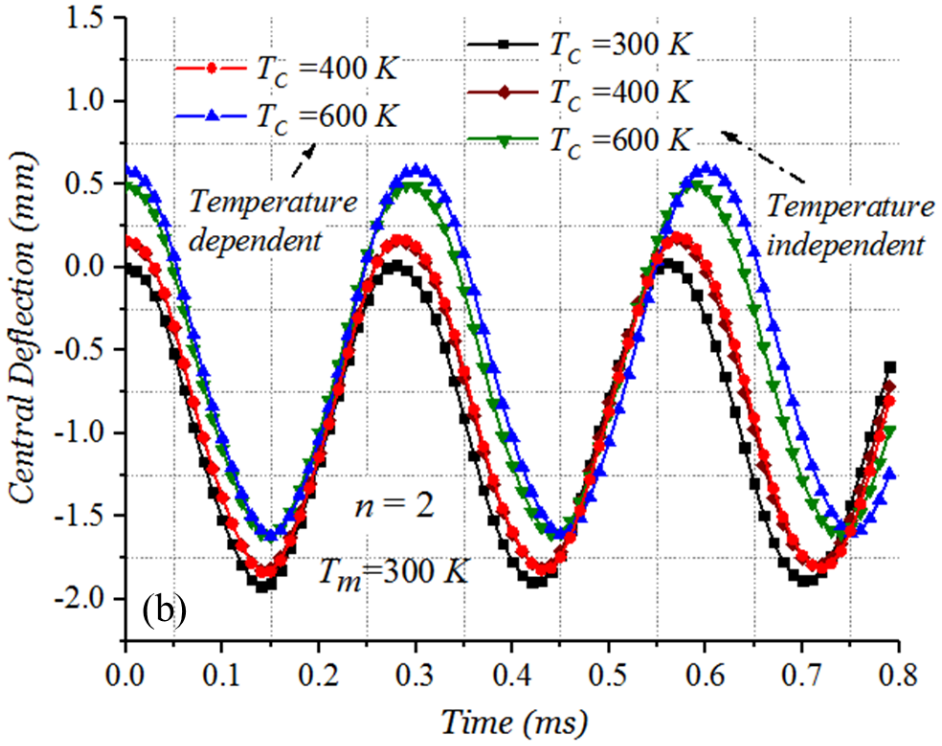
T_C =400 K
T_C =600 K
T_C =300 K
T_C =400 K
T_C =600 K
Temperature dependent
Temperature independent
n = 2
T_m=300 K
(b)
Central Deflection (mm)
Time (ms)

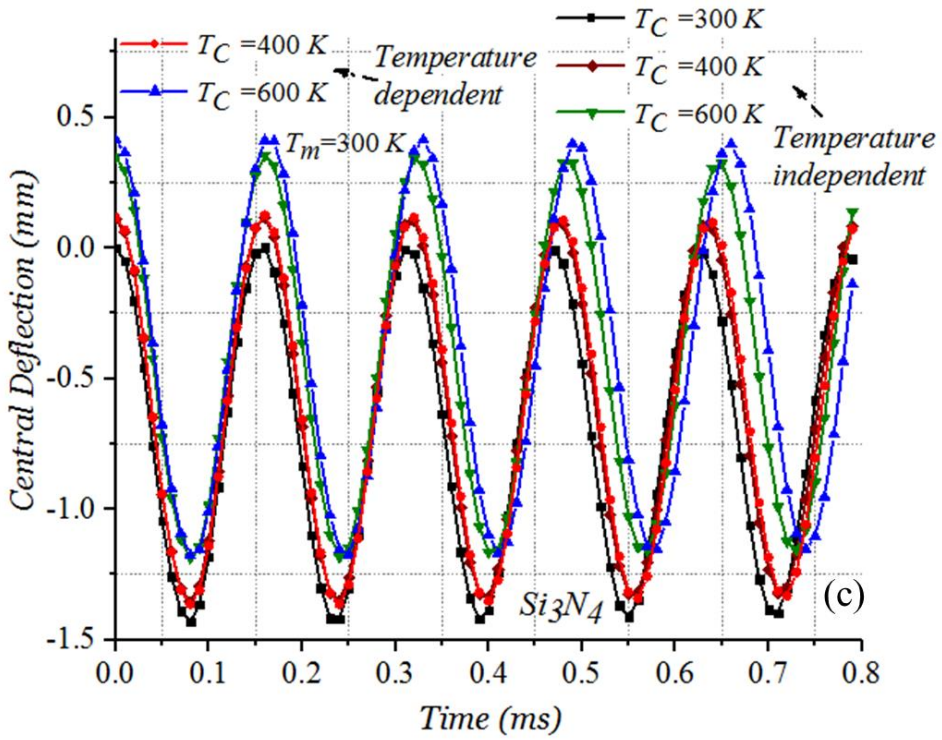
T_C =400 K
T_C =600 K
Temperature dependent
T_m=300 K
T_C =300 K
T_C =400 K
T_C =600 K
Temperature independent
Si_3N_4
(c)
Central Deflection (mm)
Time (ms)

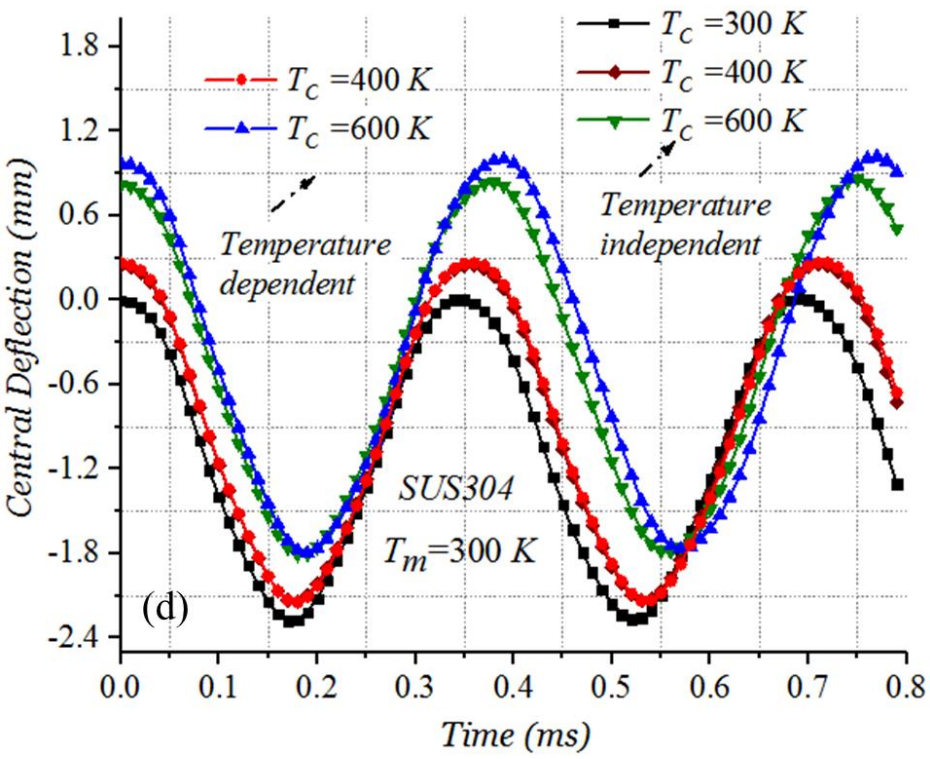

Fig. 5.10 Effect of the power-law index *n* and temperature field on the dynamic response of square plate: (a) Si_3N_4 / $SUS304$: T_c=*400 K*, (b) Si_3N_4 / $SUS304$: *n=2*, T_c=*300, 400* and *600 K*, (c) Si_3N_4 , T_c=*300, 400* and *600 K*, (d) $SUS304$, T_c=*300*, *400* and *600 K*.

The results show, that on the one hand, the temperature field and the power-law index have an important effect on the dynamic response of FGM plates. On the other hand, taking into account the material properties as temperature dependent can have a significant outcome on the overall dynamic response especially in high temperature environments. In this example, the (ZrO_2 / Ti - 6Al - 4V) material mixture seems to be more sensitive to the effect of temperature on the effective material properties than the (Si_3N_4 / $SUS304$) material mixture. It seems that this effect depends on the ration between the thermal expansion coefficient and Young's modulus for each constituent material.

2.5 Pinching of a clamped-free cylinder

One end clamped cylindrical shell is studied in this example. The shell is subjected to two diametrically opposite forces applied at the free end. This test was carried out for nonlinear analyses with FG material in [4] under purely mechanical loading. It is extended here to perform

dynamic nonlinear analysis in a thermal environment. Due to the double symmetry of geometry, loading and boundary conditions, only one-quarter of the shell is modelled. The dimensions and boundary conditions for one-fourth of the geometry are illustrated in Figure 5.11. A 6×8 elements mesh is employed for the spatial discretisation.

2.5.1 Static Analysis

Two cases are considered in this static analysis. The first case is purely mechanical (thermal conditions were not considered). The mechanical load consists of applying two diametrically opposite forces applied at the free end. The load is statically increased from 0 up to P = 100 KN. The shell's FGM is composed of Aluminium and Zirconia (Al/ZrO2) in which the materiel proprieties are considered as independent of temperature. The material properties (computed at temperature $T = 300\ K$) are listed in Table 5.1. The load-deflection curves are compared against the reference solution [4] in Figure 5.12(a). Excellent agreement between the obtained results and those of the reference is obtained.

The second loading case consists of a thermo-mechanical loading, in which, the shell is subjected to a through-thickness temperature field by holding the inner surface temperature at T_m = 300 K, while the outer surface temperature is held at T_c = 600 K. Then, the mechanical load consists of applying two diametrically opposite forces applied at the free end statically increased from 0 up to P = 10 MN. In this case, the shell's FGM is composed of $(ZrO_2 / Ti\text{-}6A1\text{-}4V)$ material mixture in which the materiel proprieties are considered as temperature-dependent.

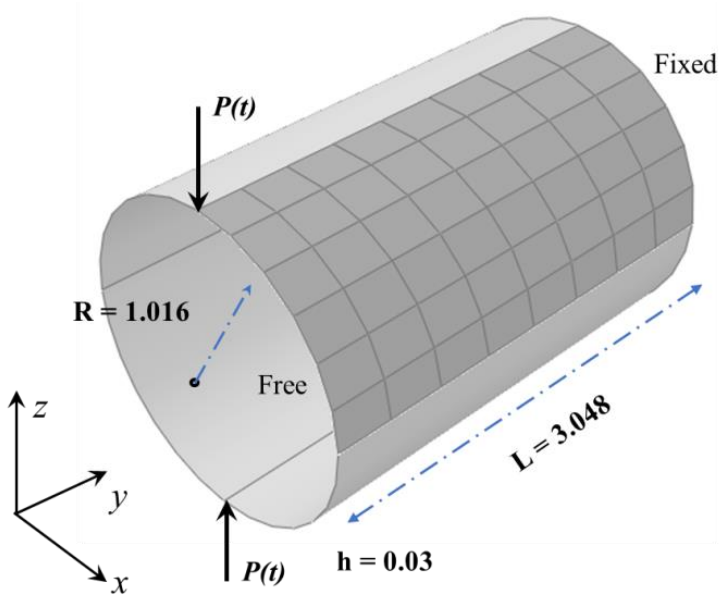

Fig. 5.11 Pinching of a short fixed-free cylinder.

The static nonlinear responses with different power low indexes for the thermo-mechanical loading are presented in Figure 5.12(b). In Figure 5.12(b) the load-deflection curves for temperature-dependent and temperature-independent material properties are shown.

It can be noticed that there is a significant difference between the responses depending on which the material properties are considered as temperature-dependent or not. It is clear that the effect of considering the material properties as temperature-dependent yields softer behaviour. However, in both cases the response of the FGM shell with the properties that are intermediate to metal and ceramic keep lies in between the responses of those made of ceramic and metal.

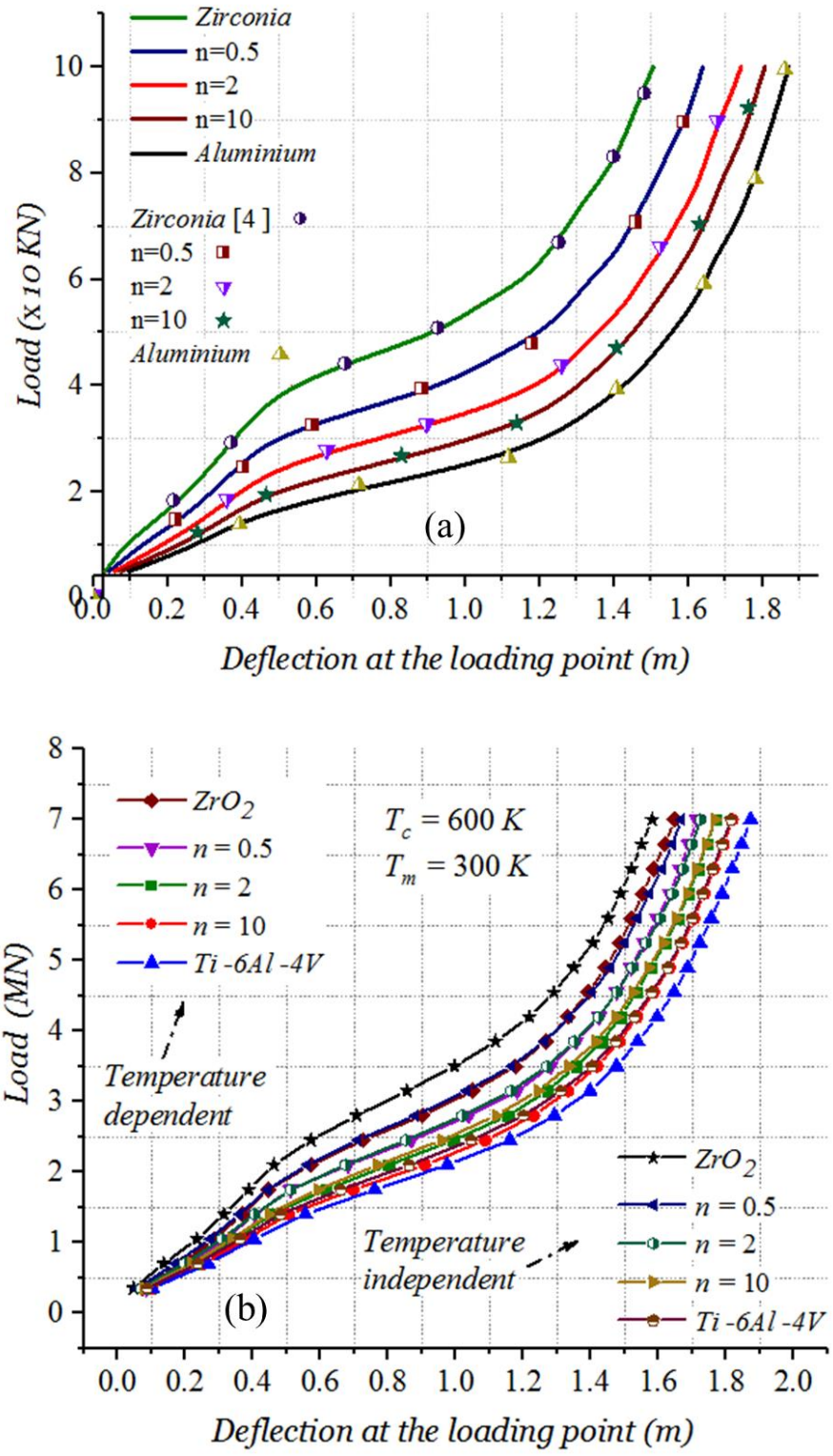

Fig. 5.12 Central deflection of the FGM fixed-free cylinder: (a) mechanical load and (b) thermo-mechanical load.

2.5.2 Dynamic Analysis

In this thermo-mechanical dynamic analysis, the inner surface temperature is held at T_m = 300 K while the outer surface temperature is raised to T_c = 600 K. Then, the cylindrical shell is subjected to two concentrated loads defined as: $P(t) = P_0\left(1-\cos(50t)\right)$, where $P_0 = 5\times10^5$ N. The analyses were performed using a time step Δt = 0.005 s.

This example is performed with ($ZrO_2/Ti\text{-}6Al\text{-}4V$) and ($Si_3N_4/SUS304$) materials. The materials mechanical and thermo-physical proprieties are taken as temperature-dependent.

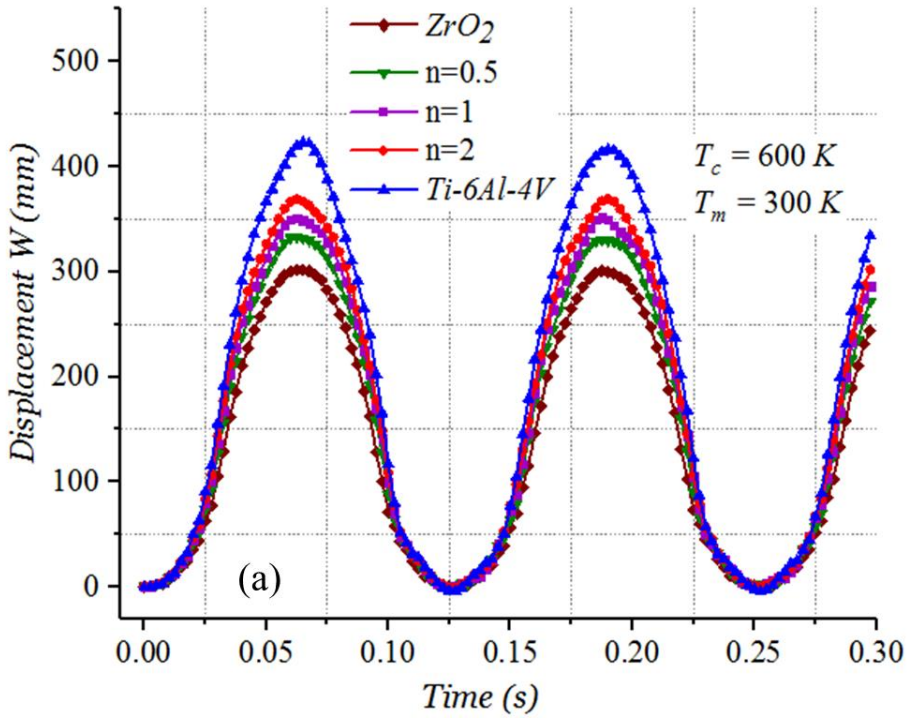

The time history responses depicted in Figures 5.13 and 5.14 show that while deflection is affected by the power-law distribution and temperature, however, they do not affect the vibrations frequencies of the cylindrical shell. Moreover, the results show that the consequences of increasing the temperature gradient are similar to that of increasing the power-law index. This is due to the fact that material properties are temperature dependent. Which means that, the temperature gradient significantly influences the material properties such as the Young's modulus and thermal expansion coefficient gradually through the thickness direction similarly to the power-law distribution on the through thickness material properties. By comparing the effect

of temperature on (ZrO_2/Ti-6A1-4V) and (Si_3N_4/SUS304) materials mixtures, it seems that the importance of this effect depends on the ratio between the thermal expansion coefficient and Young's modulus for each constituent material.

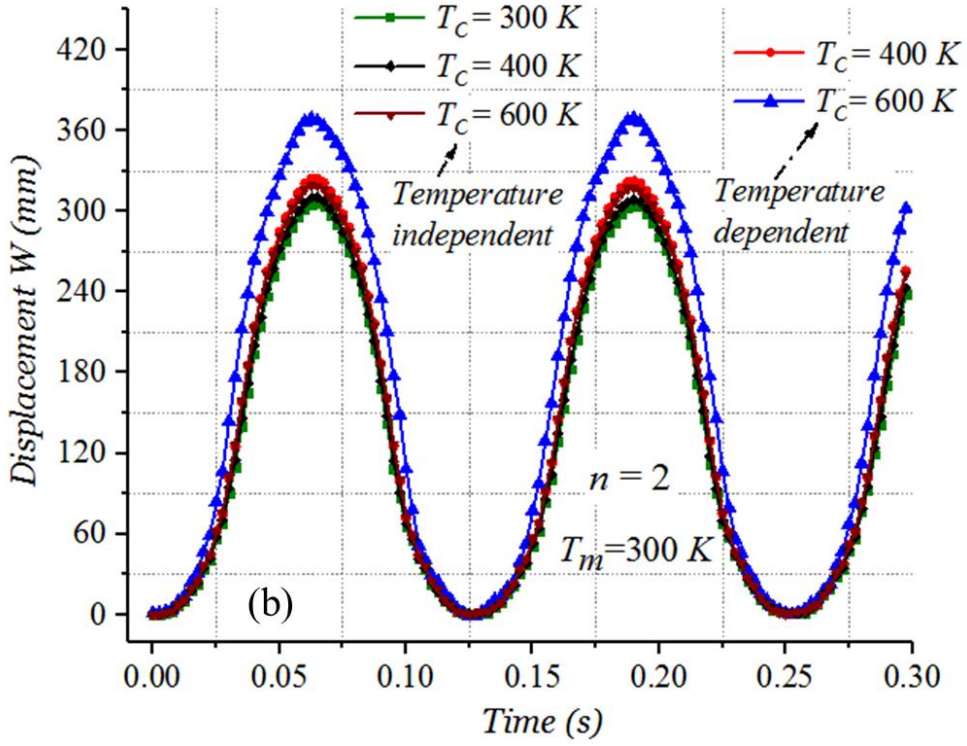

Fig. 5.13 Time history behaviour of the deflection using the conservative/decaying scheme: (a) $ZrO_2 / Ti\text{-}6Al\text{-}4V : T_c = 600\ K$, (b) $ZrO_2 / Ti\text{-}6Al\text{-}4V : n=2$, $T_c = 300$, 400 and $600\ K$.

The dynamic response of the FGM cylinder is intermediate to that of the metal and ceramic ones. A significant difference can be noticed between the maximum deflection of the time history responses of the case when material properties are considered as temperature-dependent and those when the material properties are considered as independent of temperature, especially in high temperature, see Figures 5.13(b) and 5.14(b).

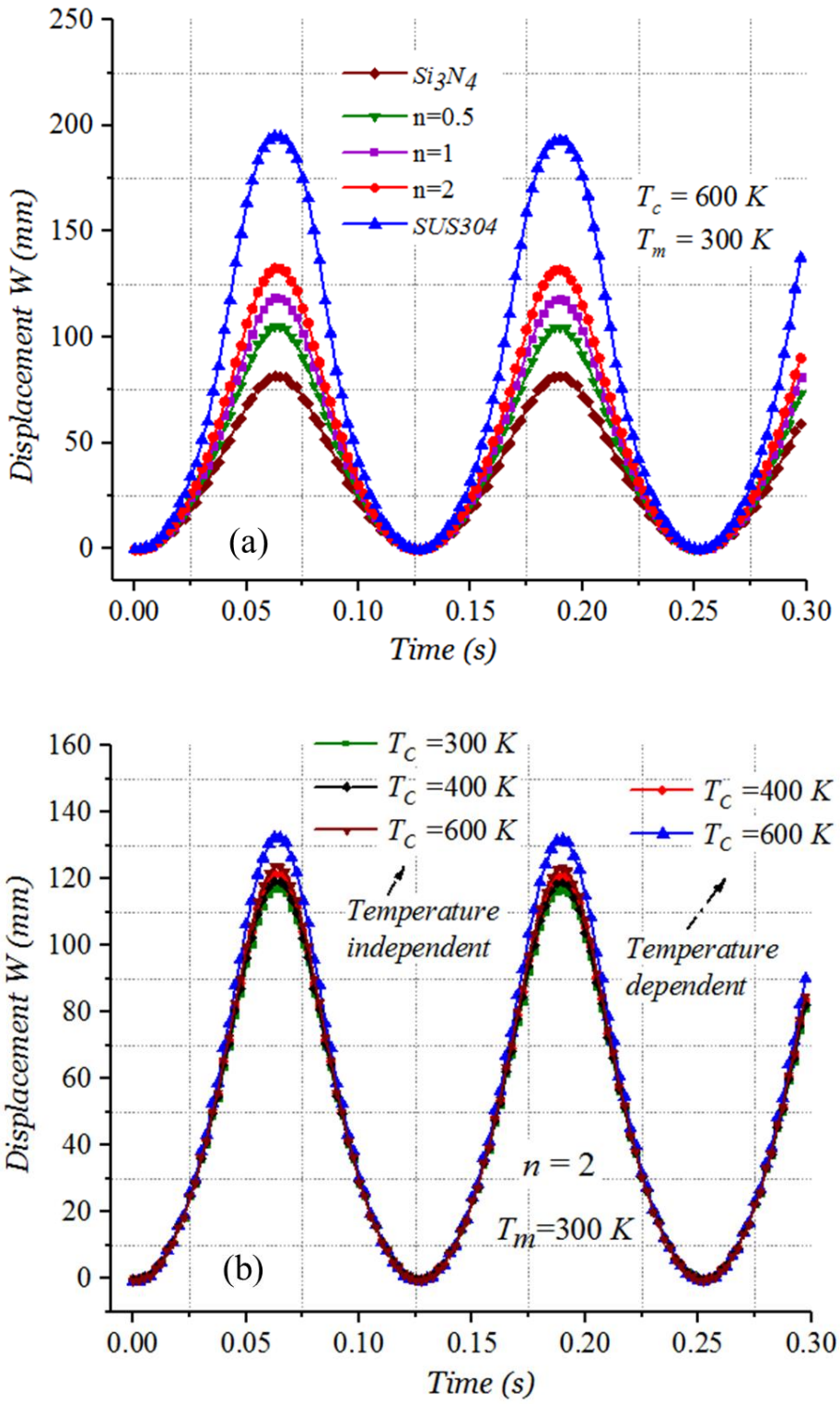

Fig. 5.14 Time history behaviour of the deflection using the conservative/decaying scheme: (a) Si_3N_4 / $SUS304$: T_c=*600 K*, (b) Si_3N_4 / $SUS304$: *n=2*, T_c=*300, 400* and *600 K*.

2.6 Dynamic Buckling of a Cylindrical Shell Panel

In this example, we investigated the nonlinear static and dynamic response of an FGM cylindrical shell panel subjected to a uniformly distributed radial load in a thermal environment. The dynamic nonlinear buckling of the FGM cylindrical shell under thermo-mechanical loading is analysed. As in the first example, we start by assessing the nonlinear static response of the present element in comparison with the solutions available in the literature. Due to the double symmetry of geometry, loading and boundary conditions, only one-quarter of the shell is modelled using 4×4 elements in both static and dynamic analysis.

2.6.1 Static Analysis

In this static analysis test, we investigated the nonlinear static response of the fully clamped FGM cylindrical shell panel subjected to a thermo-mechanical loading presented in Figure 5.15. The thermal load consists of applying a through-thickness temperature field by holding the bottom surface temperature at T_b = 20 °*C*, while the top surface temperature is held at T_t = 200 °*C*. The mechanical load consists of applying a uniform radial load statically increased from 0 up to $q = -10^7\ N/m^2$. The shell's FGM is composed of Aluminium and Zirconia (Al/ZrO_2). In this example, the material properties are considered independent of temperature as taken in [5].

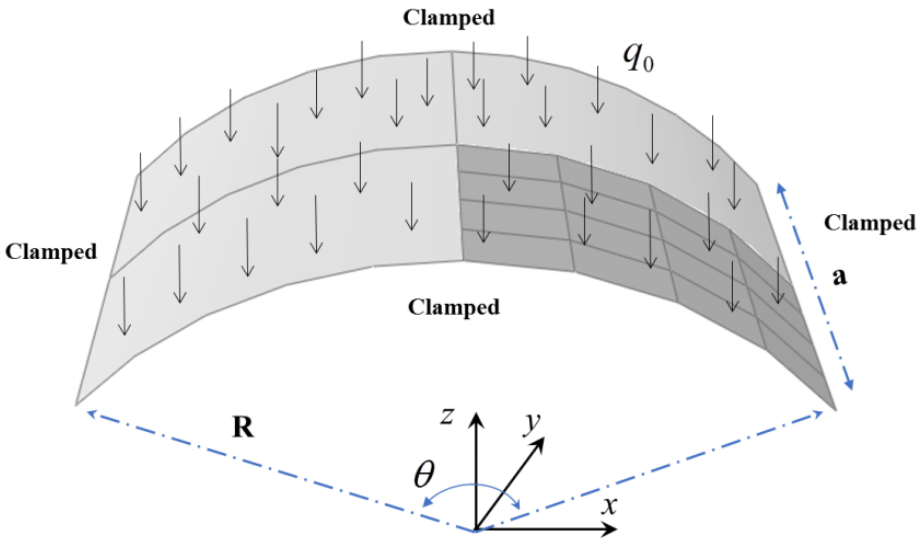

Fig. 5.15 Clamped cylindrical shell panel.

The geometric properties of the panel are a = 0.2 m, R = 1 m, = 0.2 rad and h = 0.01 m. The material properties (computed at temperature $T = 300\ K$) are listed in Table 5.1.

Figure 5.16 depicts the central deflection with the load for clamped Aluminium-Zirconia panel under a uniform load only. It is worth to mention that the displacement of the panel that corresponds to a larger volume fraction exponent is greater than that of the panel that corresponds to a smaller exponent. Note that the response of the panel with properties that are intermediate to metal and ceramic lies in between the response of the ceramic and metal. The same conclusion, the deflections are increased by increasing the volume fraction index *n*.

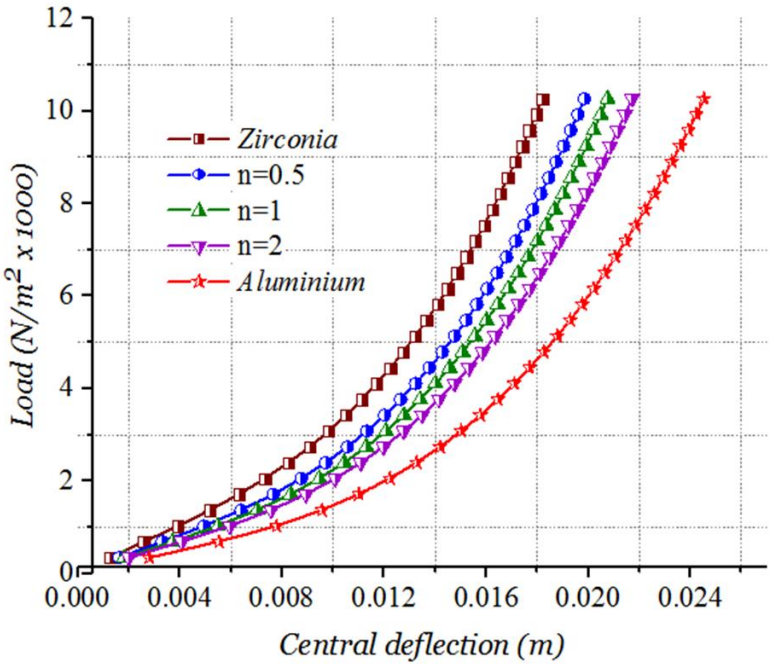

Fig. 5.16 Central deflection of FGM clamped shell panel versus load

The non-dimensional central deflection of the shell panel is depicted versus the load parameter in Figure 5.17. The non-dimensional parameters used in Figure 5.17, are the non-dimensional central deflection $\bar{w} = w/h$ and the load parameter $\bar{q} = q_0 a^4 / E_m h^4$.

It can be seen that the obtained results are in good agreement with those presented in [5]. The slight difference is due to the use of von Kármán theory in [5]. It is worth mentioning that the initial displacement in Figure 5.17 is due to the applied temperature field. Note that the initial central deflection that corresponds to a larger volume fraction exponent is greater than that which

corresponds to a smaller exponent. Under the thermo-mechanical load, the response of the FGM shell with the properties that are intermediate to metal and ceramic lies in between the responses of those made of ceramic and metal.

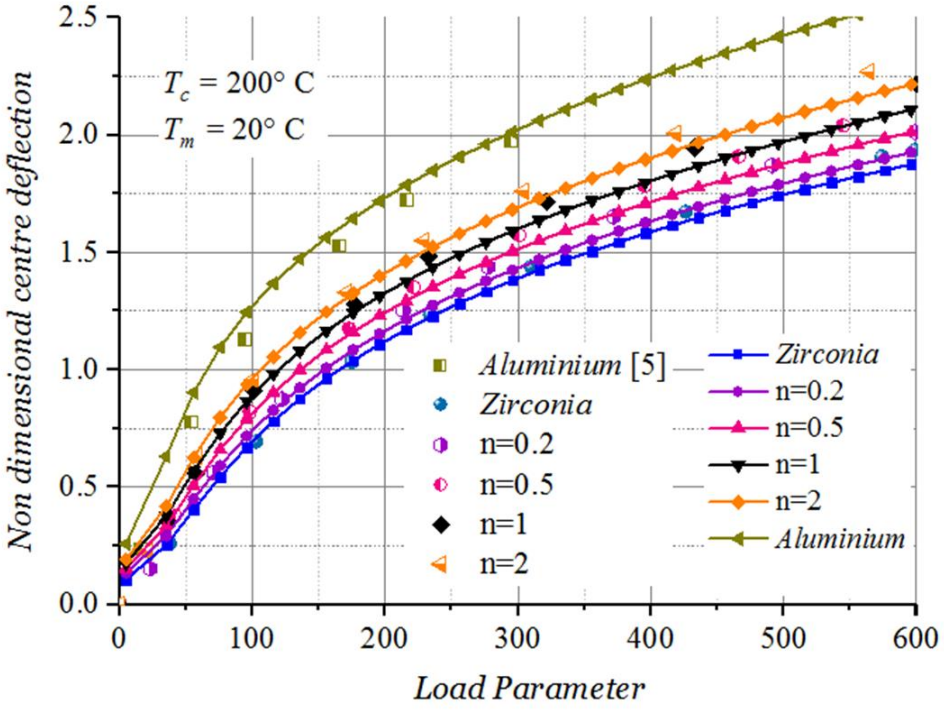

Fig. 5.17 Non-dimensional central deflection vs. load parameter.

2.6.2 Dynamic Analysis

The geometry, loading, and boundary conditions of the cylindrical shell investigated in the dynamic analysis are shown in Figure 5.18. The two straight edges of the shell are simply supported, while the curved edges are free. This example has been used extensively as a benchmark test for nonlinear shell dynamic problems [6-8]. In this dynamic analysis, a temperature field is applied by holding the bottom surface temperature at T_b = 300 K while for the top surface temperature, three cases are considered: (T_t = 300 K, T_t = 400 K, T_t = 600 K). Then, a concentrated load is applied at the central node of the shell. The value of the applied load increases linearly from 0 to 5×10^4 KN in 0.2 s and held constant at that value. This test was performed using the Newmark scheme and the conservative/decaying scheme in order to assess the stability of the conservative/decaying scheme compared to that of Newmark scheme.

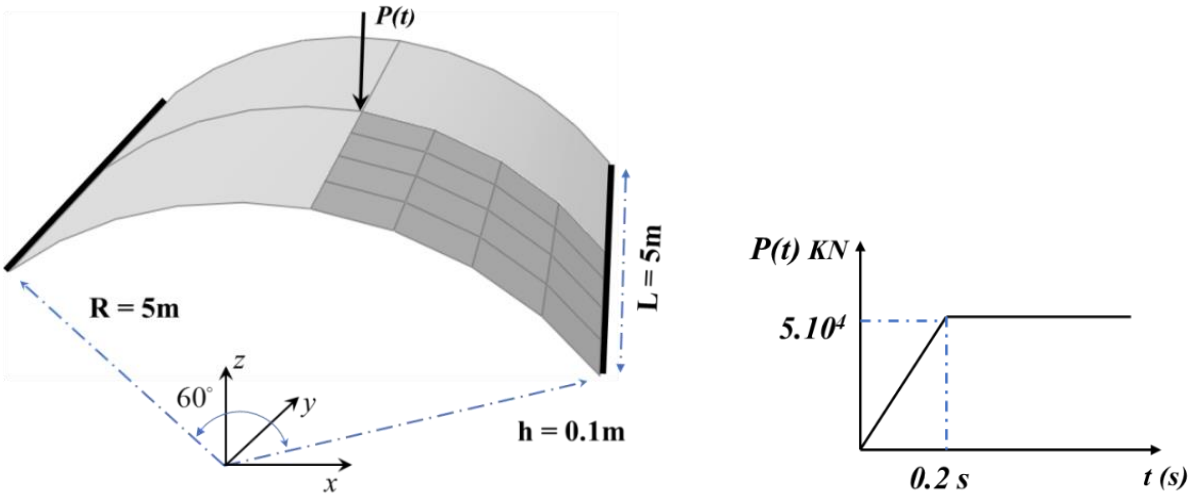

Fig. 5.18 Cylindrical shell panel: geometry, supports and loading.

The time step size for the Newmark scheme is taken equal to Δt = 0.002 *s*, while in the composite scheme is Δt = 0.004 *s* because two sub-steps are performed inside the composite scheme for each time step. In this example, the material's mechanical and thermo-physical properties are taken as temperature-dependent. Two different materials mixture is considered. The first one is the ($ZrO_2 / Ti\text{-}6Al\text{-}4V$), and the second one is the ($Si_3N_4 / SUS304$).

The results produced by the Newmark and the conservative/decaying schemes are shown in Figures 5.19 and 5.20 respectively**.** As shown in Fig. 5.19, when the Newmark scheme is used, accumulation of numerical errors is soon noticed, the energy is not properly conserved/decayed and a point is reached at which the solution cannot proceed any further. On the other hand, the conservative/decaying scheme produced a stable solution until the end of the reported time. These outcomes demonstrate the stability and effectiveness of the predicted nonlinear dynamic response of shells when using conservative/decaying schemes.

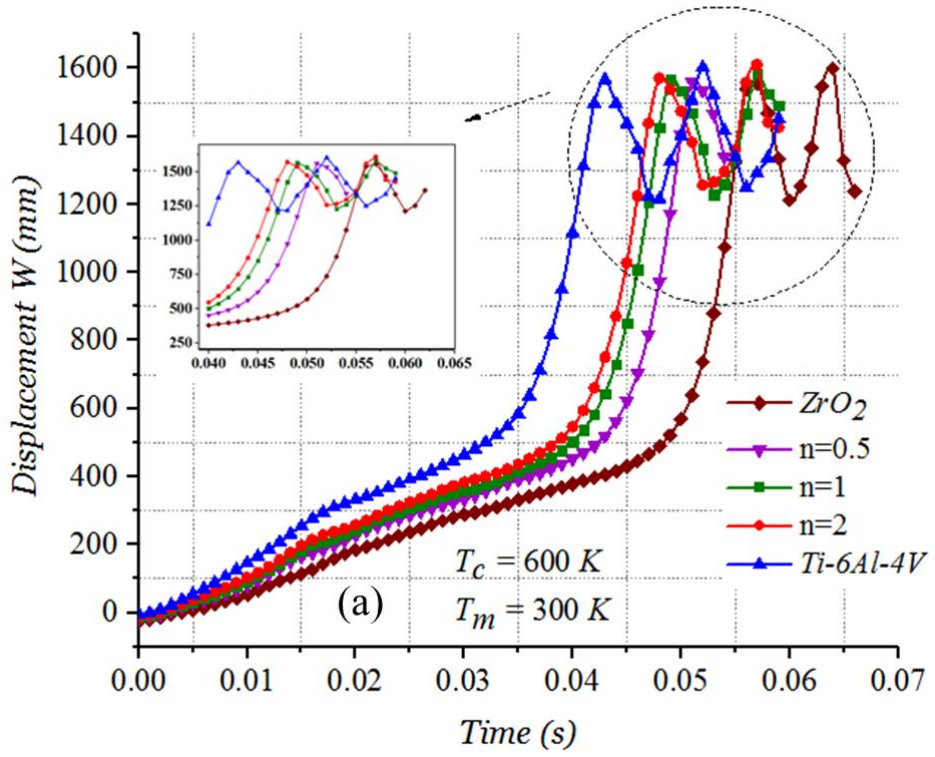
Displacement W (mm)
Time (s)
ZrO_2
n=0.5
n=1
n=2
Ti-6Al-4V
T_c = 600 K
T_m = 300 K
(a)

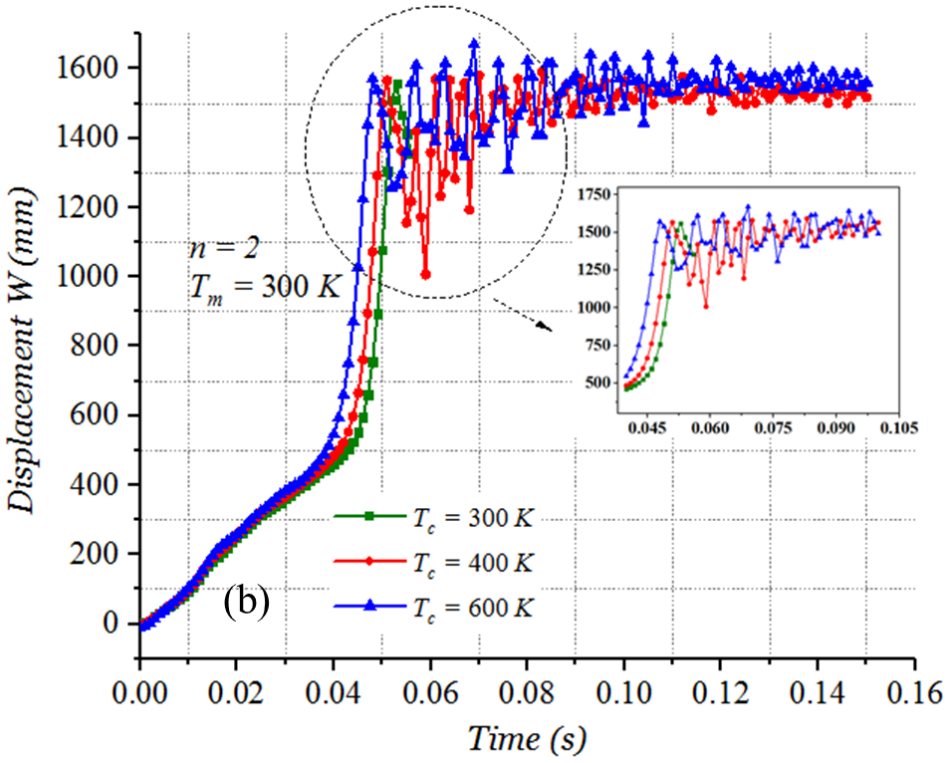
Displacement W (mm)
Time (s)
n = 2
T_m = 300 K
T_c = 300 K
T_c = 400 K
T_c = 600 K
(b)

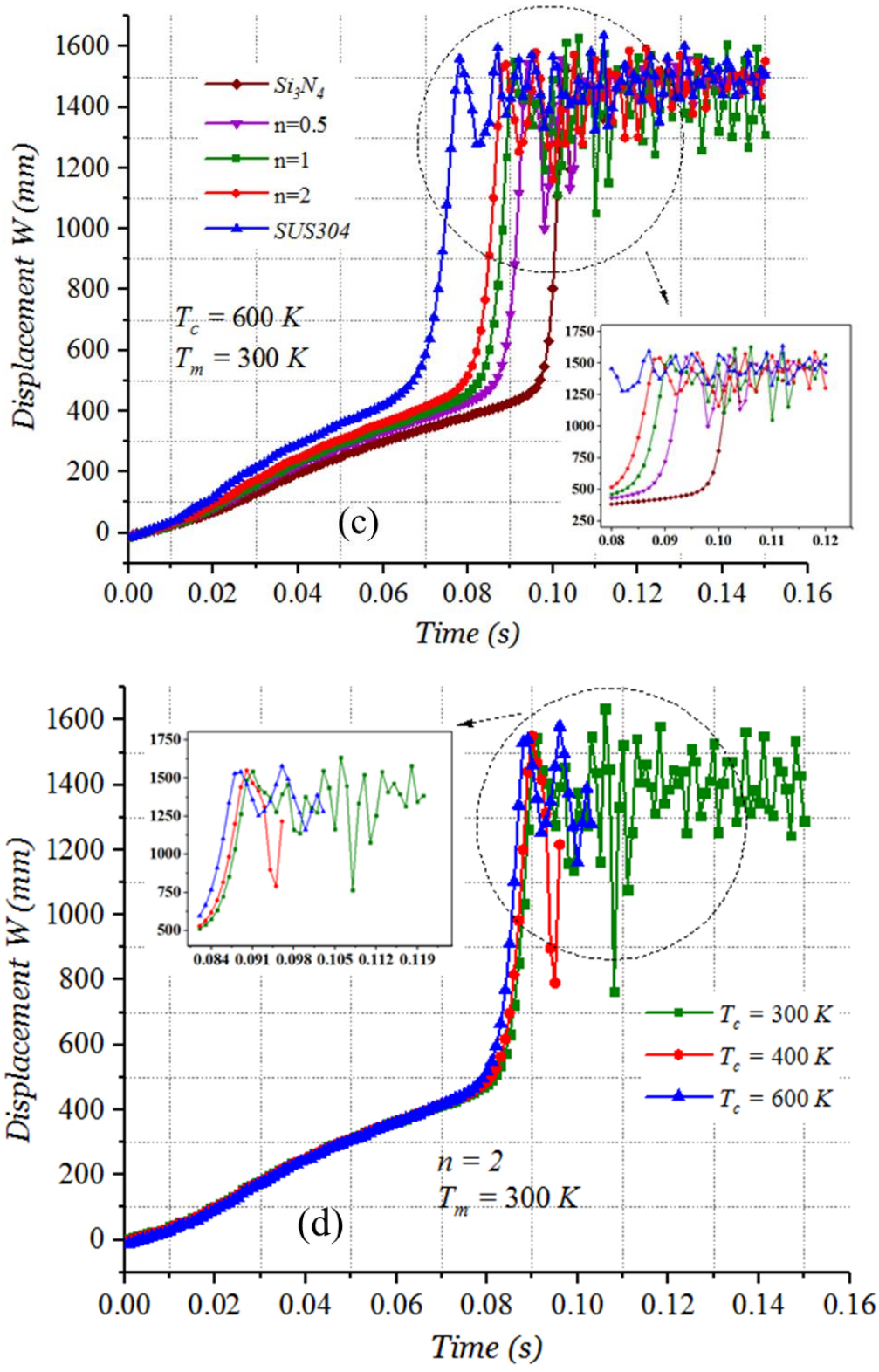

Fig. 5.19 Time history of the central deflection using Newmark scheme: (a) ZrO_2 / Ti - 6Al - 4V : T_c=600 K, (b) ZrO_2 / Ti - 6Al - 4V : n=2, T_c=300, 400 and 600 K, (c) Si_3N_4 / SUS304 : T_c=600 K, (d) Si_3N_4 / SUS304 : n=2, T_c=300, 400 and 600 K.

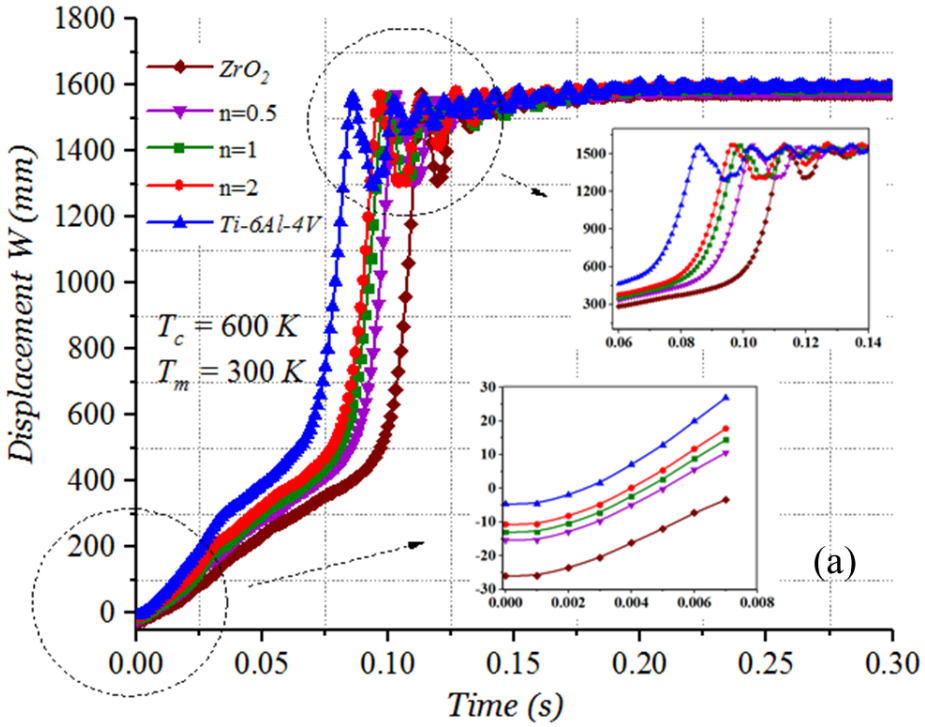
Displacement W (mm)
Time (s)
ZrO2
n=0.5
n=1
n=2
Ti-6Al-4V
Tc = 600 K
Tm = 300 K
(a)

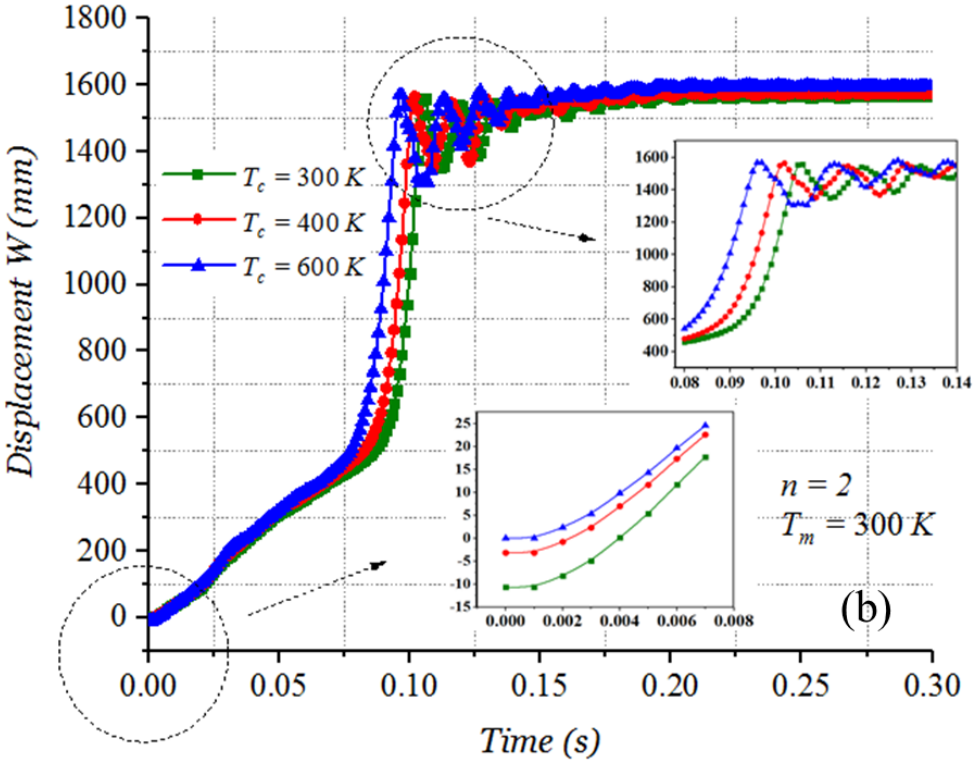
Displacement W (mm)
Time (s)
Tc = 300 K
Tc = 400 K
Tc = 600 K
n = 2
Tm = 300 K
(b)

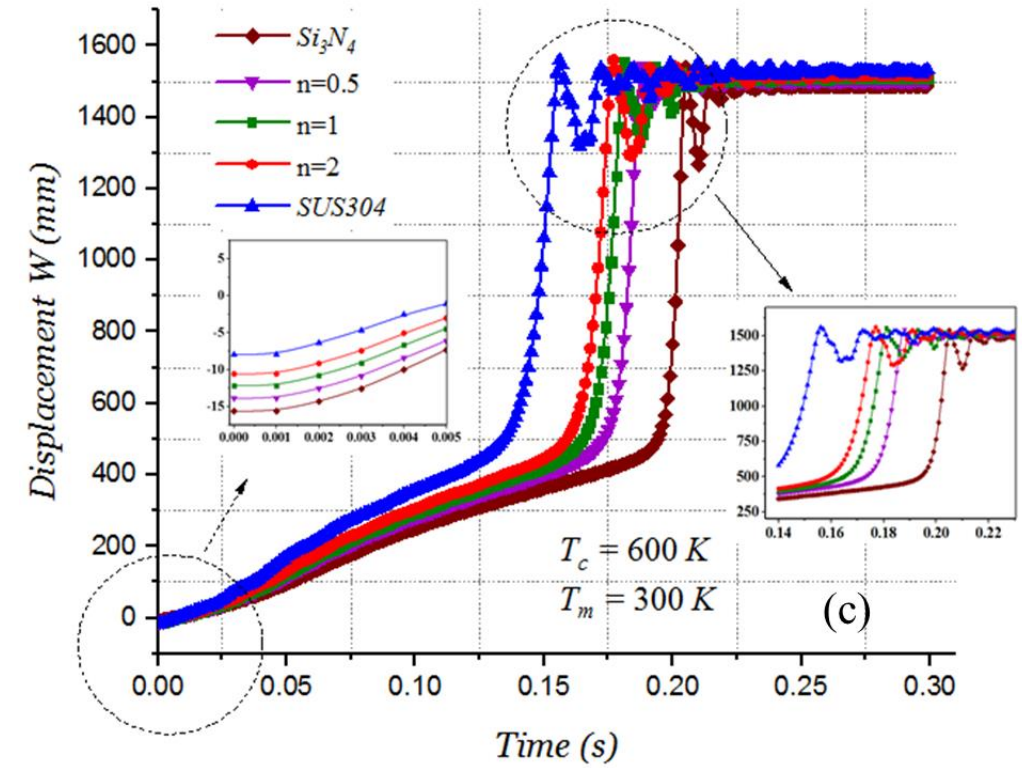
Si_3N_4
n=0.5
n=1
n=2
SUS304
Displacement W (mm)
Time (s)
T_c = 600 K
T_m = 300 K
(c)

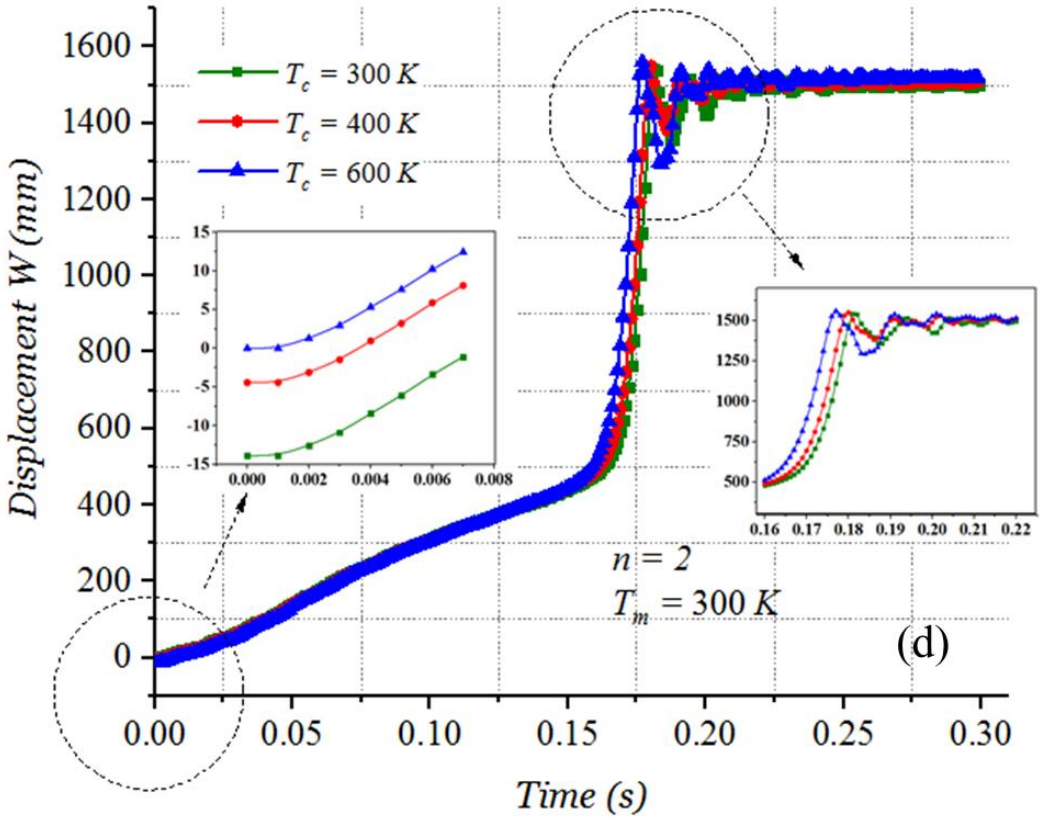
T_c = 300 K
T_c = 400 K
T_c = 600 K
Displacement W (mm)
Time (s)
n = 2
T_m = 300 K
(d)

Fig. 5.20 Time history of the central deflection using the conservative/decaying scheme: (a) $ZrO_2 / Ti-6Al-4V : T_c=600\ K$, (b) $ZrO_2 / Ti-6Al-4V : n=2,\ T_c=300,\ 400$ and $600\ K$, (c) $Si_3N_4 / SUS304 : T_c=600\ K$, (d) $Si_3N_4 / SUS304 : n=2,\ T_c=300,\ 400$ and $600\ K$.

In Figure 5.20, the pre-buckling, buckling and the post-buckling behaviours of the cylindrical panel are clearly shown. It can be seen that the buckling in the metal cylindrical panel is reached faster than that in the ceramic panel, then, the shells keep vibrating around the new equilibrium position. The response of the shell with the properties that are intermediate to metal and ceramic lies in between the responses of those made of ceramic and metal over the whole reported time.

Figures 5.19 and 5.20 clearly show that the power law index has a major effect on the pre-buckling behaviour of FGM shells. Note that the applied loading increases linearly with time and the maximum load is reached at 0.2 s. It can be seen from Figure 5.20(a) that buckling occurs before reaching the maximum load in all the tested FGM shells expect the (Si_3N_4) shell, in which, the buckling occurs after 0.2 s. On the other hand, the temperature has an important effect on the pre-buckling behaviour of the shell, especially in the ($Si_3N_4 / SUS304$) material mixture. For both materials, it can be seen that higher temperatures provoke faster buckling. One can also notice that the post-buckling behaviour has similar profile for all the studied parameters.

2.7 Dynamic-Buckling of a Spherical Cap

In this example, dynamic behaviour of clamped spherical cap with isotropic material subjected to concentrated apex load is examined, this test was proposed in [9]. Due to the double symmetry of geometry, loading and boundary conditions, only one-quarter of the shell is modelled using 8×8 elements. The time step is taken as $\Delta t = 2\ \mu s$. The nonlinear dynamic response, represented by the normalized vertical displacement at shell apex is shown in Figure. 5.21. The present results are found to be in good agreement with those reported by [9].

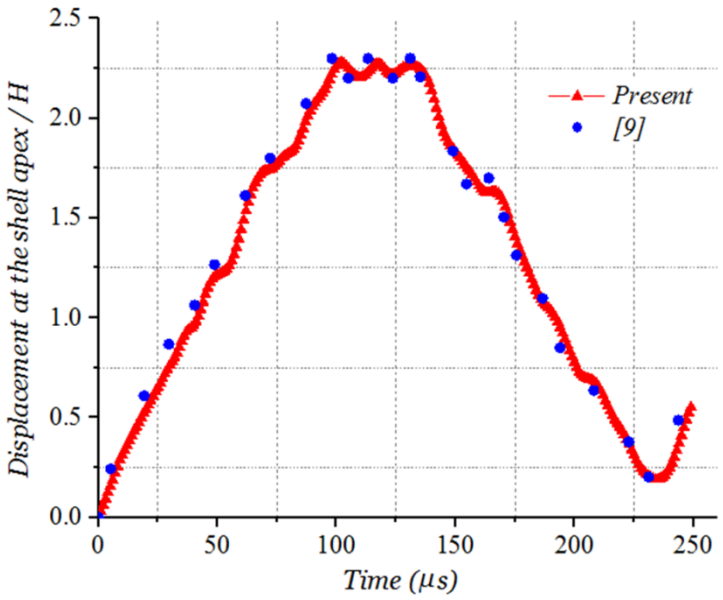

Fig. 5.21 Nonlinear dynamic response of the isotropic shallow spherical cap.

Next, dynamic nonlinear response and post-buckling behaviour of an FGM spherical cap subjected to concentrated apex dynamic load in addition to a thermal load is investigated. Material and geometric properties of the spherical cap presented in [10] are given in Table 5.3 and Figure 5.22. Two different material mixtures are considered, The first one is the (ZrO_2/Ti-6A1-4V), and the second one is the (Si_3N_4/SUS304). The materials mechanical and thermo-physical proprieties are taken as temperature-dependent.

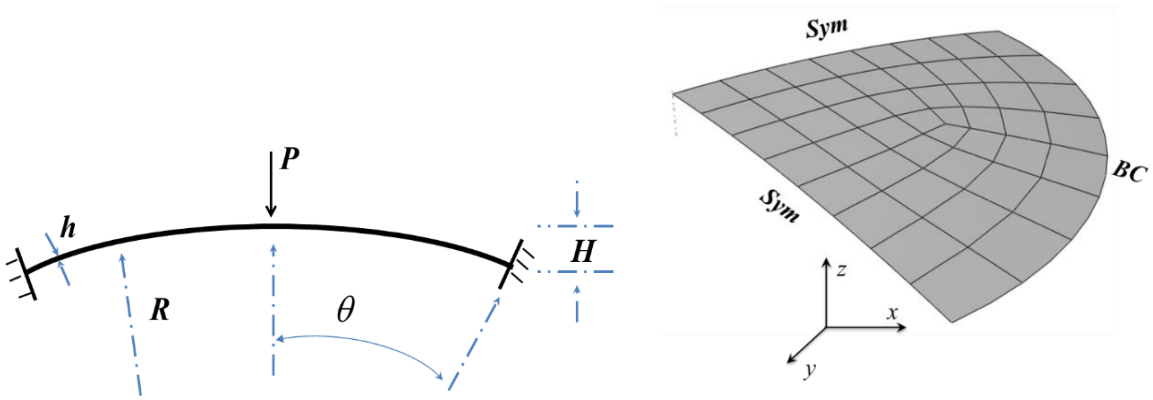

Fig. 5.22 Spherical cap: geometry, loading and mesh.

Table 5.3: Material and geometric properties of the spherical cap

Parameter	*R (mm)*	*Θ*	*h (mm)*	*H (mm)*
Value	*120.9*	*10.9°*	*0.4*	*2.182*

At first, the temperature field is applied by holding the bottom surface temperature at T_b = 300 *K* while for the top surface temperature T_t, three cases are considered: (T_t = 300 *K*, T_t = 400 *K*, T_t = 600 *K*). Then, a concentrated mechanical load is applied at the shell apex. The time step size for the composite scheme is Δt = 10 μs. Dynamic-buckling of the spherical cap is investigated with two boundary conditions:

1- Clamped Edge BC

In this case, the value of the applied mechanical load increases linearly from 0 to 2 *KN* in 100 μs and held constant at that value. The nonlinear dynamic response, represented by the normalized vertical displacement at the shell apex is shown in Figure 5.23.

It is observed that as the power-law index increases the maximum displacement of the dynamic response increases. This is due to the fact that the stiffness reduces with the increase in the power-law index. Similar behaviour is also observed by increasing the temperature gradient because Young's modulus becomes weak as temperature goes up. In this example, the (ZrO_2/Ti-6A1-4V) material mixture seems to be more sensitive to the effect of temperature than the (Si_3N_4/SUS304) material mixture. It seems that, according to the ratio between the thermal expansion coefficient and Young's modulus for each constituent material, the effect of temperature can be more or less significant than the power law index effect.

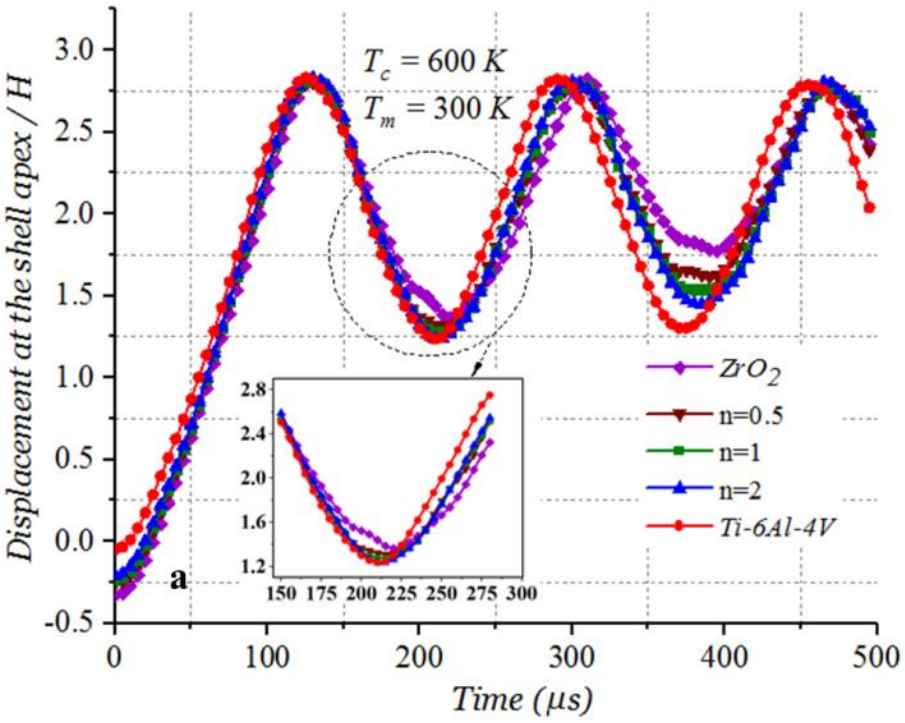
T_c = 600 K
T_m = 300 K
ZrO_2
n=0.5
n=1
n=2
Ti-6Al-4V
a
Displacement at the shell apex / H
Time (μs)

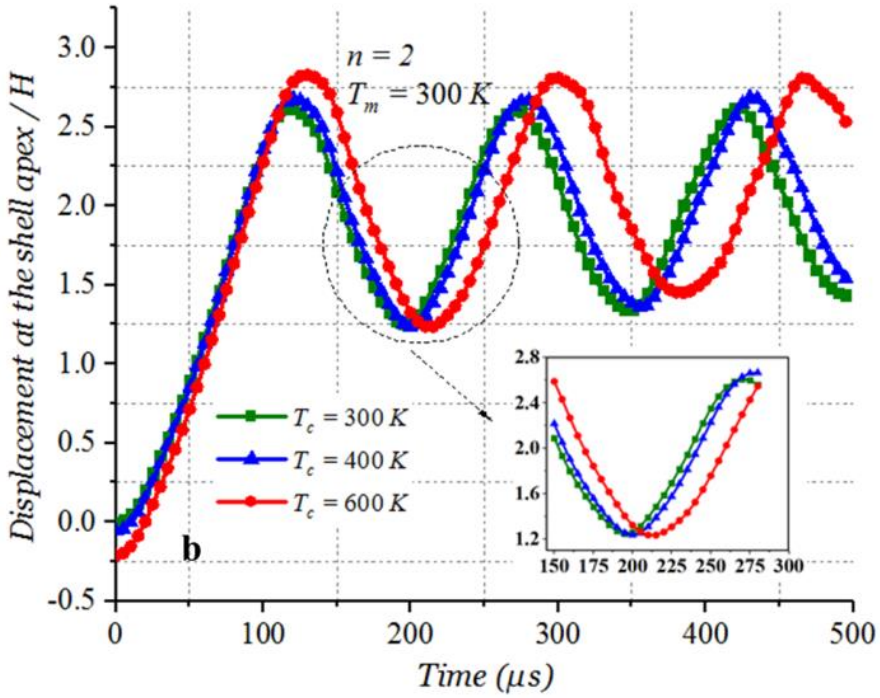
n = 2
T_m = 300 K
T_c = 300 K
T_c = 400 K
T_c = 600 K
b
Displacement at the shell apex / H
Time (μs)

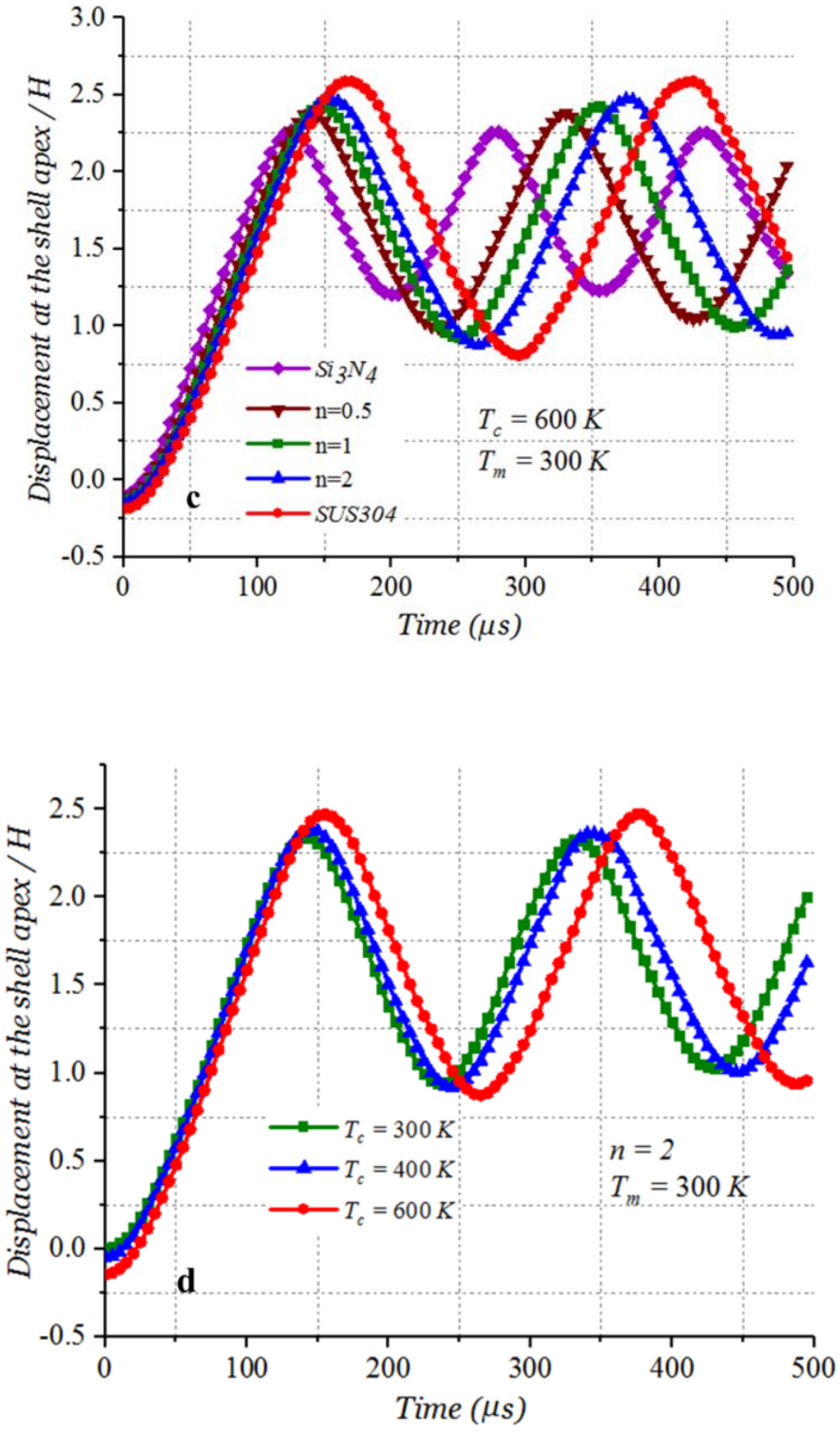

Fig. 5.23 Time history of the normalized deflection of the clamped spherical cap: (a) ZrO_2/Ti-6A1-4 : T_c=*600 K*, (b) ZrO_2/Ti-6A1-4V : *n=2*, T_c=*300*, *400* and *600 K*, (c) Si_3N_4/SUS304 : T_c=*600 K*, (d) Si_3N_4/SUS304 : *n=2*, T_c=*300*, *400* and *600 K*.

2- Hinged Edge BC

In this case, the value of the applied mechanical load increases linearly from 0 to 1 *KN* in 100 μs and held constant at that value. The adopted boundary conditions are: $u = v = w = 0$ at H=0. The nonlinear dynamic response, represented by the normalized vertical displacement at the shell apex is shown in Figure 5.24.

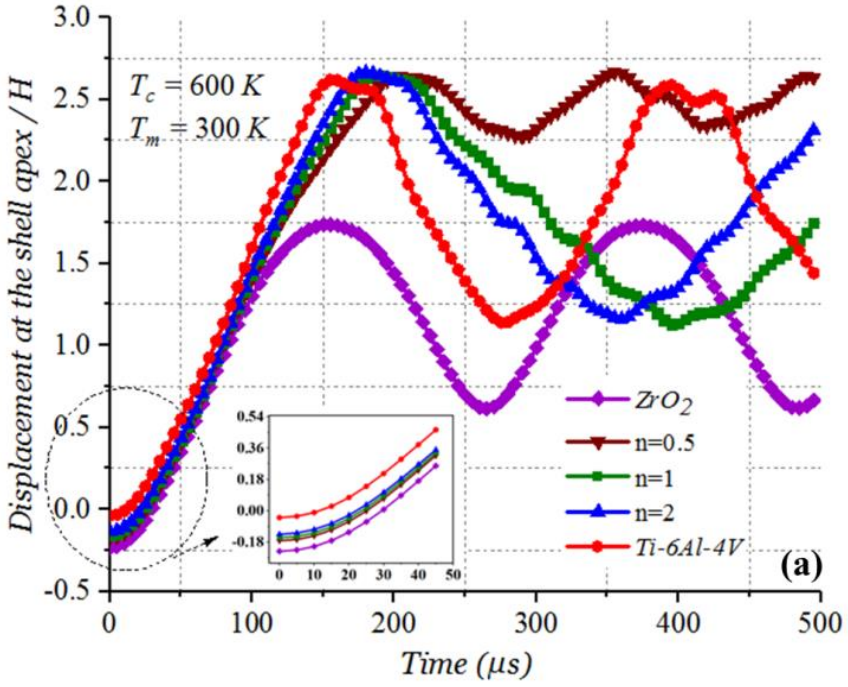

Similar behaviour is also found for hinged boundary conditions as shown in Figure 5.24. It seems that the influence of the temperature gradient on the post-buckling behaviour of the hinged spherical cap is marked and can be considerable. post-buckling behaviour can radically change by the volume fraction index as well as temperature gradient due to the shell stiffness decrease. It is worth mentioning that for the (Si_3N_4/SUS304) material mixture, in the case when T_c=*600 K* , the initial displacement due to the temperature applied field is considerable compared to the initial geometry, which leads to a considerable change of the initial stiffness and geometry of the shell. As a result, the dynamic response of the spherical cap can radically change as clearly shown in Figure 5.24(d) .

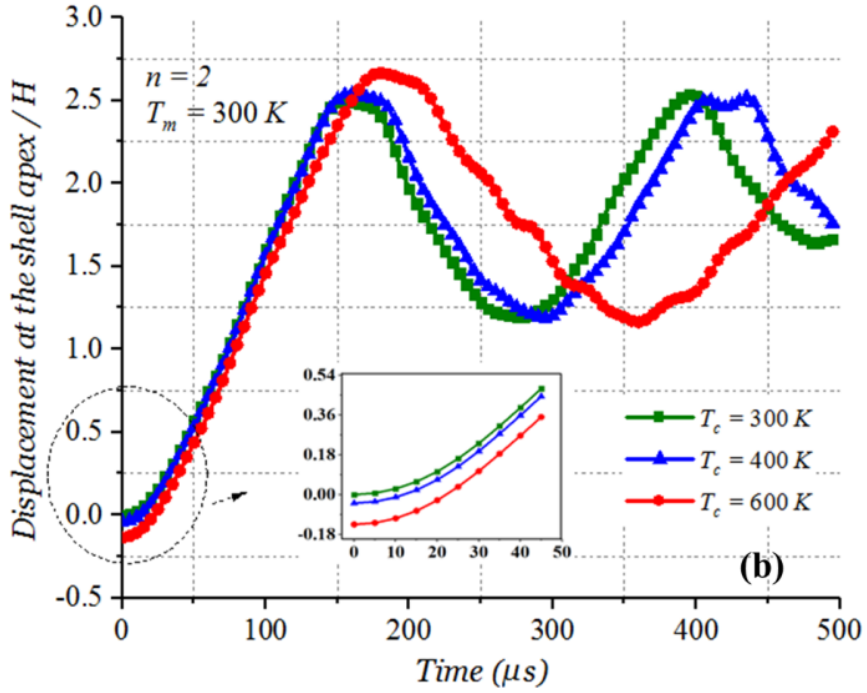
n = 2
T_m = 300 K
Displacement at the shell apex / H
Time (μs)
T_c = 300 K
T_c = 400 K
T_c = 600 K
(b)

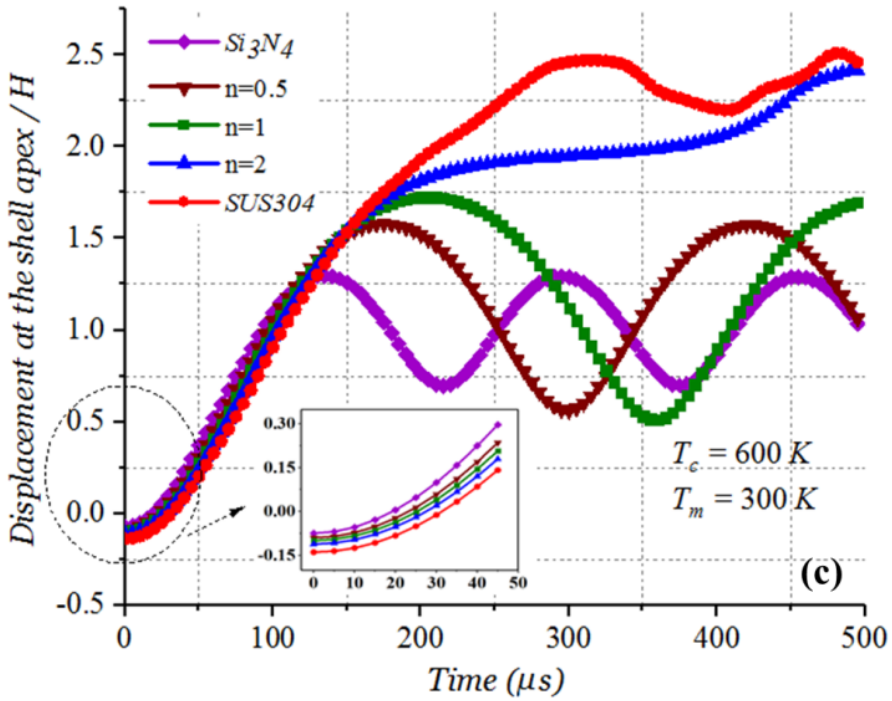
Si_3N_4
n=0.5
n=1
n=2
SUS304
Displacement at the shell apex / H
Time (μs)
T_c = 600 K
T_m = 300 K
(c)

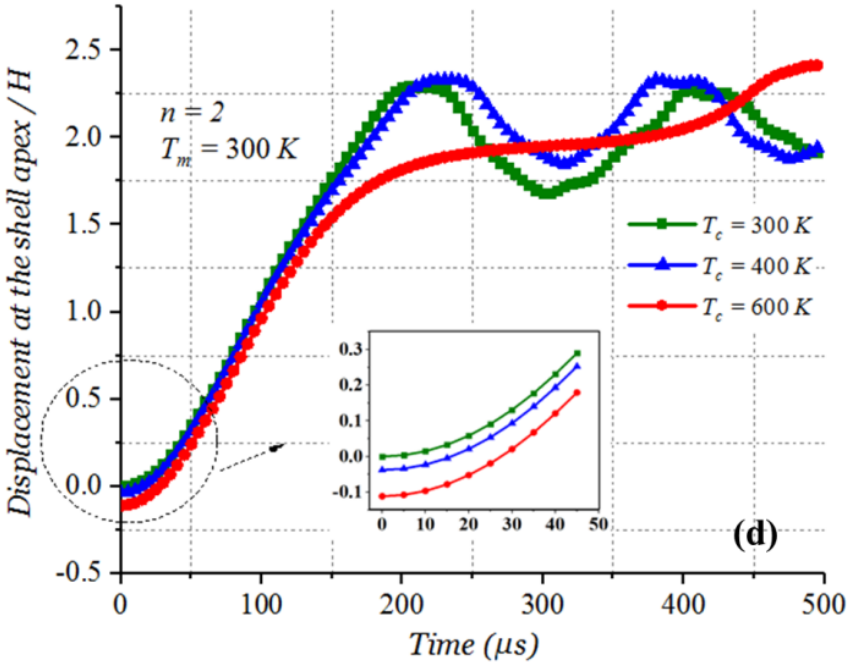

Fig. 5.24 Time history of the normalized deflection of the clamped spherical cap: (a) ZrO_2/Ti-6A1-4V : T_c=*600 K*, (b) ZrO_2/Ti-6A1-4V : *n=2*, T_c=*300*, *400* and *600 K*, (c) Si_3N_4/SUS304 : T_c=*600 K*, (d) Si_3N_4/SUS304 : *n=2*, T_c=*300*, *400* and *600 K*

Most of these results were published in an international journal as part of this study found in [11].

3. Conclusion

Nonlinear transient dynamic, dynamic buckling, and post-buckling responses of FGM plates and shells with temperature-dependent material properties subjected to thermo-mechanical loading has been investigated through using an implicit conservative/decaying direct time integration scheme. In the numerical analysis, some comparisons are shown to verify the correctness and effectiveness of the present formulation, then, the thermo-mechanical behaviour of several examples is investigated using different values of volume fraction index and under different sets of thermal environmental conditions. The parametric study show and confirm that the power-law index of the volume fraction has the most significant effect on both static and dynamic responses of FGM structures under different sets of thermal environmental conditions.

Moreover, it is shown that the influence of temperature on the effective material properties such as Young's modulus and thermal expansion coefficient is non-negligible.

Dynamic-buckling of cylindrical and spherical FGM shells in thermal environments for different volume fraction indices, temperature gradient along with different boundary conditions have been presented. It is concluded that the gradation in the material properties and the temperature field have a considerable influence on the characteristics of the buckling and post-buckling behaviour of FGM shells. The study confirm that the characteristics of the nonlinear dynamic buckling can be significantly influenced by the through thickness gradient of temperature as much as the power-law index.

The use of a conservative/decaying integration scheme allowed us to efficiently study the dynamic buckling of a cylindrical shell. The conservative/decaying scheme exhibits high stability and accuracy during the pre-buckling, buckling and post buckling phases. The study confirm that the characteristics of the nonlinear dynamic buckling are significantly influenced by the temperature and by the effect of considering the material properties as temperature dependent.

4. References

[1] Tran LV, Van PP, Lee J, Wahab MA, Nguyen-Xuan H. Isogeometric analysis for nonlinear thermomechanical stability of functionally graded plates. Comp Structures 2016; 140:655-667.

[2] Huang XL, Shen HS. Nonlinear vibration and dynamic response of functionally graded plates in thermal environments. International Journal of Solids and Structures 2004; 41(9-10):2403-2427.

[3] Moita JS, Araújo AL, Correia VF, Soares CMM, Herskovits J. Buckling and nonlinear response of functionally graded plates under thermo-mechanical loading. Composite Structures 2018; 202:719-730.

[4] Mars J, Koubaa S, Wali M, Dammak F. Numerical analysis of geometrically non-linear behavior of functionally graded shells. Lat. Am. J. Solids Struct. 2017; 14(11):1952-1978.

[5] Zhao X, Liew KM. Geometrically nonlinear analysis of functionally graded shells. International Journal of Mechanical Sciences 2009; 51(2):131-144.

[6] JinSong Y, PinQi X. Energy conserving and decaying algorithms for corotational finite element nonlinear dynamic responses of this shells. Science China Technological Scinces 2012; 55:3311-3321.

[7] Bottasso CL, Bauchau OA, Choi JY. An energy decaying scheme for nonlinear dynamics of shells. Computer Methods in Applied Mechanics and Engineering 2002; 191(27-28):3099-3121.

[8] Kuhl D, Ramm E. Generalized energy-momentum method for non-linear adaptive shell dynamics. Computer Methods in Applied Mechanics and Engineering 1999; 178(3-4):343-366.

[9] Hajlaoui A, Triki E, Frikha A, Wali M and Dammak F. Nonlinear dynamics analysis of FGM shell structures with a Higher order shear strain enhanced solid-shell element. Latin American Journal of Solids and Structures 2017; 14:72-91.

[10] Frikha A, Wali M, Hajlaoui A, Dammak F. Dynamic response of functionally graded material shells with a discrete double directors shell element. Composite Structures 2016; 154:385-395.

[11] Abuteir BW, Harkati E, Boutagouga D, Mamouri S, Djeghaba K. Thermo-mechanical nonlinear transient dynamic and dynamic-buckling analysis of functionally graded material shell structures using an implicit conservative/decaying time integration scheme. Mechanics of Advanced Materials and Structures 2021; 1-20.

Conclusion

In this thesis, we present the formulation of a curved degenerated shell element for geometrically nonlinear static, transient dynamic, dynamic-buckling, and post-buckling analysis of functionally graded plates, cylindrical and spherical shells with temperature-dependent material properties in thermal environments using a conservative/decaying time integration scheme. For this purpose, an 8-node curved degenerated shell element is used for finite element discretization. The shell element is formulated in the framework of the Total Lagrangian Formulation with thermal strains/stresses taken into account using the Green-Lagrange geometric nonlinearity. The bending and membrane strain-coupling considered in the element formulation allows to efficiently capture the high membrane-bending interaction in FGM plates/shells. Consequently, a minimal number of elements can be used to mesh plane and curved geometries, compared to plane elements, which is a crucial concern to minimise the computational time, especially in nonlinear dynamic analysis. In the presented formulation, to overcome membrane and transverse shear locking, an efficient modified reduced numerical integration scheme is adopted. Furthermore, an implicit conservative/decaying direct time integration scheme is used herein to obtain the time-history response of FGM shells. The conservative/decaying scheme is expected to be efficient in energy conservation and parasitic high-frequency dissipation providing stable and accurate dynamic responses. These desired properties of the conservative/decaying scheme allow us to efficiently study the nonlinear dynamic buckling behaviour of an FGM shell in a thermal environment.

In the numerical analysis, some comparisons are shown to verify the correctness and effectiveness of the present formulation, then, the thermo-mechanical behaviour of several examples is investigated using different values of volume fraction index and under different sets of thermal environmental conditions. The parametric study show and confirm that the power-law index of the volume fraction has the most significant effect on both static and dynamic responses of FGM structures under different sets of thermal environmental conditions. Moreover, it is shown that considering the material properties as temperature-dependent has a significant influence on the nonlinear static and dynamic behaviour of FGM shells. It is shown that the

influence of temperature on the effective material properties such as Young's modulus and thermal expansion coefficient is non-negligible. It is concluded that the gradation in the material properties and the temperature field have a considerable influence on the characteristics of the buckling and post-buckling behaviour of FGM shells. The study confirm that the characteristics of the nonlinear dynamic buckling can be significantly influenced by the through thickness gradient of temperature as much as the power-law index. The use of a conservative/decaying integration scheme allowed us to efficiently study the dynamic buckling of a cylindrical shell. The conservative/decaying scheme exhibits high stability and accuracy during the pre-buckling, buckling and post buckling phases. The study confirm that the characteristics of the nonlinear dynamic buckling are significantly influenced by the temperature and by the effect of considering the material properties as temperature dependent.

APPENDIX A

Shear correction factor pseudo algorithm:

- Calculate the stiffness matrix H_m, H_{mf}, H_f and $\overline{H}_c$.

$$\left(H_m, H_{mf}, H_f\right) = \int_{-h/2}^{h/2} \left(1, z, z^2\right) H\left(z\right) dz, \quad \overline{H}_c = \int_{-h/2}^{h/2} H_\tau\left(z\right) dz$$

- Calculate flexibility matrix F_m, F_{mf} and F_f

$$\begin{bmatrix} F_m & F_{mf} \\ F_{mf} & F_f \end{bmatrix} = \begin{bmatrix} H_m & H_{mf} \\ H_{mf} & H_f \end{bmatrix}^{-1}$$

- Initialization

$$F_{11} = 0$$

- Loop on thickness
  - Loop on integration points

$$A\left(z\right) = H\left(z\right)\left(F_{mf} + zF_f\right)$$

$$D_1\left(z\right) = -\frac{1}{2}\int_{-h/2}^{z} \begin{bmatrix} A_{11} + A_{33} & A_{13} + A_{32} \\ A_{31} + A_{23} & A_{22} + A_{33} \end{bmatrix} dz$$

$$F_{11} = \int_{-h/2}^{h/2} D_1^T H_\tau^{-1} D_1 dz$$

  End loop

End loop

$$H_c = F_{11}^{-1}$$

$$k_1 = \left(H_c\right)_{11} \Big/ \left(\overline{H}_c\right)_{11}, \quad k_2 = \left(H_c\right)_{22} \Big/ \left(\overline{H}_c\right)_{22}, \quad k_{12} = \left(H_c\right)_{12} \Big/ \left(\overline{H}_c\right)_{12}$$

APPENDIX B

The two dimensional shape function are defined as follows:

$$N_1(\xi,\eta) = -\frac{1}{4}(1-\xi)(1-\eta)(1+\xi+\eta) \qquad N_2(\xi,\eta) = -\frac{1}{4}(1+\xi)(1-\eta)(1-\xi+\eta)$$

$$N_3(\xi,\eta) = -\frac{1}{4}(1+\xi)(1+\eta)(1-\xi-\eta) \qquad N_4(\xi,\eta) = -\frac{1}{4}(1-\xi)(1+\eta)(1+\xi-\eta)$$

$$N_5(\xi,\eta) = \frac{1}{2}(1-\xi^2)(1-\eta) \qquad N_6(\xi,\eta) = \frac{1}{2}(1+\xi)(1-\eta^2)$$

$$N_7(\xi,\eta) = \frac{1}{2}(1-\xi^2)(1+\eta) \qquad N_8(\xi,\eta) = \frac{1}{2}(1-\xi)(1-\eta^2)$$

APPENDIX C

Newmark integration scheme procedure:

A. Initial calculations:

- Select time step size Δt and calculate the constants b_i.
- Initialize $u(0)=u_0$, $\dot{u}(0)=\dot{u}_0$ and solve for the initial acceleration:

  $\ddot{u}_0 = M^{-1}\left(F_{Ext}(0) - C\dot{u}_0 - Ku_0\right)$.

- Form the matrices K, M and C.

B. For each time step:

- Calculate tangent stiffness matrix : $K_T = \int_V B^T \cdot C \cdot B + G^T \cdot H^m \cdot G + G^T \cdot H^{th} \cdot G \cdot dV$.
- Form and triangularize the effective stiffness matrix : $\overline{K} = K_T + b_1 M + b_4 C$.
- Form the effective load vector $R_{t+\Delta t}$.

C. For each iteration (Newton-Raphson algorithm):

- Solve for displacements at time $t+\Delta t$: $\overline{K} \cdot u_{t+\Delta t} = R_{t+\Delta t}$.
  - The internal strains and stresses are calculated in the initial un-deformed configuration of the precedent step.
  - The new solution is obtained after linearization of the problem by calculating the internal strains and stresses in the initial un-deformed configuration of the precedent step.
  - The solution is used to proceed to the next step.
- Check for convergence of the iteration process (if OK continue, else go to C).
- Calculate velocities and accelerations at $t+\Delta t$:

$$\begin{cases} {}^{t+\Delta t}\ddot{u} = b_1\left[{}^{t+\Delta t}u - {}^{t}u\right] + b_2\,{}^{t}\dot{u} + b_3\,{}^{t}\ddot{u} \\ {}^{t+\Delta t}\dot{u} = b_4\left[{}^{t+\Delta t}u - {}^{t}u\right] + b_5\,{}^{t}\dot{u} + b_6\,{}^{t}\ddot{u} \end{cases}$$

- $t = t + \Delta t$.
- Go to B.

APPENDIX D

Bathe integration scheme procedure:

A. Initial calculations:

- Select time step size Δt and calculate the constants b_i ($\Delta t = \Delta t / 2$).
- Initialize $u(0) = u_0$, $\dot{u}(0) = \dot{u}_0$ and solve for the initial acceleration:

  $\ddot{u}_0 = M^{-1}\left(F_{Ext}(0) - C\dot{u}_0 - Ku_0\right)$.

- Form the matrices K, M and C.

B. For each time step: (Δt) is subdivided into two equal sub-steps:

- Calculate tangent stiffness matrix : $K_T = \int_V B^T \cdot C \cdot B + G^T \cdot H^m \cdot G + G^T \cdot H^{th} \cdot G \cdot dV$.
- Form and triangularize the effective stiffness matrix :

  For $t + \Delta t$: $\quad \overline{K} = K_T + \left(9/\Delta t^2\right) \cdot M + \left(3/\Delta t\right) \cdot C$

  For $t + \left(\Delta t / 2\right)$: $\quad \overline{K} = K_T + \left(16/\Delta t^2\right) \cdot M + \left(4/\Delta t\right) \cdot C$

- Form the effective load vector for the two sub-steps $R_{t+\Delta t}$ and $R_{t+(\Delta t/2)}$.

C. For each iteration (Newton-Raphson algorithm):

- Solve for displacements at time $t + \Delta t$ and $t + \left(\Delta t / 2\right)$:

  $\overline{K} \cdot u_{t+\Delta t} = R_{t+\Delta t}$ and $\overline{K} \cdot u_{t+(\Delta t/2)} = R_{t+(\Delta t/2)}$

  - The internal strains and stresses are calculated in the initial un-deformed configuration of the precedent step.
  - The new solution is obtained after linearization of the problem by calculating the internal strains and stresses in the initial un-deformed configuration of the precedent step.
  - The solution is used to proceed to the next step.
- Check for convergence of the iteration process (if OK continue, else go to C).

- Calculate velocities and accelerations at $t+\Delta t$ and $t+(\Delta t/2)$:

$$\begin{cases} {}^{t+\Delta t}\dot{u} = \dfrac{1}{\Delta t}\,{}^{t}u - \dfrac{4}{\Delta t}\,{}^{t+\frac{\Delta t}{2}}u + \dfrac{3}{\Delta t}\,{}^{t+\Delta t}u \\ {}^{t+\Delta t}\ddot{u} = \dfrac{1}{\Delta t}\,{}^{t}\dot{u} - \dfrac{4}{\Delta t}\,{}^{t+\frac{\Delta t}{2}}\dot{u} + \dfrac{3}{\Delta t}\,{}^{t+\Delta t}\dot{u} \end{cases}$$

$$\begin{cases} {}^{t+\frac{\Delta t}{2}}\ddot{u} = \dfrac{16}{\Delta t^2}\left({}^{t+\frac{\Delta t}{2}}u - {}^{t}u\right) - \dfrac{8}{\Delta t}\,{}^{t}\dot{u} - {}^{t}\ddot{u} \\ {}^{t+\frac{\Delta t}{2}}\dot{u} = \dfrac{4}{\Delta t}\left({}^{t+\frac{\Delta t}{2}}u - {}^{t}u\right) - {}^{t}\dot{u} \end{cases}$$

- Go to B.